Methods of Activation and Specific Applications

of Carbon Materials

P.Indra Neel, B. Viswanathan and T K Varadarajan

Methods of Activation and Specific Applications of Carbon Materials

160 pages and 43 figures

P.Indra Neel, B.Viswanathan & T K Varadarajan

National Centre for Catalysis Research

Department of Chemisry

Indian Institute of Technology Madras

Chennai, India

Preface

The material contained in this e book was evolved out of the efforts of the National Centre for Catalysis Research (NCCR) during their investigations on adsorptive desulphurization. The purpose of presenting this material in an e book form is to disseminate the methods of activating carbon precursor materials as well as to enumerate some of the specific applications of carbon materials. It is our hope, that carbon materials will find special emphasis in future for various applications including energy conversion and storage.

The book consists of a fairly extensive chapter on the methods of activation of carbon. This chapter brings out how the textural and surface functional groups of carbon materials can be modulated employing appropriate activation methods and agents.

Two chapters are exclusively devoted to the application of carbon materials. One of the chapters examines the suitability of carbon materials as support for electrodes in electrochemical conversion devices. The other chapter deals with the adsorptive desulphurization studies carried out in our centre. The information contained in these chapters is mostly generated from the results obtained in this centre. It is therefore reiterated that the contents of these two chapters and most of the material contained are unpublished work from National Centre of Catalysis Research. It is therefore once again appealed that the material contained in this e book may not be reproduced in any form without prior permission of the authors.

The authors will be happy to receive any comments and suggestios so that they can improve the document and make it more useful to the scientific community. The authors wish to place on record their grateful thanks to the members of the NCCR for their cooperation and suggestions at various stages of developing this e book.

Chennai 600 036   B.Viswanathan

Contents

Section I

Introduction

Carbon materials are unique and versatile in their performance. They have major industrial significance. Activated carbon materials characterized by high specific surface area and tunable porosity find utility in many vital technologies namely energy storage (super capacitors, batteries, hydrogen sorption), energy conversion (fuel cells, solar cells), sensors, environmental protection (regulate SO_x and NO_x emissions from fuel combustion in automobiles), production of fine and bulk chemicals and catalysis.

Activated carbon is a material with highly porosityre consisting of hydrophobic graphene layer as well as hydrophilic surface functional groups making them beneficial for sorption and catalytic applications. Specific industrial applications include areas such as oil and natural gas, food, pharmaceuticals, water treatment, hydro metallurgy, gold recovery and carbon-in-pulp process [1]. Activated carbon materials are effective in removing pollutants (both gaseous and liquid). The advantage of activated carbon materials as adsorbents is that the treated effluent is of high quality, the design of the process is simple, the operation of the process developed or adopted is easy. In addition carbon materials are resistant to corrosive (acidic and basic) and toxic environments [2]. In addition to purification of gases and liquids with high adsorption potential, activated carbon materials are also used as catalysts and catalyst supports. Carbon materials play an indispensable role in almost all electrochemical devices, to name a few, batteries [3], supercapacitors [4] and fuel cells [5]. The choice of carbon as the material is because of its unique properties of electrical conductivity and structural diversity.

The structure of a typical microporous activated carbon is shown in Fig. 1. Microporous carbon materials are highly disordered. In general, the structure comprises of aromatic sheets and strips. Such sheets are often bent imitating crumpled papers and wood shavings. The voids and gaps of molecular dimensions, between such aromatic

sheets are regarded as micropores. Again the microporosity is dependent on the carbon precursor as well as the method of preparation [6].

Fig.1. Structure of Activated Carbon - A schematic representation (reproduced from ref. 6)

The demand for activated carbon is increasing owing to the increased utility of the carbon materials in pollution control. As a result, cost of activated carbon is also growing depending on the application. Designing ways for the production of activated carbon through economic ways is the need of the hour. A range of low cost, easily available, carbon rich and low ash precursors and sources are being explored for the production of carbon materials.

Most of the commercial activated carbons are either coal based [7, 8] or petroleum pitch based [9] which are prone to exhaustion. Their global distribution is non uniform. As the applications of activated carbon are immense, the gap between demand and supply is ever widening. This may in due course result in scarcity of the material in addition to becoming expensive. This situation necessitates the need for the exploration of new sources of carbon materials with desired physico chemical properties namely, high specific surface area, micro or meso porosity or both, depending on the end application, surface functionality, thermal stability, carbon purity, adsorptive capacity and chemical composition (inherent or induced presence of hetero atoms like B, N, S and P).

Lignocellulosic materials have been and will be with mankind for ever and they hold a promise of renewable and inexhaustible supply of carbon materials provided

suitable methods of production are developed. In addition they are more evenly distributed throughout the globe relative to either coal or petroleum. Thus the lignocellulosic material, a regenerable natural resource, is a viable option for the generation of carbon materials rather than fossil fuels.

It is interesting to note that Carbon has come to the rescue of even Thomas Alwa Edison, the greatest inventor of modern times, in his backbreaking toilsome efforts to invent high-resistance incandescent lamp, where in either Pt or PtIr alloy failed to provide an antidote. To our surprise, the carbon filament that was originally used was from biomass [10].

In the biological lignocellulosic material, the carbohydrate (holo cellulose and cellulose) component is intimately bound to lignin. Lignin is a 3-dimensional cross linked aromatic polymer with phenyl propane units [11]. Next to cellulose, lignin is the major constituent of plant cell wall. Lignin possesses a complicated chemical structure with both phenolic (aromatic) as well as alcoholic (aliphatic) hydroxyl groups being present in the structure [12]. The main repeating unit of lignin is 3-(4-hydroxy phenyl) prop-2-eneol. Lignin is an aromatic amorphous biopolymer deposited as a reinforcing agent in plants offering mechanical support to the fibrous tissues of the plant [13]. Thus the main function of lignin is to impart strength and rigidity to the cell wall by acting as structural matrix. The carbon precursor and the method of preparation are the determining factors of the textural and surface properties of carbon materials [14]. Taking into consideration some specific properties like volatile matter, ash content and fixed carbon content as well as the derivable porosity, several researchers have studied the possibility of producing carbon materials from different lignocellulosic materials.

Ganan *et al*., [15] have employed *Almond tree pruning* as precursor for producing activated carbon (specific surface area, SSA ~ 959 m^2/g). A two step process of activation comprising of pyrolysis followed by catalytic air oxidation is employed. Oxides of Co and K were used as catalysts. Mariyam Kazemipour *et al*., [16] have employed *Almond (Amygodolus) shells, Apricot (Armeniaca bulgar) stones, Hazel nut (Corylus avellana), Pistacio (Pistaca) and Walnut (Jouglans regia L.)* as precursors for producing activated carbon materials with SSA values of 1208, 861, 786, 635 and 941 m^2/g by the method of carbonization in inert atmosphere at 1073 K. The activated carbon

materials from Almond shell, hazel nut and walnut were effective in the removal of 99.8 % Cu, 96.9 % Pb and 71% Zn respectively from industrial effluent water.

Onal *et al*., [17] have employed *Apricot stones* as precursor for producing activated carbon (SSA ~ 1060 m^2/g) using $ZnCl_2$ as activating agent. The activated carbon thus produced was found to be an effective sorbent for Naproxen Sodium (maximum sorption capacity ~ 49.75 mg/g of carbon). Demirbas *et al*., [18] have employed *Apricot stones* as precursor for producing activated carbon (SSA ~ 560 m^2/g) at an activation temperature of 523 K in air oven using H_2SO_4 as activating agent. The carbon material thus produced was effective in the sorption of astrazon yellow 7GL, a basic dye (adsorption capacity – 221 mg/g of carbon material). Mansoorech Soleimani *et al*., [19] have produced activated carbon with a SSA of 1387 m^2/g from *Apricot stone* using H_3PO_4 as activating agent at an activation temperature of 373 K. The carbon material was found to be an effective sorbent for the removal (98 % removal achieved) of gold from industrial (gold-plating) waste water. Cigdem Sentorun-Shalaby *et al*., [20] have produced activated carbon (SSA ~ 1092 m^2/g) from *Apricot (Kabaasi) stones* using steam activation at an activation temperature of 1073 K. An inverse relationship between the S content of the carbon precursor and the BET surface area values was observed. The decrease in the surface area with an increase in S content was attributed to the enhanced gasification rate of the carbon material because of the presence of increased surface functional groups upon SO_2 pretreatment of the carbon precursor. Kobya *et al*., [21] have prepared activated carbon from *Apricot stones* using sulphuric acid as activating agent at an activation temperature of 473 K. The material (SSA ~ 566 m2/g) thus obtained was found to be effective in the removal of heavy metals like Cr (VI) (99.99 % at pH = 1), Cd (II) (99.68 at pH = 6), Co (II) (99.11% at pH = 6), Cr (III) (98.99 at pH = 6), Ni (II) (98.51% at pH = 6), Cu (II) (97.48 % at pH = 6) and Pb (II) (99.93 % at pH = 6) from industrial waste water.

Hameed *et al*., [22] have employed *Bamboo (bambusoidae)* for producing activated carbon by adopting a physico chemical method of activation using KOH as well as CO_2 as activating agents at an activation temperature of 1123 K. The activated carbon material with SSA, total pore volume and pore diameter values of 1896 m^2/g, 1.109 cm^3/g and 2.34 nm was effective in the sorption of methylene blue (454.2 mg/g). Yong-

Jung Kim *et al*., [23] have produced activated carbon from *Bamboo* using KOH activation method at 1073 K in Ar atmosphere. The activated carbon produced exhibited potential as electrode material for electric double layer capacitors. The carbon material (produced with a char to KOH (wt./wt.%) ratio of 1:3) with a specific surface area value of 894 m^2/g and the highest mesopore to micropore fraction showed maximum value of specific capacitance. The higher capacitance was attributed to the better mobility of the electrolyte ions in the presence of larger pores (mesopores).

Dinesh Mohan *et al*., [24] have employed *coconut shell fiber* as a precursor for producing activated carbon (SSA`~ 512 m^2/g) using H_2SO_4 as well as thermal means to activate the material. The activated carbon material thus produced was found to be effective in the removal of Cr (III) (sorption capacity – 16.1 mg/g).

Jeremias *et al*., [25] have employed *coir pith, coir fiber and endocarp from coconut shell* to generate activated carbon material using physicochemical activation process. $ZnCl_2$ as well as CO_2 were used as activating agents at 1073 K in N_2 atm. The activated carbon produced from coir pith possessed a specific surface area value of 1880 m2/g where as those carbon materials from coir fiber and endocarp exhibited specific surface area values of only up to 540 m^2/g .

Badie S Girgis *et al*., [26] have employed *Peach stone shells* as precursor for producing activated carbon materials (SSA ~ 1053 – 1404 m^2/g) using H_3PO_4 as activating agent. The carbon materials exhibited promising sorption capacities for p-nitro phenol (435 mg/g), methylene blue (543 mg/g) and Pb^{2+} ions (204 mg/g).

Ru-Ling Tseng *et al*., [27] have produced activated carbon material (SSA ~ 2300 m^2/g) from the cane pith of *sugar cane (Saccharum Officinarum)* through activation with KOH at 1053 K in N_2 atm. The high specific surface area was attributed to the catalytic smelting action of KOH which is analogous to the fermentation of flour. The carbon material showed promise in the sorption of dyes such as acid blue 74, methylene blue and basic crown.

In addition to the above mentioned biomass, several other lignocellulosic materials, namely, apple pulp [28 - 32], cane bagesse [33 - 35], corn cob [36 - 39], coconut shell [40-55], corn stalks [56], date pits [57 – 59], eucalyptus wood [60], guava seeds [61], oat hulls [62, 63], olive-stone [64 – 76], pea nut hulls [77], pecan shell [78],

pine wood [80], rice husk [80-88], rice straw [90 – 92], rock rose [93, 94], saw dust [95, 96] and walnut wood [97] have also been exploited by researchers for producing activating carbon materials.

I. 1. Reactions leading to Char formation from Lignocellulosic carbon precursor:

During pyrolytic decomposition of lignin and cellulose certain reactions result in the scission of chemical bonds leading to the fragmentation and also depolymerization of parent polymer. In addition to bond scission, formation of new bonds too takes place. Such creation of new bonds will stabilize the adjacent carbon atoms there by resulting in the formation of a non-volatile and stable carbon framework. Certain fragments formed during pyrolysis evolve as volatile products where as the other fragments gets reconnected to the carbon framework undergoing thermal reformation to form char [98].

I.1.1. The factors that affect the char yield and carbon content of the activated carbon

The terrestrial plants can be classified into three taxonomic groups in general, namely, soft wood trees, hard wood trees and the grasses. Plant tissue is made up of lignocellulosic material. The lignocellulosic material consists of plant cell wall and also the intracellular substances. The cell wall is made up of holocellulose which is a combination of cellulose and hemicellulose and lignin. In general, the intracellular substances are termed as extractives based on the analytical method of extraction. The abovementioned components, namely, lignin, cellulose and extractives are known to vary in chemical structure and initial carbon content. The cellulose is a linear polymer of glucose with a theoretical carbon content of 44.4 %. Lignin is a three dimensional polymer of aromatic alcohols with a carbon content of 60 – 63%. As a result the carbon content of a lignocellulosic material is dependent on the relative abundance of its constituents. Thus it can be said that greater the carbon content of the lignocellulosic precursor greater will be the carbon content of the char. The carbon yield obtained from extractives lies between the yields obtainable from lignin and cellulose. Most of the

extractives, intra cellular material, contain compounds analogous to lignin, but of relatively smaller molecular weight, and are usually termed as Brawn's lignins. Also some of the components of extractives like terpenes are relatively volatile and do not contribute to char formation during pyrolysis. Thus the yield of carbon from each component is directly related to the carbon content of the respective components. Holocellulosic fraction with lowest carbon content results in lowest carbon yield where as lignin with the highest carbon content exhibits highest carbon yield. Thus the carbon yield upon pyrolysis of lignocellulosic material is dependent on the composition of the precursor material. In general, greater the aromaticity and molecular weight of the precursor, greater will be the char yield. The low carbon yield in the case of cellulose is due to the fact that significant amount of carbon is lost from the glucose derivatives due to volatilization and as a result the char yield is low. The high yield of carbon in the case of lignin is because of the high aromatic content as well as the complex polymer structure of lignin. Interestingly, the char yield from cellulose is known to be enhanced by the presence of inorganic compounds (mineral matter). In plants Na^+ and K^+ ions are of physiological important. Plant cells are intelligent in differentiating Na^+ and K^+ by some complexing mechanism [99].

Increasing the inorganic content upto 2 – 15% (catalytic saturation limit) increased the char yield. The crystallinity of cellulose also affects the char yield. In the lignocellulosic materials, cellulose is known to be present in both crystalline and amorphous phases and the char yield was found to be higher with crystalline cellulose. Unlike cellulose, hemicellulose is only amorphous. The initial carbon content, the char yield and carbon yield from lignin were respectively 63, 53 and 76%. On the contrary, the carbon content, the char yield and carbon yield from cellulose were 44, 18 and 40% [98]. Thus lignin contributes to higher carbon content to the activated carbon compared to cellulose.

I.1.2. Cellulose and Lignin transformation into condensed aromatic system

Tang and Roger Bacon [100] provided a detailed reaction mechanism for the transformation of cellulose into a condensed aromatic system and is illustrated in Fig. 2.

11

Cellulose is known to undergo thermal decomposition without the presence of a melting state resulting in the formation of a strong carbonaceous reside. In the process of aromatization of cellulose, four stages were supposed to be crucial.

During state I, physisorbed water molecules are removed in the temperature range of 298 – 423K. Such a desorption of physisorbed water increases the degree of lateral order. In stage II, the structural water, involving hydrogen and hydroxyl moieties in the equatorial position, is stripped off from the cellulose in the temperature range of 423 – 413 K due to thermal excitation. Such dehydration process is essentially intramolecular. Major thermal degradation of cellulosic structure takes place in stage III at temperature above 413 K. Thermal scission of C-O and C-C bonds as well as dehydration takes place in stage III-a in the temperature range of 413 – 673 K yielding tar as well as carbonaceous residue. Tar formation is supposed to be through Levoglucosan. Upon pyrolytic decomposition cellulose depolymerizes through the scission of 1, 4 glycosidic linkage and also the subsequent intramolecular rearrangement of cellulosic units results in the formation of levoglucosan which results in the formation of tar. Even though the tarry portion is a complex mixture, the main constituent of the tar was indentified to be dehydrated cellulose (mass = 144). The final breaking down of each of the cellusic ring units takes place in Stage III c resulting in the formation of carbon residue containing four – carbon atoms (nos. 3, 4, 5 and 6). Thus four of the six carbon atoms in each glucose monomer are retained in the char. Such four carbon atom intermediates, a very – short lived radical species, serve as "building blocks" for the repolymerization forming carbon polymer and subsequently a graphitic structure in Stage IV in the temperature range of 673 – 973 K.

Both cellulose and lignin contribute the aromatic carbon content. But the precursors containing hexagonally arrayed carbon, as those found in lignin, would readily reform to stable graphitic arrays. In the case of cellulose such structural advantage is missing.
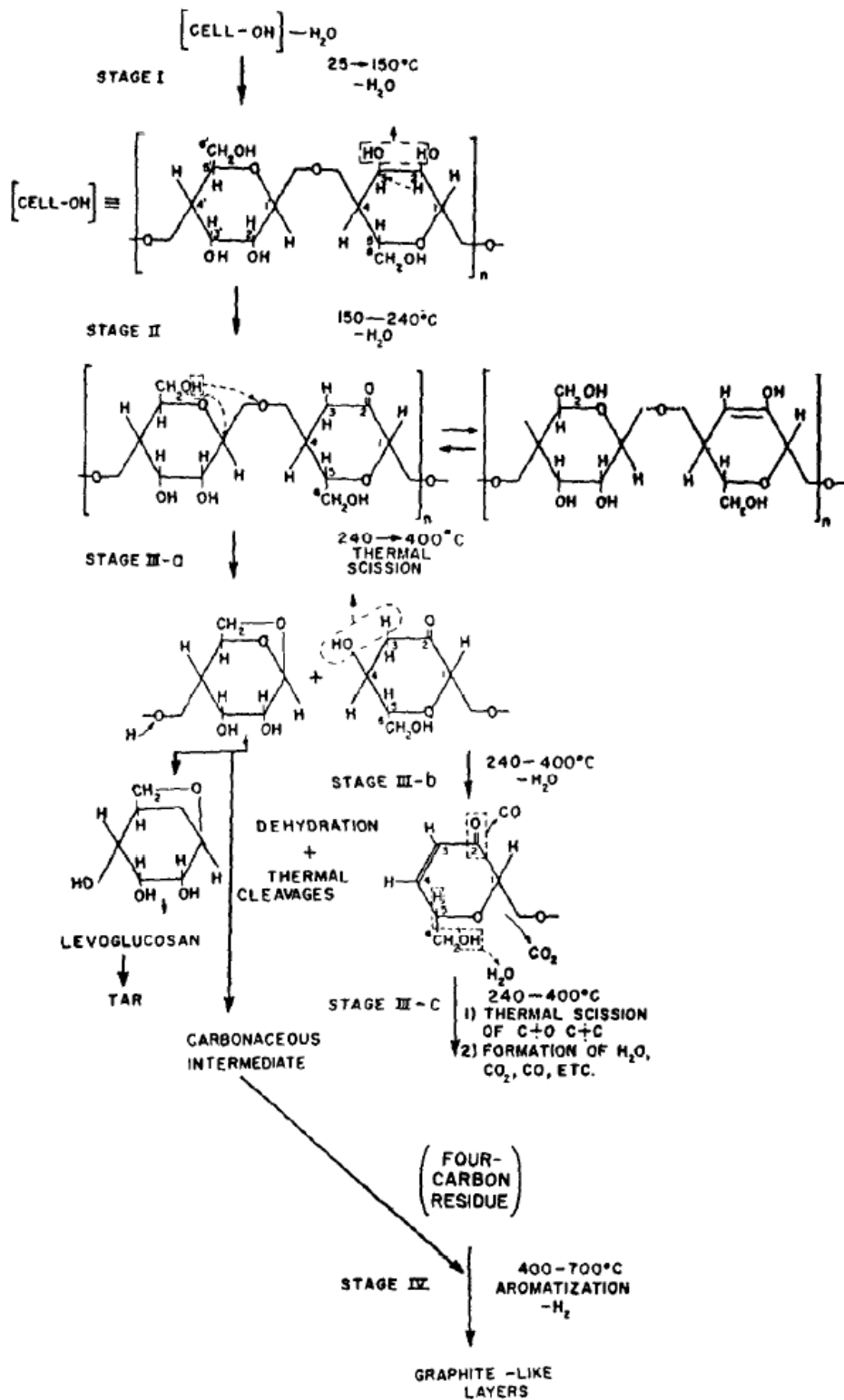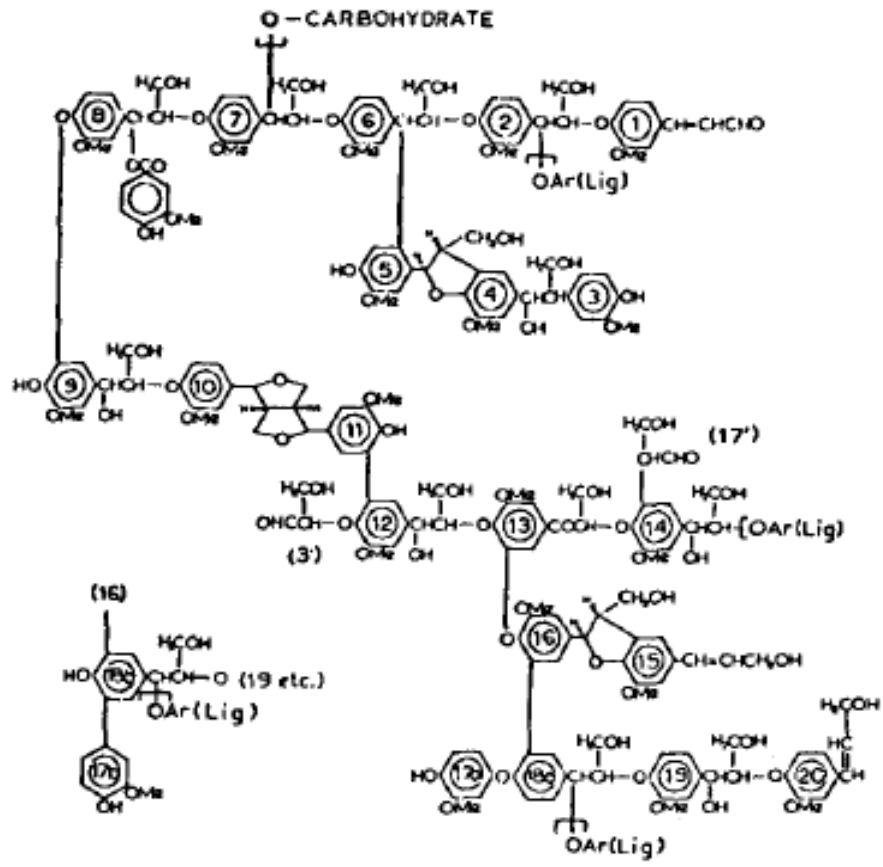
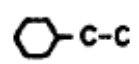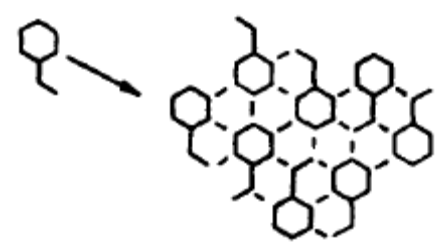Fig. 2. Proposed mechanism for the transformation of cellulose to aromatic carbon (reproduced from ref. 100)

Fig. 3. Conceptual mechanism for the transformation of lignin to aromatic carbon: (a) typical structure of lignin, (b) basic building block of lignin structure and (c) conceptual geometry for the formation of graphite like layer from the structural units formed during pyrolysis (reproduced from ref. 98)

Mackay and Roberts [98] have proposed a conceptual mechanism of aromatization of lignin upon pyrolysis as represented in Fig 3. The structure of lignin comprises of inherent and inbuilt aromatic building blocks. Such subunits are geometrically well suited for the formation of condensed aromatic system as shown in Fig. 3. (c).

I.1.3. Suitable Lignocellulosic Materials for the production of Activated Carbon Materials:

Wolfgang Heschel *et al*., [101] have evaluated several lignocellulosic materials, namely, chery stones, coconut shells, hazel nuts, peach stones, plum stones and walnut shells, to derive information regarding the specific properties of the parent lignocellulosic materials that determine their suitability for the production of activated carbon. Wood materials with a coarse cellular structure with inherent porosities greater than 35 % were found to be disadvantageous in terms of poor mechanical strength of the activated carbon derivable from such materials. Mechanical stability of the activated carbon material is desirable because sorption properties namely, adsorption capacity, hardness and granularity are mechanical strength dependent. In addition to the nature of the precursor material, the conditions of preparation have a bearing on the properties (porosity, hardness and density) of the activated carbon material. The structure of the raw material as well as the production process governs the adsorption properties of activated carbon produced. Raw materials that offer cokes with resistance to abrasion, low macroporosity and high yield are in general preferred and are suitable sources for the production of activated carbon. Among the materials investigated, woods are found to be of highest porosity (46 – 49 %) and nut shells and fruit stones were of lower porosity. No correlation was observed between the porosity and the chemical composition (O/C atomic ratio) of raw material where as the chemical composition of the precursor has a bearing on the coke yield obtainable. The coke yield increased with an increase in the lignin content of the precursor. This is because lignin contains lower amount of structural oxygen compared to hemicellulose or cellulose. No correlation was found between the hardness and the O/C ratio of the coke implying that the suitability of the

lignocellulosic material should not be assessed based on the O/C ratio alone. Rather the cell structure (porosity) of the plant is an important parameter in the choice of lignocellulosic materials. The morphology of the plant cell is the main factor responsible for the hardness, density and the porosity of the coke. Thus the morphology of the plant cell with peculiar cross linking between cellulose, hemicellulose and lignin determines whether a particular lignocellulosic material is suitable for the production of activated carbon. In essence for a lignocellulosic material to be chosen as precursor for activated carbon, the inherent porosity of the raw material should not be greater than 35 %. Also upon pyrolysis the ratio of mass loss (Δm) to volume (ΔV) shrinkage should be close to 1. Among the raw materials investigated the order of suitability for the production of activated carbon is as follows: coconut shells > peach stones > plum stones > hezel nut shells > walnut shells > cherry stones.

A multitude of activating agents has been extensively employed for the production of activated carbon materials with desired pore structure. The purpose of activation is to create and develop (volume and size) porosity in the carbon material and there by increase the adsorptive capacity. All the available methods of activation can be classified in to two types, namely, physical activation or chemical activation depending on whether a gaseous or solid activating agent is used. Each of these methods has its own merits and demerits.

1.1.4. Chemical method of activation

On the other hand, chemical activation is a single step process for the preparation of activated carbon where in carbonization of organic precursor in the presence of chemical agents takes place. In this method a solid activating agent like alkali and alkaline earth metal containing substances and some acids are used. The activating agents employed function as dehydrating agents that influence pyrolytic decomposition inhibiting the formation of tar and thereby enhancing the yield of carbon. The temperatures used in chemical activation are lower than that used in the physical activation process. As a result the development of a porous structure is better in the case of chemical activation method. In spite of the above mentioned virtuous aspects the

chemical method has its own inherent drawbacks like the need for washing of the product to remove the residual inorganic material which causes serious pollution problem.

I.1.5. Physical method of activation

Physical activation involves two steps, namely carbonization of the carbonaceous precursor in an inert atmosphere and subsequent activation of the resulting char in the presence of carbon gasification reactants (gaseous) such as carbon dioxide, steam or air or a suitable combination of the above mentioned gaseous activating agents. In the method of physical activation, the reaction involved is between carbon atom and the oxidizing gas. It is this reaction that gives rise to the pore creation and development as some parts of the char structure are reacted faster than the others. During this reaction if carbon atoms were to be removed from the interior of incipient pores formed as a result of devolatilization during carbonization enlargement of opened micropores and the opening up of the closed micropores takes place. If the burn off were to be from outside of the particle no new porosity results but it facilitates the reduction of particle size. Since physical activation uses gaseous activation agents and does not produce waste water this method is considered to be an environmentally benign technology. But all is not well with this process. It takes long time and much energy for producing microporous activated carbon through physical activation methods. Also another inherent draw back of this method is that large amount of internal carbon mass is eliminated to obtain well developed pore structure. And thus one has to satisfy himself with limited carbon yields if one were to go in this route.

Section II

On the Methods of Activation (Based on the chemical nature of activating agent) of Carbon Nano Materials

Chemical methods of activation utilize the microexplosion behaviour of chemical agents. Carbon nanomaterials have unique electrical and structural properties thus making them useful and indispensable in energy conversion and storage devices (as electrode material), catalytic processes (as support material) and purification technologies (sorbents). One of the main factors limiting their applicability is their low specific surface area (in the range of $200 - 300$ m^2/g). Several activation methods are known to improve the porosity and specific surface area of carbon nanomaterials.

The questions of interest are:

(i)   what is (are) the possible reaction(s) between carbon material (precursor to activated carbon material) and the activating agent?

(ii)   How does such reaction(s) contribute to evolution of porosity and an accompanied improvement in specific surface area?

(iii)   How does the surface chemistry of carbon materials alter upon activation?

(iv)   How does the process of activation increase the sphere of usefulness of carbon materials?

In spite of the availability of vast literature on various activation methods meant for improving the performance of carbon materials, detailed knowledge of the process of activation is still poor.

II. 1. Activation with Alkali Metal Hydroxides

Among the alkali metal salts, KOH is the most effective activating agent in producing activated carbon materials.

## II. 1.1. KOH as activating agent

The studies of Harry Marsh and Dennis S Yan [102] were aimed at understanding the reactions between carbonaceous material and KOH and subsequently knowing how the process of activation leads to the transformation of a non-porous, low surface area carbon precursor into a high surface area porous carbon material. The researchers could offer a convincing description of the process of activation of carbon precursor by KOH. Based on the thermodynamic considerations, the reaction between KOH and carbon precursor can result in the formation of functional groups such as –OK using oxygen of the alkali salt.

$$K_2O + C \longrightarrow C\text{-}O\text{-}K + K$$
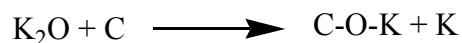
The presence of such potassium and oxygen bond in the char leads to the oxidation of cross linking carbon atoms in the adjacent lamella during the process of activation. Surface functional groups are created at the edges of the lamella. As a result of removal of cross linking between adjacent lamella and also the formation of new functional groups on individual lamella, the lamellas of the crystallite are disturbed from their normal (completely flat) form into a slightly wrinkled or folded or puckered form. Also the potassium metal produced in the process of activation, *in-situ*, **intercalates** in to the lamella of the crystallite. After the activation process, when the carbon material is washed with water, the potassium salts present in the carbon particles are removed by leaching. At the same time, the lamella cannot return to their original state (non porous state) creating interlayer voids. Thus the lamella remains apart causing porosity and yielding high surface area carbon [102].

The intellectual propositions of Harry Marsh and Denis S Yan on the process of KOH activation found experimental verification by the studies of Seong – Ho Yoon *et al.,* [103] on the activation of CNF's by KOH. The studies of Seong – Ho Yoon *et al.,* were aimed at understanding the structural changes involved in the carbon nanofibers

upon activation and also the impact of activation on the textural properties of the resulting activated CNF's. In their study, CNF's were prepared at 873 K using Cu-Ni based catalyst and a mixture of C_2H_4 together with H_2 as carbon precursor. The as prepared CNF's were activated with KOH (KOH:CNF = 4:1, wt./wt.%) at three different activation temperatures, namely 1073, 1123 and 1273 K. The specific surface area of the CNF's upon activation increased from 174 to 439, 587 and 1212 m^2/g respectively at activation temperatures of 1073, 1123 and 1273 K. The most striking aspect of the study is the understanding of the structural transformation the original as synthesized CNF underwent upon increasing the severity of KOH activation (increasing the activation temperature from 1073 to 1273 K). Two important structural parameters namely the average (002) interlayer spacing (d_{002}) and the average stacking height of carbon (002) planes ($Lc_{(002)}$) were derived from XRD studies to gain insight into the mechanism of KOH activation. It was observed that under mild activation conditions, when the specific surface area of the activated CNF is lower than 400 m^2/g, there was only little change in the (002) inter layer spacing (d_{002}) but there was a drastic decrease, (from 4.6 nm to 1 nm), in the stacking height of the (002) planes of carbon. This observation indicates selective consumption of graphenes in certain parts of the crystallite of carbon (gasification or partial oxidation). As a result of such selective gasification, a ladder like structure is formed. But the fiberous morphology of the CF's was still retained (as observed from SEM studies). Upon increasing the severity of the activation process, in the case of CNF's with surface area values greater than 400 m^2/g, an increase in the (002) inter layer spacing (d_{002}) with no change in the stacking height ($Lc_{(002)}$) is observed. Such an increase in (002) interlayer spacing is a result of broadening and subsequent collapse of over all (002) plane interspacing leading to the rearrangement of the fiber structure. Keeping in view the afore mentioned observations, Seong-Ho Yoon *et al.*, have proposed a model depicting the KOH activation process as represented in scheme 1. The important features of the model being: selective gasification of graphenes by -C-OK, K_2O, and K_2CO_3 species formed *in situ* during the KOH activation process; local removal or broadening of graphene layers (lamellas of carbon crystallite) and finally the collapse of the fibrous morphology by rearrangement of the graphene layers.
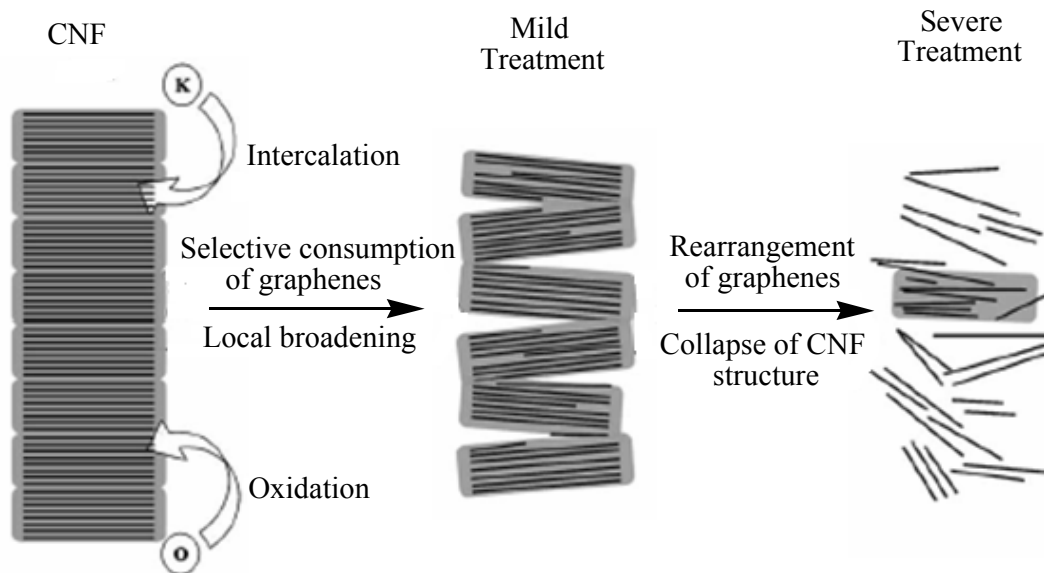
Scheme 1. Model for the activation of carbon nanofibers (CNF's) by KOH between 773 – 1273 K in N_2 atmosphere (reproduced from ref. 103)

Byung-Joo Kim *et al*., [104] have examined the process of KOH activation of graphitic nanofibers. Based on the XRD and SEM observations, a mechanism as shown in scheme 2 was proposed to explain the development of porosity on KOH activation. Graphitic nanofibers were known to contain layered structure. Three path ways, namely, breaking of longer fibers to shorter fibers, expansion of the graphene layers by K intercalation (widening of pores) and exfoliation (involving a combined effect of separation of grapheme layers and also the breaking of fibers) were operative in generating the porosity. The as prepared graphitic nanofibers possessed a specific surface area value of 320 m^2/g. But upon activation with KOH at three different temperatures, namely, 1172,1273 and 1373 K, the specific surface area values improved to 500, 580 and 790 m^2/g respectively.

Increasing the severity of the activation process by increasing the activation temperature brought about significant changes in the intensity as well as the width of the diffraction peak at a 2θ value of 25 ^{0} which can be ascribed to the (002) diffraction of graphitic carbon. The intensity of the above mentioned signal decreased with increasing activation temperature indicating the induced irregularity into the layered structure of the graphitic nanofibre. In addition to the decrease in the intensity of the diffraction signal

from the (002) plane of graphitic carbon, the peak was broadened on increase of activation temperature and this change in width of the peak can be attributed to the widening or expansion of the grapheme layers in the individual crystallite by K interaction and the subsequent collapse of the fiberous shapes (disintegration to smaller crystallites).
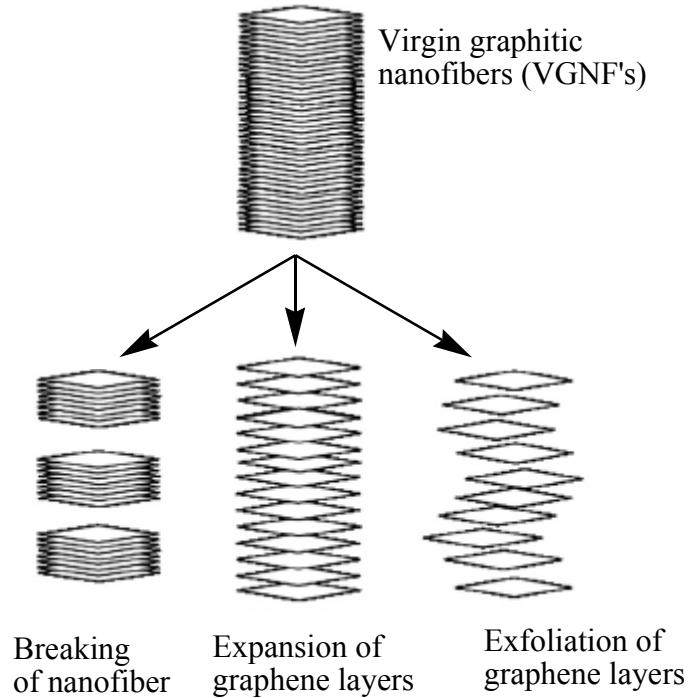

Scheme 2. Schematic Representation of the mechanism of activation of graphitic nano fibers (GNF's) by KOH (reproduced from ref. 104)

In addition to the development of porosity and improvement in specific surface area, another prominent advantage with KOH activation is the creation of -OH surface functional groups on the carbon surface. The (-OK) groups formed on the carbon surface upon KOH activation gets transformed to (-OH) groups on washing with water by ion exchange reaction.

Thus, in addition to creation of voids by the removal of K, upon washing with water, polar functional groups like –OH are created in large numbers making the carbon surface hydrophilic. In fact, producing water soluble (hydrophilic) CNT's by itself is an important research problem being pursued currently.
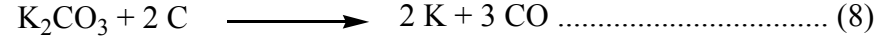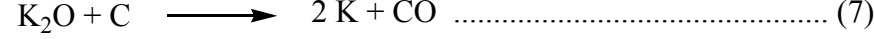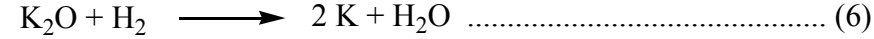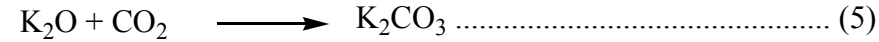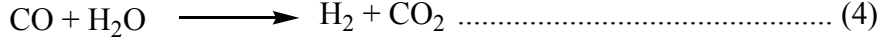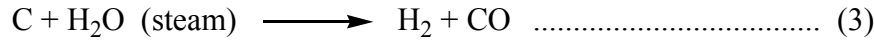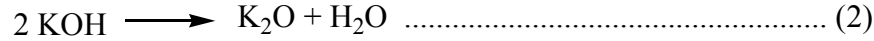
Yupeng Guo *et al*., have proposed the following mechanism for the activation of carbon materials by KOH [105].

In general the chemical reaction between KOH and carbon material can be written as follows:

$$4 \text{ KOH} + \text{C} \longrightarrow \text{K}_2\text{CO}_3 + \text{K}_2\text{O} + 2 \text{ H}_2 \quad ....(1)$$
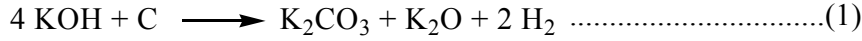
KOH reacts with disordered or amorphous carbon at high temperatures to form K_2CO_3 as well as the decomposition product K_2O along with the evolution of hydrogen.

Considering the decomposition of KOH into K_2O as well as the reducing ability of carbon, additional reactions do take place during the process of activation as shown:

$$2 \text{ KOH} \longrightarrow \text{K}_2\text{O} + \text{H}_2\text{O} \quad .... (2)$$

$$\text{C} + \text{H}_2\text{O} \text{ (steam)} \longrightarrow \text{H}_2 + \text{CO} \quad .... (3)$$

$$\text{CO} + \text{H}_2\text{O} \longrightarrow \text{H}_2 + \text{CO}_2 \quad .... (4)$$

$$\text{K}_2\text{O} + \text{CO}_2 \longrightarrow \text{K}_2\text{CO}_3 \quad .... (5)$$

$$\text{K}_2\text{O} + \text{H}_2 \longrightarrow 2 \text{ K} + \text{H}_2\text{O} \quad .... (6)$$

$$\text{K}_2\text{O} + \text{C} \longrightarrow 2 \text{ K} + \text{CO} \quad .... (7)$$

$$\text{K}_2\text{CO}_3 + 2 \text{ C} \longrightarrow 2 \text{ K} + 3 \text{ CO} \quad .... (8)$$

The steam generated in (step 2) causes removal of amorphous carbon as CO as shown in (step 3) leading to formation of pores. Additional carbon is also consumed for reducing K^+ to K as shown in steps (7) and (8). All these carbon losses contribute to the creation of porous network in the carbon material. It is interesting to note that KOH activation has the benefit of activating the carbon material or the carbon precursor with steam (step 3) as well as activation with K_2CO_3 (step 8).

Caution should be exercised in considering reaction (8) where in amorphous carbon is gasified to CO and also yielding K which subsequently intercalates in to the carbon lamella. Yong bin Ji *et al*., [106] have proved from XRD studies that reaction (8) is only possible in ungraphitizable carbon materials but not in graphitizable carbon materials possessing structural regularity. The researchers have observed only little attenuation in the diffraction peak at the 2θ value of $26°$ (corresponding to the (002) plane of graphite crystallite) upon activation (with K_2CO_3) of meso carbon micro beads (MCMB) relative to unactivated MCMB implying that there is hardly any change in the

structure of the graphene layers in the original MCMB upon activation with K_2CO_3. Thus reaction (8) is not possible in graphitizable carbon materials like MCMB.

The following reaction between K_2O and silica is specific to carbon materials produced from natural sources where silica is unavoidable.

$$K_2O + SiO_2 \longrightarrow K_2SiO_3 \quad \text{... (9)}$$
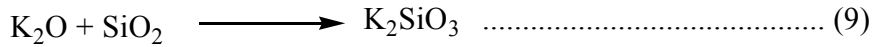
Reaction (9), where in silica is removed leaving porous structure, is important for the additional activation of carbon materials from natural sources. Thus during activation with KOH, amorphous carbon as well as silica are removed from the carbon precursor resulting in porous structure and a corresponding improvement in values of specific surface area.

Zengmin Shen *et al*., [107] have inferred that during the KOH activation process, surface species (such as alkalides, -OK) as well as molecular species like K_2CO_3 and K_2O are formed. The potassium salts thus formed react further with carbon leading to the formation of K and CO. The researchers have proposed two path ways, namely, formation of mesopores and pore widening, for the development of porosity during KOH activation. In general, the process of pore widening takes place at a higher activating agent (KOH) to activate carbon precursor ratio. In addition the pore widening process is accelerated as the activation temperature is raised from 1073 to 1225 K and this can be attributed to the fact that at higher temperatures of activation, the melt of K_2CO_3 and K_2O as well as the vapour of K possess higher kinetic energy accelerating the pore widening process.

Zengmin Shen *et al.,* [107] have evaluated the effect of the amount of activating agent (KOH) on the process of activation. The activation of meso carbon micro beads (MCMBs) was carried out with different wt./wt.% ratios of activation agent to the carbon precursor, namely, 3, 5, 7, 8, 10 and 12. It was observed that upto a ratio (activating agent to carbon precursor, wt./wt.%) of 8, the specific surface area value increased upto 3182 m^2/g. The improvement in the specific surface area value was attributed to the extensive oxidation of carbon atoms (gasification) and the accompanied development of porosity. The micropore widening process predominates over the formation of new micropores. This is because of the availability of large number of reaction sites in the interior of the micropores rather than on the external surface. Such pore widening

process results in the transformation of miroporous carbon material to mesoporous carbon material. But further increase in the ratio of the activating agent to the carbon precursor (> 8 wt./wt.%) excess carbon loss results and this cause the collapse of pore wall and the loss of mesoporosity and subsequently the specific surface area is reduced.

The effectiveness of KOH activation relative to either physical activation methods or activation by other chemical agents can be attributed to the ability of K to form intercalation compounds with carbon easily. In addition, the K_2O formed during the process of KOH activation, *in-situ,* can easily infiltrate into the pores. K_2O is reduced to K by carbon resulting in carbon gasification with a subsequent emission of CO_2 leading to the formation of pores. Also K atoms that intercalate into the lamella of the carbon crystallites widen the space between the adjacent carbon layers (intercalation phenomenon), resulting in an increase in the value of specific surface area. [106].

The problem of inducing microporosity in to mesoporous carbon materials by either physical or chemical activation methods is being pursued actively in recent times. Joanna Gorka *et al*., [109] have activated the phloroglucinol-resin based mesoporous carbon with KOH to tune (alter) the porosity of the material. For preparing the mesoporous carbon material, a soft template method is employed. Usually, the tri block copolymer, poly (ethylene oxide) – poly (propylene oxide) – poly (ethylene oxide) (PEO – PPO – PEO) is used as the soft template. Organic compounds such as phenol (resorcinol or phloroglucinol) and formaldehyde are incorporated into the hydrophilic nanodomains of the template. Poly condensation reaction of phloroglucinol and formaldehyde in the hydrophilic nanodomains of the triblock copolymer results in the formation of carbon precursor (polymer). The carbon precursor on removal of the sacrificial polymeric template (the triblock copolymer) from the polymeric nanocomposite (polymer of phloroglucinol and formaldehyde + triblock copolymer), is transformed to the ordered mesoporous phenolic resin which upon carbonization transforms to mesoporous carbon. Upon KOH activation of the mesoporous carbon, the researchers could increase the microporosity substantially with simultaneous rentention of mesoporosity. The specific surface area of the mesoporous carbon material increased from 497 to 901 m^2/g; the micropore volume increased from 0.04 to 0.22 cm^3/g while there is almost no change in the mesopore volume (0.66 cm^3/g before activation and 0.64

cm^3/g after activation). The process of KOH activation of mesoporous carbon material results in the generation of significant amount of microporosity while keeping the mesoporosity intact is depicted pictorially in Fig. 4.

KOH activation

N_2 atm., 700 °C

Mesoporous
Carbon Material

Micro- and Mesoporous
Carbon Material
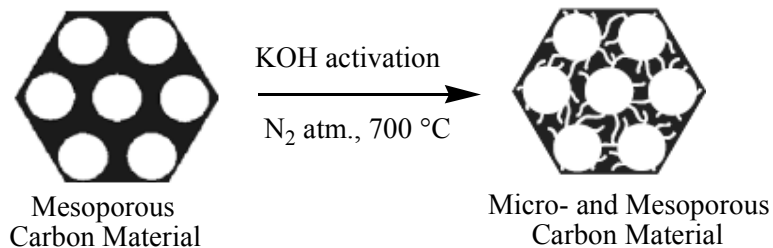
Fig. 4. Pictorial representation of the formation of micropores in the mesoprous carbon upon actaivation with KOH at 973 K in N_2 atmosphere (reproduced from ref. 8)

II. 1.1. A. Typical examples emphasizing the advantages of KOH activation

II. 1.1.A. (i) KOH Activated Carbon Nano Tubes (CNT's) for Super Capacitor Application:

High specific surface area as well as the narrow pore size distribution is the essential features for the carbon materials to be exploited for hydrogen storage, catalysts supports and electrode materials for super capacitors. But the main disadvantage with multiwalled carbon nanotubes is their low specific surface area. This has practically hindered the sphere of usefulness of carbon nanotubes and limited the applications [110].

Producing CNT's with high specific surface area as well as controlled pore structure is an important research problem. For closed single walled carbon nanotubes (SWNT's) the theoretical external specific surface area is 1315 m^2/g where as for the opened SWNT's the value is 2630 m^2/g. But in reality, the as-grown CNT's, in particular, the MWNT's exhibit lower specific surface area values than the theoretical values predicted. One of the ways of improving the specific surface area of the as grown CNT's is to resort to either physical or chemical methods of activation [111].

Qi Jiang *et al.,* [110] have produced CNT's by the method of chemical vapour deposition using CH_4 as carbon source. La_2NiO_4 was used as catalyst precursor. The catalyst precursor was reduced to a mixture of La-Ni by H_2 at 1073 K for 1 h. The temperature is reduced to 953 K under N_2 atm. CH_4 was allowed to pass through the

catalyst chamber for 1 h where in the CNTs growth takes place. The temperature was then lowered to ambient conditions. The catalyst metal particles were removed by nitric acid treatment. The specific surface area of the as prepared CNT's was ~ 194 m^2/g. Upon activation with KOH, the specific surface area value increased from 194 to 510m^2/g and the specific pore volume increased from 0.66 to 0.91cm^3/g.

KOH activated CNTs were exploited as electrode material for electro chemical super capacitor (ESC) application. ESC's are of particular importance in the field of energy storage owing to their large capacitance, long cycle life and environmental friendliness (free from toxic materials). Jiang *et al*., have found that activated CNT's have out performed the non-activated CNT's. The electrochemical capacitance offered by activated CNT based electrodes is double (50.0 F/g) that of the electrodes fabricated from nonactivated CNT's (25.0 F/g). The improvement in charge storage capacity was attributed to the increase in specific surface area (nearly 3 times – from 194 to 510m^2/g) and specific pore volume (1.5 times – 066 to 0.91cm^3/g) of the activated CNT's compared to the non activated CNT's. It should be noted that specific surface area, specific pore volume and pore size distribution are the crucial parameters that govern the performance of the electrode materials in super capacitor applications [112].

Yungang Liu *et al.,* have produced CNT's by the method of catalytic pyrolysis. Benzene was used as carbon source; ferrocene is used as catalyst precursor with thiophene. The specific surface area of the as – grown CNT's was ~ 24 m^2/g. But upon activation with KOH (KOH : C = 7:1 (wt./wt.%)) 15 times improvement in the specific surface area value has been reported i.e., from 24 m^2/g to 360 m^2/g [111].

### II. 1.1. A (ii) KOH Activated Carbon Material from Coal and Pitch for Capacitor Application

Low cost carbon materials produced from natural sources are attractive candidates for capacitor applications.

Small aromatic lamellae, poorly packed because of peripheral functional groups, are present in the precursor (coal or pitch or char) for activated carbon. During KOH activation, the aliphatic substituents as well as the heteroatom (other than C like N, O, S)

containing functional groups, were preferentially burnt-off, leading to the formation of partially ordered, defective graphene layers in the activated carbon [113].

In the electric double layer capacitors (EDLC's) the charge is accumulated at the electrode/electrolyte interface by the electrostatic forces of attraction. For a practical device that can store large charge in small volume, the carbon materials employed for electrode fabrication should be of high specific surface area. It should be noted that there is no direct proportionality dependence of the capacitance measured on the specific surface area of the carbon material. Size constraints and hence all pores are acessible to adsorbate molecule (gaseous N_2 used for evaluating the specific surface area) may not be accessible to solvated anions and cations and in turn such pores do not contribute to the capacitance even though they contribute to the improved surface area. Thus, in addition to the specific surface area value, other parameters such as pore size distribution, surface wettability and surface functionality are critical for the performance as an electrode.
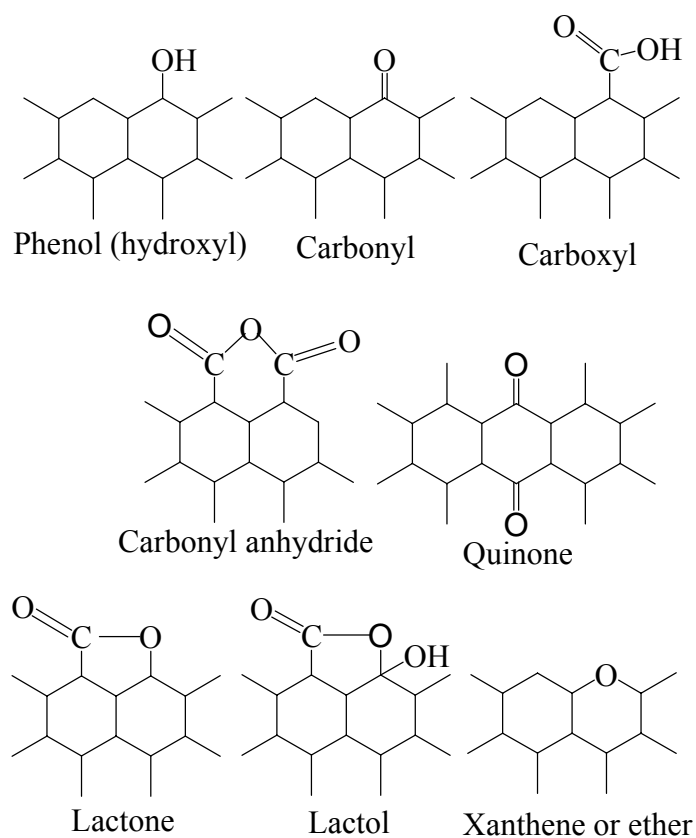
Scheme 3. Schematic representation of oxygen surface functional groups on the surface of carbon material (reproduced from ref. 114)

Common oxygen surface functional groups present on the surface of carbon materials, in general, are shown in scheme 3.

Kierzek *at al*., [113] have activated coal sample (highly volatile bituminous coal) with KOH. The resulting activated carbon material showed a specific surface area value of 3150 m^2/g and a total pore volume of 1.612 cm^2/g. The activated carbon material when evaluated for capacitor applications showed excellent performance as electrode material with a capacitance and specific capacitance values of 300 Fg^{-1} and 9.9μFcm^{-2} respectively. For comparison, the performance of the commercial activated carbon PX 21 was also evaluated for capacitor applications and the capacitance and specific capacitances values were only 240 Fg^{-1} and 8 μFcm^{-2}. Thus the activated carbon material produced from bituminous coal upon activation with KOH exhibited superior performance compared to commercial activated carbon PX 21. But all is not well with KOH activation. KOH activation creates carbon surface rich in oxygen functional groups. Such oxygen containing surface functional groups, even though advantageous for electrode applications in fuel cells when used as support of noble metals, retarded the durability (cycle life) of the capacitor electrodes by enhancing the capacity loss, leakage current and self - discharge. Kierzek *et al*., [113] have suggested the use of carbon materials with out surface functionality as far as EDLC applications are concerned.

Now there arises a question as to how the process of KOH activation of carbon materials can be tuned so that the advantage of obtaining high specific surface area is retained and at the same time the disadvantage (for EDLC application) of the inevitable creation of oxygen surface functional groups is eliminated. Yong bin Ji *et al*., [106] adopted micro wave treatment method, rather than the usual electric furnace method, to bring about reaction between KOH and activated carbon precursor (Meso carbon micro beads, MCMBs). From FT-IR studies, the researchers have found that KOH activated carbon materials obtained by microwave treatment contained remarkably low or negligible hydroxyl functional groups (identified by the band around 3430 cm^{-1} characteristic of the stretching vibration of –OH bond) unlike the sample heated in an electric furnace where in the creation of –OH functional groups is inevitable upon KOH activation. In addition to avoiding the formation of –OH groups, it was further noted that, the intensity of the bands arising from other oxygen containing functional groups,

such as carbonyl, lactonic, carboxylic and carboxylate moieties was lowered in the case of activated carbon materials from micro wave treatment compared to the samples obtained from heating in electric furnace.. Such carbon materials, where in the advantage of high specific surface area is retained in addition to getting rid of surface oxygen functional groups, are particularly beneficial for EDLC applications.

II. 1.2. NaOH as activating agent

The main cost of the production of activated carbon lies in the consumption of activating agent. The activating agent that produces the highest specific surface area carbon material per unit weight is the most economical one. Activation by NaOH is less expensive and environmentally benign. Chemical activation process has an edge over physical activation. Relatively larger specific surface area values with enhanced micorporosity as well as narrow pore size distribution were obtained through chemical activation process.

Formation of metallic K or Na is inevitable, upon activation of carbon material with either KOH or NaOH. The general stoichiometric reaction between the activating agent and the carbon precursor is [115]:

$$6 \text{ MOH} + 2 \text{ C} \longrightarrow 2 \text{ M} + 3 \text{ H}_2 + 2 \text{ M}_2\text{CO}_3$$

where M = Na or K
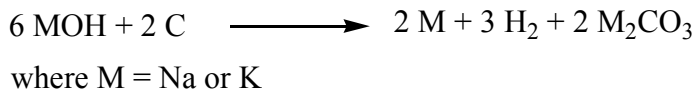
The striking difference between the activation process by NaOH and KOH is that atomic species, K, formed *in situ* during KOH activation intercalates between the grapheme layers of the carbon crystallite. Such intercalation is more pronounced and predominant in the case of well ordered graphitic carbon materials. On the contrary, NaOH is an effective activating agent for disordered carbon materials. There is hardly any evidence for the intercalation of Na with carbon. The activation process with NaOH proceeds through a surface reaction where highly defective sites are present. Formation of alkali metal carbonates and their subsequent decomposition to evolve CO and CO_2 at higher reaction temperatures (> 1073 K) are common features to activation by both NaOH and KOH. The evolution of gases like CO and CO_2 also occur by the process of

devolatilization of the carbon precursor (lignocellulosic materials and coals with high volatile content).

Ru-Long Tseng [116] has compared the NaOH activation process of char to that of fermentation of flour used for preparing cake. The generation of carbon materials with huge variation in the specific surface area values (113 to 1887 m^2/g) was likened to the preparation of loose cakes of different porosities from the same quantity of the flour. The flour used was analogous to the char empolyed for activation where as the final cake prepared (lose and well fermented) was analogous to the final activated carbon.

From the studies on the effect of NaOH/Char wt/wt.% ratio, during the activation process, on the textural properties (specific surface area and pore volume) and surface morphology (SEM studies) Ru – Long Tseng proposed a two step activation mechanism involved in the generation of carbon materials by NaOH activation. It was observed that when the NaOH : Char (carbon precursor) ratios were in the range of 0 – 1, the specific surface area of the samples decreased from 290 to 113 m^2/g. This is regarded as stage I of the activation process and was attributed to surface pyrolysis. When the NaOH/char (wt./wt.%) ratio is in the range of 2-4, an increasing trend in the surface area values (from 1478 to 1887 m^2/g) was observed. It should be noted that when the wt./wt.% ratio (NaOH/char) was changed from 1 to 2, an order of magnitude increment in specific surface area values (from 113 to 1478 m^2/g) was observed. This is regarded as stage II of the activation process and was attributed to the etching and swelling processes.

Thus the stage I of the NaOH activation process can be likened to the preparation of a dense cake from a not well fermented flour where as the stage II of the process of activation can be likened to the loose cake prepared from well fermented flour. The huge increase in specific surface area as well as porosity was attributed to the oxygen loss ratio (the ratio of weight loss of a certain element (O or C or H) in the char upon activation to the weight of that element in the char before activation).

Ru-Ling Tseng [116] has proposed the following reactions for elucidating the NaOH activation process.

$$4\,NaOH + C \longleftrightarrow 4\,Na + CO_2 + 2\,H_2O \quad \text{........................ (1)}$$
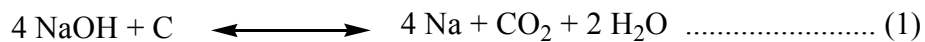
Na produced in reaction (1) is oxidized to Na_2O and subsequently hydrated to NaOH.

$$2\ Na \xrightarrow{\text{Oxidation}} Na_2O \xrightarrow{\text{Hydration}} NaOH \ \text{............ (2)}$$
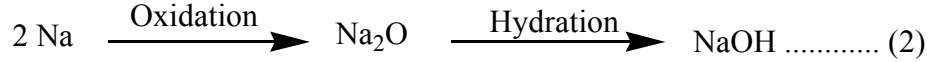
Lillo – Rodenas *et al.*, [115] have shown that the process of chemical activation of anthracite coal and NaOH comprises of the reaction between carbon and NaOH with the reaction products being metal carbonate, metal compound and hydrogen. Based on the observations the following reaction was proposed (3).

$$6\ NaOH + 2\ C \longleftrightarrow 2\ Na + 2\ Na_2CO_3 + 3\ H_2 \ \text{.......(3)}$$

If reaction (3) alone were to be operative, the observed oxygen loss ratio cold not be accounted. To account for the observed oxygen loss ratio (between the char and the activated carbon), it was proposed that the elemental Na formed in (3) reacts with oxygen of the char to form Na_2O as shown in reaction (2).

But reaction (2) is an over all reaction during the process of activation which is insufficient to provide the detailed mechanism of the activation process. In order to delve deep in to the reactions occurring between carbon and hydroxide during the activation process, Lillo – Rodenas *et al.*, [115] have activated coals of different ranks, namely, lignite, sub bituminous and anthracite using NaOH. The process of activation, simulated in a TPD instrument is monitored by the evolution of H_2 which is an indication of the beginning of the reaction between solid carbon and the activating agent. The evolution of H_2 is monitered by mass spectrometer. An analogy was drawn between carbon-air reaction and carbon-NaOH reaction. The order of reactivity between carbon and air (lignite > sub bituminous > anthracite) and carbon and NaOH (temperature of beginning of reaction monitored by the first evolution of H_2) were found to be same. It was observed that the beginning of the reaction was dependent on the reactivity between the carbon precursor (lignite, sub-bituminous and anthracite) as well as the activating agent used (NaOH or KOH). A decrease in the amount of H_2 evolution is observed with an increase in the rank (i.e., decrease in reactivity of carbon towards the activating agent). Also the percentage reactivity of the carbon with the activating agent decreased as the coal rank is increased. The carbon was removed from the solid coal as sodium carbonate. But no evolution of either CO or CO_2 is observed at a reaction temperature below 1023 K. Only H_2 evolution was observed. Probably at higher reaction temperatures, the Na_2CO_3 formed in (3) gets decomposed to release CO_2 and CO.

Lillo-Rodenas *et al.,* [115] have attributed the evolution of hydrogen to the conversion of hydroxide as observed in reaction (3). This is contrary to the proposal of Yasumasa Yamashita and Koji Ouchi [117] who have attributed the hydrogen evolution to the dehydrogenation of the active methylene groups (4) as well as the aromatic rings (5) resulting from the addition of –ONa groups in the presence of NaOH.

$$CH_2 + NaOH \longrightarrow H_2 + CH-O-Na$$

.... (4)

.... (5)
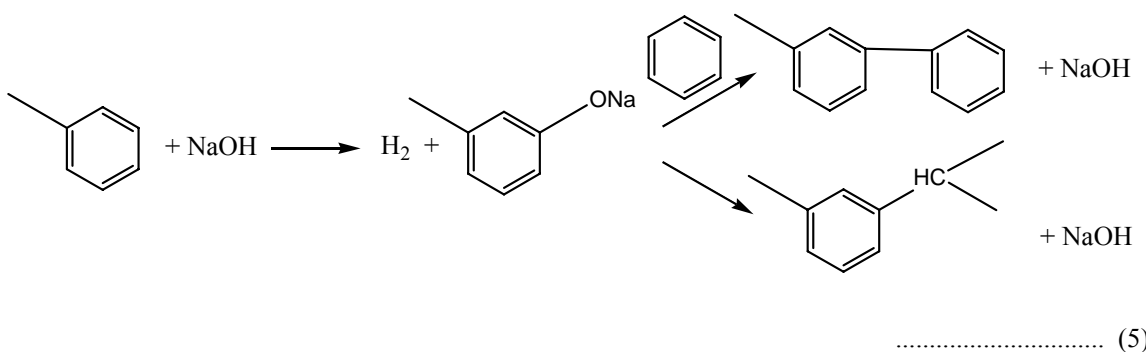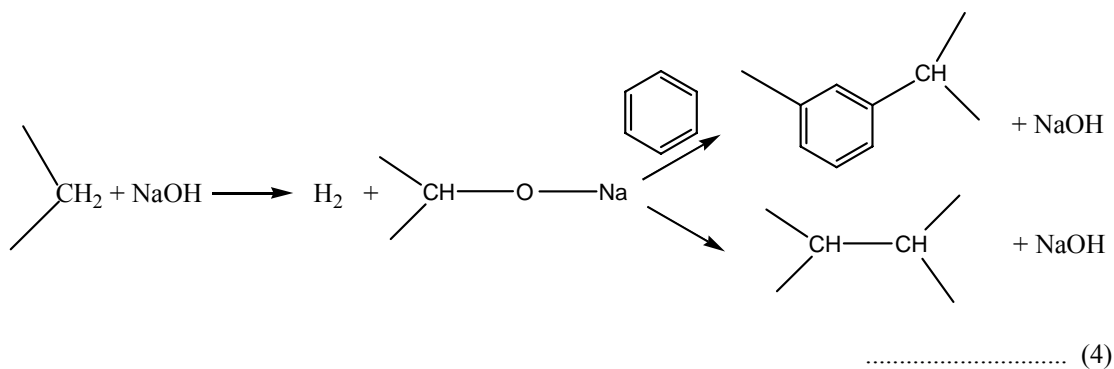
Jair C. C. Freitas *et al.,* [118] through ^{23}Na MAS NMR studies on the sodium species present in the activated carbon material produced from rice hull char by NaOH activation confirmed the presence of Na^+ ions bonded to oxygen surface functional groups present at the edges of the graphene planes with in the carbon pore network. This result has authenticated the reactions (4) and (5) based on the formation of surface –ONa groups proposed by Yasumasa Yamashita and Koji Ouchi [117].

The nature of bonding between the carbon and metallic species (ions) such as Li, Na, K, Fe and Mn which are commonly present in the activated carbon materials is not well understood. This type of information is particularly important because of the significant role played by the metallic species in the electro chemical reactions when the carbon material is employed. In order to gain an understanding of the nature of bonding between the Na species generated in the carbon material upon NaOH action and the

carbon surface, Jair C. C. Freitas *et al.,* [118] have carried out ^{23}Na MAS NMR studies on the activated carbon sample.

The activated carbon material was prepared from rice hull char activated with NaOH at 1073 K with a NaOH/carbon precursor (wt./wt.%) ratio of 3:1. The mixture of carbon precursor along with the decomposition products (carbonates and silicates) of the activated agent obtained after activation process was washed thoroughly with distilled water to remove the carbonates and silicates. In spite of washing with water, Na^+ ions remain bound to the carbon surface. The nature of such surface bound Na^+ species was examined by ^{23}Na MAS NMR. From the values of chemical shift and the quadrupolar coupling constant corresponding to the Na moieties, useful information on the chemical environment of Na^+ in the porous network of carbon material was deduced. Aqueous solution of NaCl was used as primary reference or the powdered NaCl was used as a secondary reference.
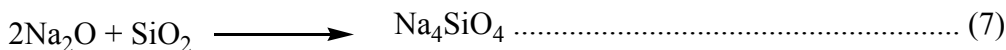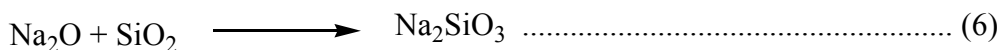
The resonance signal observed in the ^{23}Na MAS NMR spectrum is associated with the central transition of (1/2 ↔ -1/2) of the quadrupolar split energy levels associated with the multiplet of [23]Na nucleus.

The observed chemical shift value is − 2.8 ppm. The following aspects are considered logically to assign a particular chemical environment to the signal with a chemical shift of − 2.8 ppm. The Na-O bond distance in several inorganic and organic sodium compounds is 2.4 Å. The mean pore size of the carbon material produced is 16 Å. If sodium atoms were to be intercalated between the grapheme planes forming intercalation compounds, large positive shift in the chemical shift values is expected. But the observed chemical shift value is − 2.8 ppm ruling out the possibility of the presence of metallic Na. Also the formation of intercalation compounds by Na is less likely compared to either K or Cs (heavier alkaline elements than Na). Even direct interaction between the diamagnetic Na^+ and π electron cloud of phenyl rings is expected to result in large up field shift which was not the case. Thus the observed chemical shift value of − 2.8 indicates the bonding of Na^+ through oxygen functional groups at the edges of the graphene planes.

Several functional groups like carboxylic, carbonyl, phenol, ether and lactone are present at the edges of the graphene lamella in the carbon material.   The observed

chemical shift value of – 2.8 ppm was attributable to the presence of Na^+ ions bonded to oxygenated groups on the carbon surface. Presence or absence of moisture has not affected the δ_{iso} value (observed isotropic chemical shift value) but has a strong influence on the values of quadrupolar coupling constant. Presence of moisture increased the symmetry around Na sites there by decreasing the value of quadrupolar coupling constant (from 1.8 to 1.2 MHz). Upon dehydration or drying of the sample, larger quadrupolar coupling constant value (1.8 MHz) is observed indicating distorted environment around the Na^+ ions.

Jair C C Freitas *et al.*, [119] have investigated the NaOH activation process of rice hull char by analyzing the chemical nature of the reaction products formed during activation. A decrease in the ash content is observed upon activation of the char and subsequent washing of the activated material with water. This is indicative of the involvement of inorganic matter (particularly silica) in the process of activation by NaOH and the subsequent formation of water soluble sodium silicates resulting in the decrease in the ash content upon activation and water washing. In rice hulls silicon is present as amorphous hydrated silica. Some part of the silicon species were found to be chemically bonded to the functional groups of carbon. Such silicon plays a prominent role during the activation process. The following reactions can be proposed to account for the formation of water soluble sodium silicates (based on XRD and ^{23}Na MAS NMR studies) by the reactions between silica and the Na containing species (Na_2O) generated in situ during activation process.

$$Na_2O + SiO_2 \longrightarrow Na_2SiO_3 \quad\text{...} (6)$$

$$2Na_2O + SiO_2 \longrightarrow Na_4SiO_4 \quad\text{...} (7)$$

$$Na_2O + SiO_2 + H_2O \longrightarrow Na_2SiO_3.6\,H_2O \text{ (hydrated species) ....} (8)$$

$Na_2SiO_3\,6H_2O$ is found in the activated carbon when the activation temperature is 973 K; when the activation temperature is increased to 1073 K, compounds such as Na_2SiO_3 and Na_4SiO_4 were observed in the activated carbon material (prior to washing with water) authenticating reactions (6, 7 and 8). No traces of sodium silicates but only sodium carbonate was observed in the activated carbon (before water washing) when the activation process was carried out with the char which was treated *a prioi* with HF (for

removing the silica present in the char). Thus acid treatment is an effective process to remove silica completely there by preventing the formation of sodium silicate materials during the activation process with NaOH. The formation of Na_2CO_3 in abundance during activation, as shown in (3), is an indication of the effectiveness of the activation process.

The S_{BET} values of the activated carbon materials produced from char with silica and with out silica (HF treated char) are 450 and 1400 m^2/g. Thus the presence of silica in the char has retarded the effectiveness of the activation process by competing with carbon for the activating agent (NaOH) to form sodium silicates. As a result, the availability of NaOH for reaction with carbon decreases and reaction (3) is hindered by the presence of silica in the char. Removal of silica associated with carbon matrix by acid treatment of the char, results in the generation of incipient porosity even before the beginning of the activation with NaOH.

Formation of inorganic material *in situ* during the NaOH activation process was inferred from the thermogravimetric curves when the ash content of the activated carbon was found to be greater than that of the char (HF treated to remove silica prior to activation). Such inorganic material was retained in the activated carbon material even after washing with either water or HNO_3. The only possible inorganic material formed during NaOH activation process is Na-containing species. In fact from spectrophotmetric analysis of the ash from the activated carbon, the presence of elemental Na was identified. The important questions to be addressed are:

(i)   What is the chemical nature and environment of such Na containing species?

(ii)   How are such Na containing species bound to the carbon matrix?

Jair C C Freitas *et al*., [119] from their ^{23}Na MAS NMR studies, have given a detailed account of the nature and chemical environment of Na containing species formed during NaOH activation and retained in the activated carbon matrix even after washing with either water or HNO_3. The spectra were recorded with a rotor having a speed of 6.0 kHz with 4000 transients at a frequency of 105.7 MHz and at a magnetic field strength of 9.4 T. Aqueous NaCl (0.1 M) was used as standard. ^{23}Na MAS NMR spectra were recorded on the activated carbon materials prior to washing with water as well as after

washing with water so as to examine the details of both water soluble and insoluble Na containing inorganic compounds formed *in situ* during the process of activation.
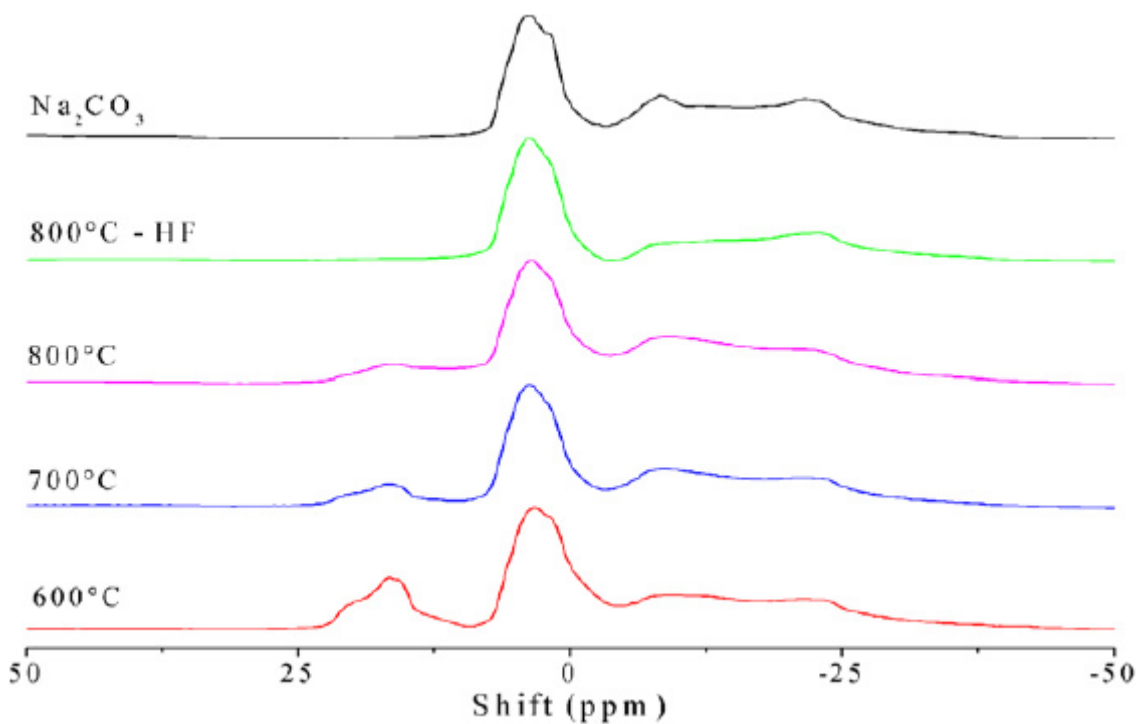
Fig. 5. ^{23}Na MAS NMR spectra of activated carbon materials *prior to water washing* (prepared from rice hull char through NaOH activation) [reproduced from ref. 5]

The ^{23}Na MAS NMR spectra recorded on non washed activated carbon materials are shown in Fig. 5. The spectra marked as 873 K, 973 K and 1073 K corresponds to the activated carbon material obtained from the rice hull char activated at 873, 973 and 1073 K respectively. The spectra labeled as 1073 K – HF corresponds to the activated carbon produced from the char which was treated with HF prior to activation to remove silica followed by activation at 1073 K. For comparison the ^{23}Na MAS NMR spectrum of Na$_2$CO$_3$ is also shown in the same plot. In all the cases, the unwashed activated carbon material showed features characteristic of Na$_2$CO$_3$ (broad bands extending between 10 to − 38 ppm). This implies that irrespective of the presence or absence of silica in the char and also irrespective of the temperature of activation (from 873 to 1073 K), the formation of Na$_2$CO$_3$ is inevitable during activaton by NaOH as represented in (3). In addition to the presence of Na$_2$CO$_3$, the spectra labelled as 873, 973 and 1073 K showed an

additional resonance signal at 16 ppm attributable to the crystalline Na_2SiO_3 authenticating reaction (6). Another interesting feature observed in the spectra shown in Fig. 5. is that with an increase in the activation temperature from 873 to 1073 through 973 K, the intensity of resonance signal at - 16 ppm (crystalline Na_2SiO_3) decreased with a concomitant increase in the resonance signal at - 10 ppm (new (Na, Si)- based product). This observation is a result of the gradual consumption of Na_2SiO_3 by the reaction with Na_2CO_3 to form a new (Na, Si)- based compound.

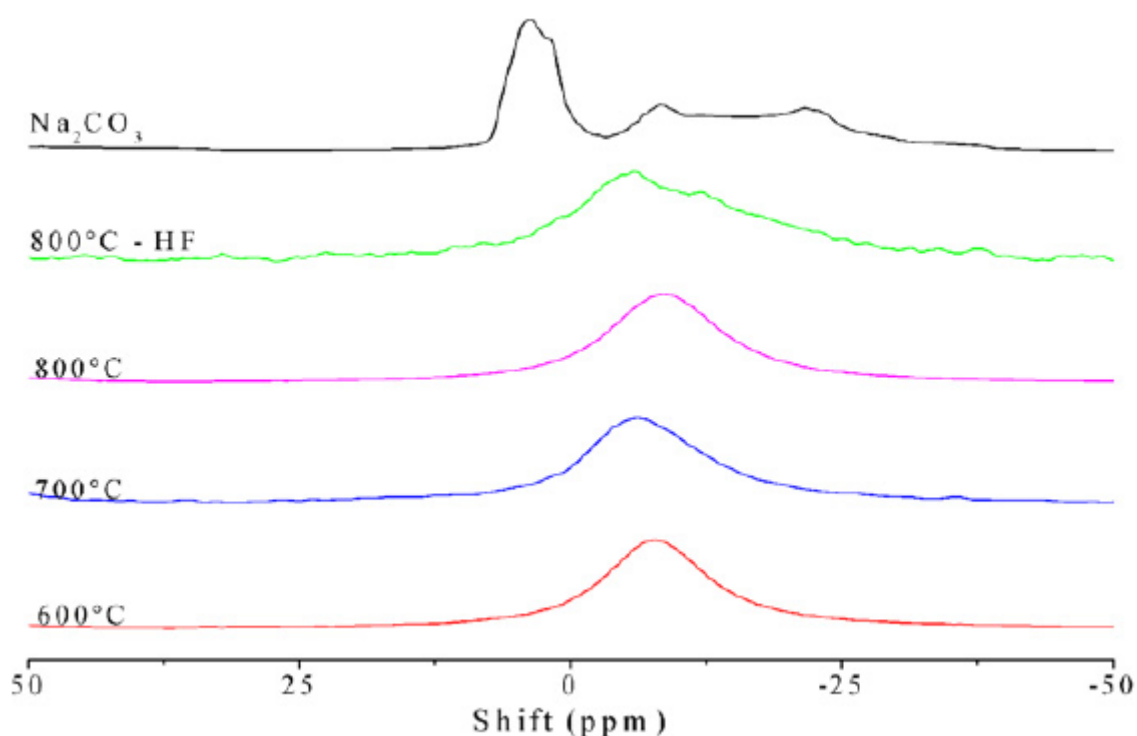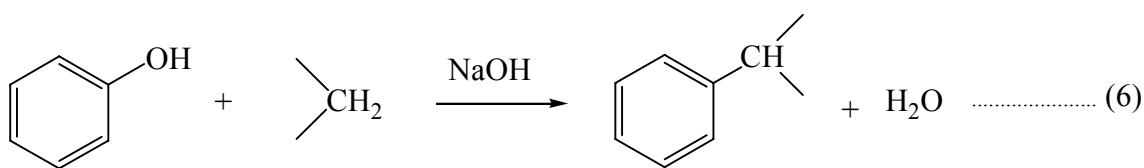Fig. 6. ^{23}Na MAS NMR spectra of activated carbon materials *after water washing* (prepared from rice hull char through NaOH activation) [reproduced from ref. 5]

The ^{23}Na MAS NMR spectra of activated carbon material after washing with H_2O are shown in Fig. 6. Striking differences in the ^{23}Na MAS NMR spectra were observed on washing the activated carbon with water (compare Figs. 5 and 6). No features characteristic of either sodium silicate or sodium carbonate are observed in the activated carbon material upon washing with water indicating the effectiveness of washing with water in removing sodium silicate and sodium carbonate species formed during the

process of activation.   Interestingly, the ^{23}Na MAS NMR spectra of water treated activated carbon consisted of a broad featureless resonance signal extending from 7 to - 30 ppm and centered around − 5 to − 10 ppm. Such features are characteristic of the presence of Na species bound to carbon surface through oxygen atoms at the edges of the aromatic lamella. Even though washing with water effectively removed silicates and carbonate of Na formed during NaOH activation, some amount of sodium remains bound to the carbon network through surface oxygen functional groups. In fact, the retention of Na in the activated carbon was more in the case of carbon material produced from char containing silica. The presence of Na in the activated carbon may be because of some chemical interaction between Si, Na and organic functionalities. In other words, the decreased Na content in the case of activated carbon material prepared from char with out silica (silica removed by HF treatment) is attributed to the higher specific surface of the activated carbon material obtained from such a char making the water washing step effective to remove more Na.

The amount of H_2 evolved during the activation of lignite, sub-bituminous and anthracite with NaOH were 22, 759, 13, 563 and 3, 860 µmol/g of the carbon precursor – NaOH mixture. Even though Lillo-Rodenas *et al*., [115] have estimated the evolution of the total amount of H_2 (22, 759 µg/mol during lignite activation with NaOH) from reaction (3) alone but this may not be true. Yasumasa Yamahita and Koji Ouchi [117] observed the evolution of significant amount of H_2O and a little of H_2 during the NaOH activation of low rank coal. The evolution of H_2O (6) was attributed to the reaction between the hydrogen atoms of the active methylene group and the polar –OH groups which are, in general, present in abundance in low rank coal.

$$\text{(structures)} \quad + \quad \text{CH}_2 \quad \xrightarrow{\text{NaOH}} \quad \text{(structures)} \quad + \quad H_2O \quad \text{...............} \quad (6)$$

There is a possibility that under the high temperature of activation, the steam generated (H_2O) (1 and 6) may react with metallic Na, formed *in situ* (1 and 3), and the water may split to form H_2 and Na_2O as shown in (7).

$$2\,Na + H_2O \longrightarrow Na_2O + H_2 \quad \text{..} \quad (7)$$
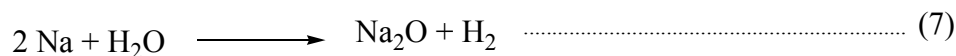
Thus the hydrogen evolved during activation process is contributed from steps (3), (4), (5) and (7).

There is a need for pursuing isotope labeling studies to resolve the ambiguity related to the hydrogen evolution reaction during the process of NaOH activation. Also there is the possibility of developing the reaction between carbon (low rank coal) and alkali hydroxides as a new method for the production of hydrogen gas.

The effectiveness of the activation process is not only depended upon the nature of the carbon precursor but also on the activating agent used. Greater the reactivity between the carbon precursor and the activating agent, lower is the temperature of the beginning of the reaction (evolution of H_2 is observed at a lower temperature). When KOH is used as activating agent, the reaction between carbon and activating agent started at a relatively lower temperatures compared to NaOH indicating that KOH is more reactive with carbon compared to NaOH.

Hye – Ryun Hwang *et al*., [108] have found KOH to be better activating agent than NaOH. The improved performance of KOH was attributed to the greater ionic radius of K^+ (0.2666 nm) compared to the ionic radius of Na^+ (0.190 nm). The researchers have systematically analyzed the variation in the performance of KOH and NaOH as activating agents by employing sewage sludge and coal tar pitch as precursors to carbon material. Under identical conditions of activation temperature (1073 K), activation time (1.5 h) and activating agent concentration (1 mol/l) the specific surface area values, total pore volume values and the pore size values of the samples from KOH and NaOH activation process were found to be 450 and 381 m^2/g, 0.394 and 0.37 cm^3/g and 38.72 and 36.72 Å respectively. Thus KOH activation resulted in carbon materials with higher specific surface area values, pore volume values and pore diameter values compared to the samples activated with NaOH indiacting the significance of the ionic radius of the cation of the activating agent on the textural properties of the carbon material.

Sodium carbonate, metallic sodium, hydrogen, carbon monoxide and carbon dioxide were known to be formed during activation of carbon precursor with NaOH.

Alejandro Robau – Sanchuez *et al*., [120] have observed, for the first time, the formation of cyanide species (NaCN, Na_2CN_2), carbide species (Na_2C_2) and acetylene (C_2H_2) during the process of NaOH activation. Upon washing the activated carbon with

water the filtrate contained NaCN. For the formation of cyanide, it is essential that carbon and nitrogen should react. Two possibilities exist for the reaction between carbon and nitrogen. This is because of the two different sources of nitrogen present in the activation process: one source of nitrogen is the structural nitrogen inherently present in the char structure (0.37 wt.%) and the other source of nitrogen being the gaseous nitrogen used as reaction medium or purging gas. It is peculiar that gaseous nitrogen takes part in the activation process leading to the formation of NaCN. Experiments of Alejandro Robau – Sanchez *et al.*, [120] have ascertained the participation of the structural nitrogen present in the char as well as the gaseous nitrogen present in the medium of activation. Such revelations were in fact new to the chemical activation process. To confirm the authenticity of the participation of the gaseous nitrogen in the cyanide forming reactions the activation process was carried out in Ar as well as N_2 atmospheres. NaCN formation was observed even in the case of Ar environment and in this case the nitrogen for the formation of cyanide is contributed solely by the structural nitrogen of the char. Interestingly, the amount of NaCN formed when the activation process is carried out in N_2 atmosphere is 6 times more than the amount of NaCN formed in Ar environment establishing the participation of gas phase N_2 in the activation process.

Also during the water washing step of the activated carbon, the gaseous products evolved were analyzed by mass spectrometry. Surprisingly a signal at m/z value of 26 corresponding to acetylene evolution was observed. The immediate implication of the release of acetylene during water washing is that sodium carbide, Na_2C_2, could be a reaction product in the chemical system NaOH – C - N_2. The following reaction was put forward to account for the evolution of acetylene upon water treatment of activated carbon.

$$Na_2C_2 + 2\ H_2O(g) \rightleftharpoons 2\ NaOH_{(l)} + C_2H_{2(g)} \quad \Delta G = -24.48\ kCal\ at\ 25\ °C$$
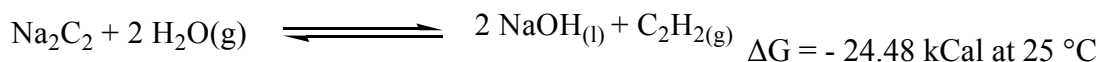
Giving allowance for the formation of reaction products like cyanide and carbide and also considering the thermodymic feasibility of the occurance of possible chemical reactions (Fig. 7), Alejandro Robau – Sanchez *et al.,* offered the following reaction mechanism to expain the NaOH activation process.
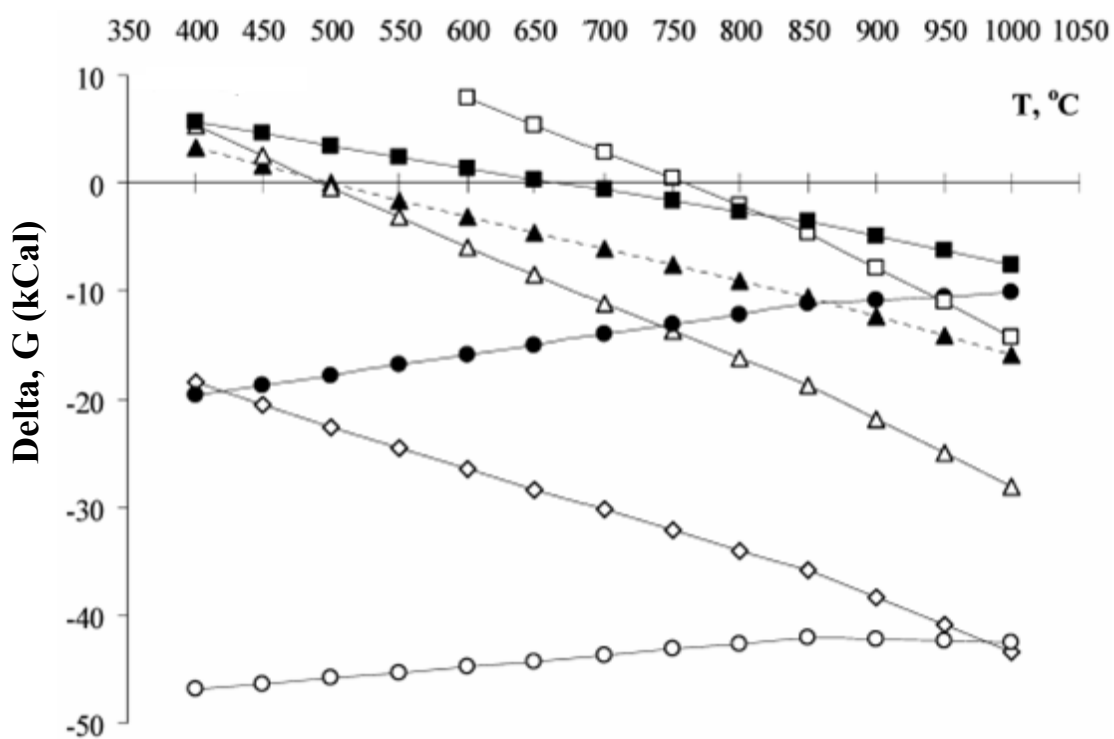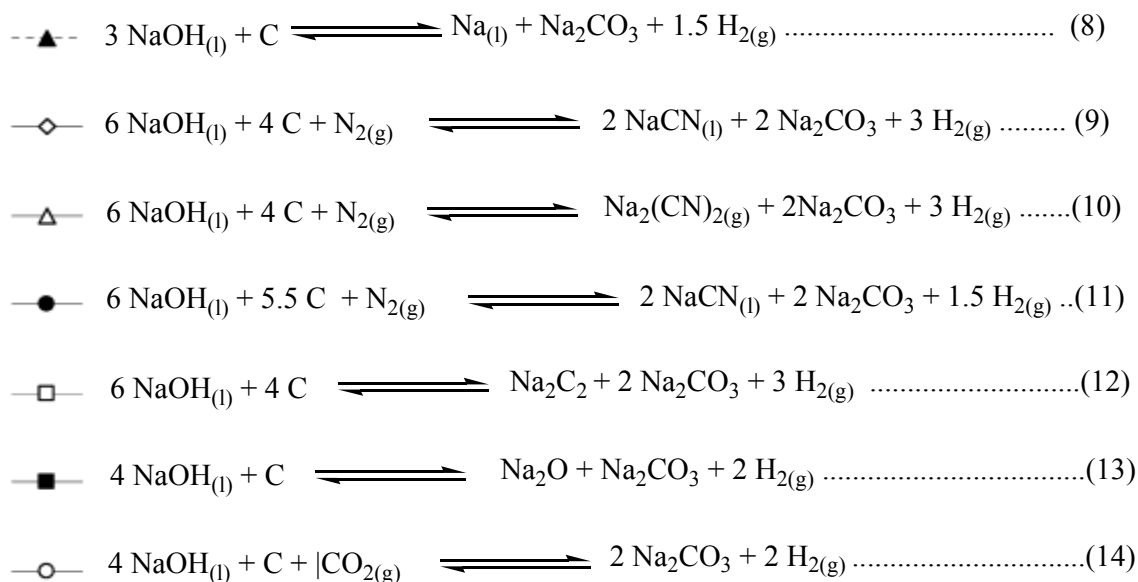
$--\blacktriangle--$ $3\ NaOH_{(l)} + C \rightleftharpoons Na_{(l)} + Na_2CO_3 + 1.5\ H_{2(g)}$ .... (8)

$--\diamond--$ $6\ NaOH_{(l)} + 4\ C + N_{2(g)} \rightleftharpoons 2\ NaCN_{(l)} + 2\ Na_2CO_3 + 3\ H_{2(g)}$ .... (9)

$--\triangle--$ $6\ NaOH_{(l)} + 4\ C + N_{2(g)} \rightleftharpoons Na_2(CN)_{2(g)} + 2Na_2CO_3 + 3\ H_{2(g)}$ ....(10)

$--\bullet--$ $6\ NaOH_{(l)} + 5.5\ C + N_{2(g)} \rightleftharpoons 2\ NaCN_{(l)} + 2\ Na_2CO_3 + 1.5\ H_{2(g)}$ ..(11)

$--\square--$ $6\ NaOH_{(l)} + 4\ C \rightleftharpoons Na_2C_2 + 2\ Na_2CO_3 + 3\ H_{2(g)}$ ....(12)

$--\blacksquare--$ $4\ NaOH_{(l)} + C \rightleftharpoons Na_2O + Na_2CO_3 + 2\ H_{2(g)}$ ....(13)

$--\circ--$ $4\ NaOH_{(l)} + C + |CO_{2(g)} \rightleftharpoons 2\ Na_2CO_3 + 2\ H_{2(g)}$ ....(14)

Fig. 7. Gibbs free energy changes for the primary reactions of NaOH − C − N₂ system (reproduced from ref. 120)

Activation medium (purging gas, N_2 or CO_2 or H_2O) also influences the textural properties of the activated carbon. The effect of atmosphere of the reaction on the NaOH activation process was evaluated by considering three different atmospheres, namely, CO_2, H_2O and N_2. Use of N_2 medium during NaOH activation yielded positive results. Flow rate of N_2 gas is an important factor influencing the textural properties of the carbon materials. As the flow rate of the N_2 gas increased, improvement in the porosity was observed. This is because, with an increase in the flow rate of carrier gas or purging gas, the evolved gases (during the activation process, namely, CO, CO_2, Na_2CN_2) are removed (flushed out) at a faster rate. As a result the activation reaction is shifted towards forward direction forming more products and hence improving the effectiveness of the activation process. NaOH activation process was retarded in CO_2 atmosphere. The pore development process was hindered in CO_2 environment because of the preferential carbonation reaction between CO_2 and NaOH rather than the CO_2 – C and NaOH – C reactions. NaOH activation process in the presence of steam resulted in carbon materials with good porosity. The improvement in the effectiveness of activation process is due to the combined effect of the hydroxyl – carbon and the steam – carbon reaction. Compared to CO_2 and steam, N_2 was found to be a good choice for the activation environment.

II. 2. Activation with Alkali Metal Carbonates:

Even though, the use of alkalimetal hydroxides like KOH and NaOH as activating agents offers the advantage of producing high specific surface area carbon materials, they (alkali metal hydroxides) are corrosive, hazardous and environmentally unfriendly. Use of alkali metal carbonates such as K_2CO_3 can be a substitute to the use of alkali metal hydroxides.

Kiyoshi Okada et al., [121] have evaluated the effect of the nature of activating agent (Li_2CO_3, Na_2CO_3, K_2CO_3, Rb_2CO_3, Cs_2CO_3) on the process of activation of carbon material produced from news paper waste. The textural properties (specific surface area values and specific pore volume values) were found to be a function of the size (radii) of the alkali metal cation. From Li to Cs through Na, K and Rb the physical properties,

namely, the atomic size, melting point and the basal spacing of the intermatallic compounds of alkali metals (C_nMe) vary systematically as shown in Table 1.

Table 1. Alkali metal atoms – Alteration in Physical Properties

| S. No.	Element	Atomic size (nm)	Melting point[a] (K)	Basal Spacing[b] (nm)
1	Li	0.314	891	0.374
2	Na	0.382	1124	0.460
3	K	0.470	1164	0.540
4	Rb	0.500	1110	0.565
5	Cs	0.544	Decomposes[c]	0.594

a. alkaline carbonate

b. Intercalation compounds, C_nMe (Me: alkaline metal), basal spacing of graphite is 0.335 nm

c. Melts with decomposition at 880 K [122]

Such a variation in physical properties of the alkali metal cation of the activating agent was found to have a profound effect on the textural properties of the activated carbon. Salts of K were found to act as better activating agents than others owing to the formation of atomic K during the activation process as shown in (1), which subsequently intercalates into the inter layers of adjacent hexagonal network plane of C atoms.

$$2\,C + K_2CO_3 \longrightarrow 2\,K + 3\,CO \quad \text{.......................................} \quad (1)$$
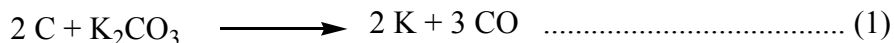
The adjacent graphene planes were separated because of the K intercalation. Even after removal of K, either by washing with H_2O or acid, the rearranged or disordered graphene sheets of the carbon crystallite cannot go back to their original position thus leaving pores and voids. This results in an activated carbon material with high porosity and specific surface area value.

Kiyoshi Okada *et al.,* [121] have examined the effect of cation size of the activating on textural properties of the resulting carbon materials. The specific surface area values as well as the values of pore volume of the activated carbon materials obtained using different activating agents, namely, Li_2CO_3, Na_2CO_3, K_2CO_3, Rb_2CO_3 and

Cs_2CO_3 were 790, 610, 880, 1230, 1370 m^2/g and 0.64, 0.65, 0.58, 0.75 and 0.85 cm^3/g respectively when the process of activation is carried out at 1073 K for 2 h and at the activating agent to carbon precursor (wt./wt. %) ratio of 1. When the activation process was carried out at 1173 K with other conditions being similar as in the previous case the specific surface area and the pore volume values were 680, 790, 1740, 1200, 1310 m^2/g and 0.53, 0.78, 1.15, 0.77 and 0.80cm^3/g. The size of the cation of the activating agent has a significant effect on the textural pore volume and specific surface area (S_{BET}) of carbon materials. Even though the S_{BET} values varied widely, the researchers have classified the activating agents into three groups based on the S_{BET} values obtainable. Activated carbon materials produced using activating agents with smaller cationic size (Li_2CO_3 and Na_2CO_3) possessed S_{BET} values lower than 1000 m^2/g and these are termed as group I activating agents. Activating agents with larger cationic size (Rb_2CO_3 and Cs_2CO_3) yielded carbon materials with S_{BET} values greater than 1000 m^2/g and such activating agents were classified as belonging group II. With either group I or group II activating agents there was only little variation in S_{BET} values with increase in temperature from 1023 to 1173 K. K_2CO_3 showed a special behaviour and is being termed as belonging to group III. There was a significant variation in the S_{BET} value as the temperature is varied from 1023 to 1173 K when K_2CO_3 is used as an activating agent with a maximum S_{BET} value of 1740 m^2/g (obtainable at 1173 K) which has been the largest of all the activated carbon materials obtained from various activating agents. For comparison, the carbon precursor was activated by physical means using steam as activating agent in N_2 atmosphere at 1123 K for 2 h. It was observed that the S_{BET} value (1086 m^2/g) and the specific pore volume, Vp, (1.01 cm^3/g) values were lower than those carbon materials obtained by chemical activation with K_2CO_3. A strong correlation between specific surface area value and the product yield were observed (in the physical activation process) with the maximum value of S_{BET} value obtainable when the yield was 10 %. The unique advantage of the physical activation process is the retention of the original microstructure of the carbon precursor in the final activated carbon which is not possible in chemical activation process. Another important distinguishing feature between physical and chemical activation methods is that the physical activation process

comprises of surface activation where in surface erosion predominates over the pore formation reaction.

Larger the cationic size (Rb, Cs) of the activating agent larger is the specific surface area value and smaller the cationic size of the activating agent smaller is the specific surface area value. Thus the size of the alkali metal cation is an important parameter determining the effectiveness of activating agent in the chemical activation process.

Kiyoshi Okada *et al*., [121] have optimized the method of preparation of activated carbon through chemical activation and found that single step activation involving direct impregnation of the carbon precursor with activating agent and subsequent activation in N_2 atmosphere in an electric furnace at 1173 K for 2 h (method i) yielded better results than other methods of preparation. Apart from the above mentioned method, another three methods of preparation were evaluated, namely: method (ii) is a two step activation process (oxidation – activation) where in the waste news paper is oxidized in air at 523 and 573 K for 2 h and then the char obtained is activated as in method (i); method (iii) is again a two step activation process (carbonization – activation) where in the news paper waste is first carbonized at 773, 873 and 973 K in N_2 atmosphere for 2 h and the char thus obtained is then activated as in method (i); method (iv) is a three step activation process (oxidation – carbonization – activation) involving the process of oxidation as in method (ii) and the char thus obtained in carbonized as in method (iii) and the carbonized product thus obtained is activated as in method (i). After thorough evaluation of the textural properties, it was observed that direct single step activation with out any oxidation or carbonization is the best method yielding activated carbon material with higher specific surface area values and pore volumes.

The chemical nature of the activated carbon surface (produced from news paper waste by K_2CO_3 activation at 1173 K for 2 h in N_2 atmosphere) was examined by X - ray photo electron spectroscopy. The nature of the surface functional groups was studied by deconvolution of the X-ray excited Auger electron Spectroscopy.

The C 1s XPS spectrum of activated carbon material possessing a specific surface area value of 1740 m^2/g from K_2CO_3 activation carried out at 1173 K is shown in Fig.8.

A broad intense peak at a binding energy value of 283.9 eV attributable to the C-C bond of graphitic carbon is observed in the spectrum. Tailing of the spectrum towards higher binding energy values is observed. The spectrum was deconvoluted into several overlapping peaks as indicated in the figure. The attribution of binding energy values of each of the deconvoluted peaks to specific chemical bonds is shown in Table 2.
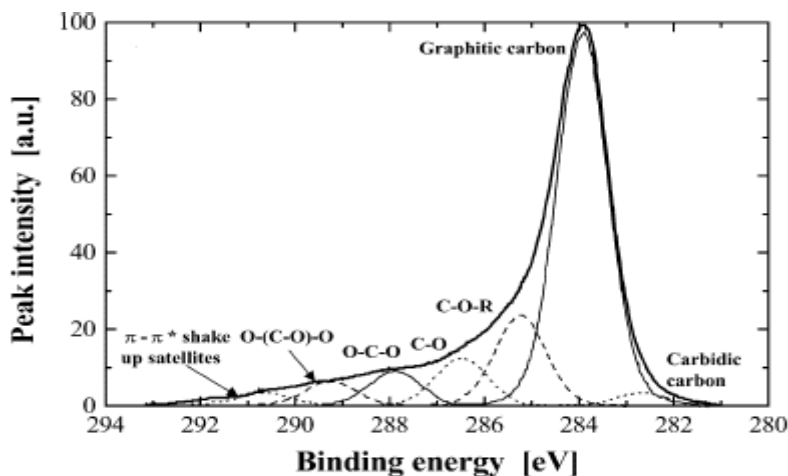
Fig. 8. X-ray photoelectron spectrum of C 1s level of activated carbon prepared from waste news paper using K_2CO_3 as activating agent at 1173 K at a carbon precursor to activating agent wt./wt.% ratio of 1:1 in N_2 atmosphere {reproduced from ref. 121)

Table 2. Assignment of binding energy values of the peaks in the C 1s XPS spectrum to the surface chemical bonds in activated carbon from news paper waste

Peak No.	B. E. (eV)	Assignment
1	282.5	C-Si bond of carbidic carbon
2	284.0	C-C bond of graphitic carbon
3	285.5	C-O bond of the C-O-R group
4	286.8	C-O bond of the C=O group
5	288.3	C-O bond of the O-C-O group
6	289.7	C-O bond of the O-(C-O)-O group
7	291.1	π-π* shake-up satellites of the benzene ring

David A Fox and Alfred H White [123] have quantitatively estimated the amount of CO and Na formed during the reaction between coke and sodium carbonate carried out in air at 1273 K. Metallic Na and CO were found to be the reaction products. Quantitative estimation of the amount of Na and CO formed as a consequence of reaction between coke and Na_2CO_3 was carried out. The ratio of moles of CO evolved to the atoms of Na formed was found to be approximately 1.512 (Moles of CO/Atoms of Na = 3.03/2.00). The following reaction (2) was proposed accounting for the quantitative amounts of products formed:

$$Na_2CO_3 + 2\,C \rightleftharpoons 3\,CO + 2\,Na \quad .... (2)$$

In fact, David A Fox and Alfred H White [123] have adopted a simple but reliable method for the quantitative estimation of the reaction products of the gasification of coke in presence of Na_2CO_3 and there by deduced the reaction path way. In the typical method of estimation, the CO evolved during the gasification reaction is oxidized by the air stream to CO_2. The CO_2 thus formed is passed through caustic potash solution (KOH) to form K_2CO_3. The amount of CO_2 evolved was estimated by titrating the caustic potash solution containing the dissolved CO_2 (leading to K_2CO_3 formation) with H_2SO_4 using phenolphthalein and methyl orange indicators. The difference between the phenolphthalein and methyl orange end points in potash solution yielded the amount of carbonate formed. The carbonate determination was then calculated back to moles of CO. The Na vapours formed were known to condense instantly on the cooler parts of the reaction chamber. The Na metal thus formed is subsequently oxidized to Na_2O (as the gasification reaction is being carried out in air stream). To estimate the amount of Na formed in the process, the product, Na_2O is agitated with water and then titrated for alkali (NaOH) with H_2SO_4 in the presence of methyl orange indicator. The amount of H_2SO_4 consumed for the neutralization of the alkali corresponds to the amount of Na_2O formed from the Na metal during the gasification reaction.

The slightly higher value (1.512) of the ratio of moles of CO to the atoms of Na compared to the theoretical value (1.500) corresponding to reaction (2) is attributed to the small amount of the thermal dissociation of sodium carbonate into non volatile sodium

peroxide and carbon dioxide. The CO_2 evolved from the thermal dissociation of Na_2CO_3 and the CO_2 formed from the oxidation of CO (from the carbothermal reduction of Na_2CO_3 by coke (2)) are not distinguishable as both of them are transformed to carbonate species by passing through caustic potash solution (KOH) during the process of quantitative estimation by titrimetry. Thus the CO_2 released from the thermal dissociation of Na_2CO_3 as shown in (3) is the cause of the experimentally observed slightly higher value (1.512) of the ratio of number of moles of CO to the number of atoms of Na.

$$Na_2CO_3 \rightleftharpoons Na_2O + CO_2 \quad \text{.. (3)}$$
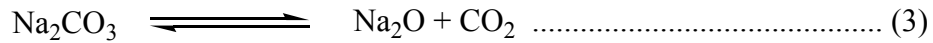
In fact, reaction (3) is not as insignificant as David A Fox and Alfred H White [123] have assumed. Reaction (3) plays a key role not only in the early (at a lower temperature, ≈ 500 K) evolution of CO_2 but also facilitates the formation of well dispersed active sites (metal oxide clusters) on the char at a stage where the structural rearrangement of either the coal or the lignocellulosic material is at its incipient stage. Such highly dispersed metal oxide clusters act as gasification sites at high temperature of activation leading to the development of porosity [122]. Thus the important factor for the evolution of microporosity is the earlier evolution of CO_2 due to the thermal decomposition of alkali metal carbonate in the presence of carbon char and the subsequent formation of well dispersed metal oxide clusters which serve as activation sites.

In addition, as the gasification of coke with Na_2CO_3 was carried out in air, to know the nature of the reaction products formed and to subsequently arrive at a conclusive understanding on the mechanism of activation (2), David A Fox and Alfred H White [123] have grossly neglected the contribution of Na_2O formed in gasifying the char if the activation were to be carried out in inert atmosphere (which is the usual way) rather than in air.

Yasumasa Yamashita and Koji Ouchi [124] have activated 3, 5 dimethyl phenol – formaldehyde resin with NaOH where in Na_2CO_3 and Na_2O are formed in situ during the activation process. The researchers have observed the evolution of significant amount of CO. The evolution of CO was not solely attributed to the carbothermal reduction of Na_2CO_3 with carbon as proposed by David A Fox and Alfred H White [123] in (2) but

was also attributed to the equally possible carbothermal reduction of Na_2O as shown in (4).

$$Na_2O + C \longrightarrow 2\,Na + CO \text{ .... (4)}$$

Interestingly, Addoun *et al.,* [2] have found that the amount of CO released, measured by mass spectrometry during the Cs_2CO_3 activation of a low rank coal (Menouna (H)), is nearly equal to a sum of three times the amount of undecomposed Cs_2CO_3 according to reaction (2) and an equal amount of CO to that of the CO_2 formed during the thermal decomposition of Na_2CO_3 (3). This is so because, each mole of the undecomposed Cs_2CO_3 upon carbothermal reduction yields three moles of CO (2). Also each mole of thermally decomposing Cs_2CO_3 yields one mole of CO_2 and one mole of Cs_2O (3). One mole of CO is formed per each of the mole of Cs_2O undergoing carbothermal reduction (4) implying that the amount of CO_2 formed in (3) and the amount of CO formed in (4) are equal. The experimental observation of amount of CO evolved, as monitered by mass spectrometry, is in a reasonably good agreement with that of the theoretically expected amount of CO indicating that reactions (2), (3) and (4) are operative during the chemical activation with Cs_2CO_3, in particular, and alkali metal carbonates in general excepting the case of Li_2CO_3 where in the carbothermal reduction of Li_2O to Li is not possible [124].

Addoun *et al.,* [122] have elucidated the effect of the nature of alkali metal carbonate on the evolution of porosity of the carbon materials through the activation of a low rank coal using different activating agents, namely, Li_2CO_3, Na_2CO_3, K_2CO_3, Rb_2CO_3 and Cs_2CO_3. Increase in micropore volume was observed as the radii of the cation of the alkali metal carbonate increased (Li < Na < K << K < Rb < Cs). In addition to the ionic radii of the alkali metal cation of the activating agent, the thermal stability of the alkali metal carbonate in the presence of carbon material was also found to have profound influence on activation process. The lower the thermal stability of the activating agent, the greater is the effect of activation on the evolution of porosity. In fact the amount of CO_2 released during the activation of coal at 1070 K with equal loadings of K_2CO_3 and Na_2CO_3 were found to be equal to 1.4 and 0.9 $mmolg^{-1}$ respectively indicating that K_2CO_3 is thermally less stable than Na_2CO_3 in the presence of carbon

material (char or coal or carbon precursor). Also the rate of evolution of CO_2 was found to be higher in the case of activation with Cs_2CO_3 compared to Rb_2CO_3 activation.

Carbon reduces K_2CO_3 at elevated temperatures. As a result of the carbothermal reduction process (5) potassium vapour and carbon monoxide are formed [124]. The occurrence of reaction (5) is verified experimentally using Knudsen cell mass spectrometry. Potassium vapour and CO were detected in the gas phase during the reaction between carbon and K_2CO_3 in vacuo at temperatures in the range of $773 - 973$ K.

$$2\,C + M_2CO_3 \rightleftharpoons 2\,M + 3\,CO \quad \text{.......................................} \quad (5)$$
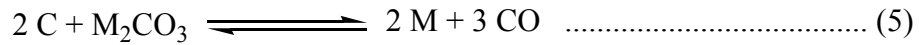
$$M = Na,\ K$$
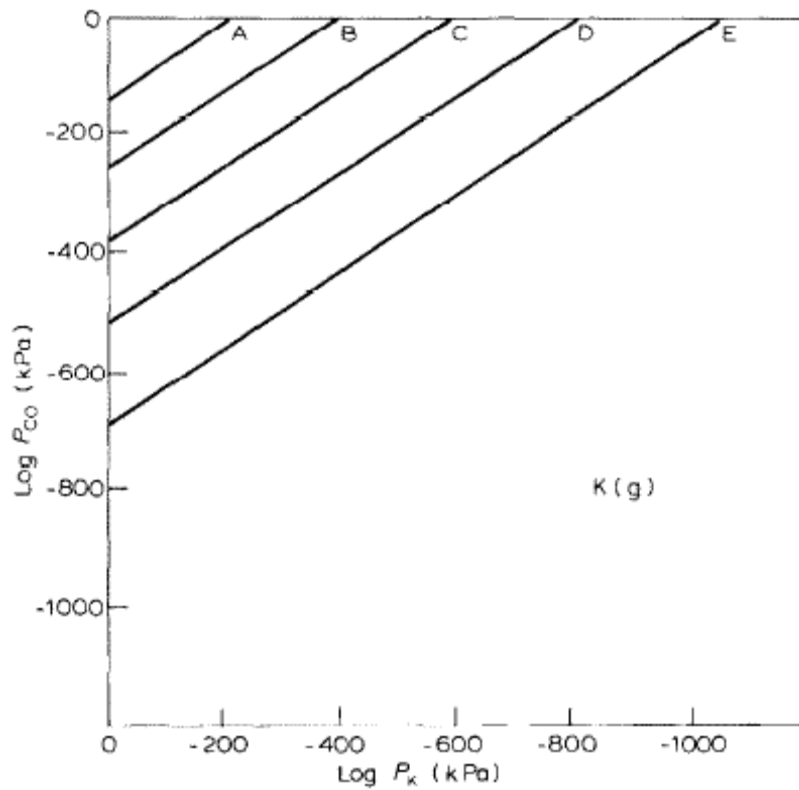
Fig. 9. Equilibrium stability regions of K (g) and K_2CO_3 (s) for the reaction (2) as functions of temperature, P_{CO} and P_K (atm).(A. 1273 K, B. 1173 K, C. 1073 K, D. 973 K and E. 873 K)

Douglas W Mckee [124] succeeded in finding out the stability regimes of the metallic species (vapour form) as well as the unreacted potassium carbonate (solid) as a function of temperature (873 – 1273 K) during the carbon gasification reaction (5) based on thermodynamic considerations. The results obtained from the calculation of the equilibrium stability values of K (g) and K_2CO_3 (s) are shown in Fig. 9. The calculations were performed assuming the occurrence of reaction (5) using the following free energy relation:

$$\Delta G = \Delta G^0 + RT \ln P_{CO}{}^3 \, P_K{}^2$$

The observed reaction rate constant for the gasification of graphite in presence of potassium carbonate (5) carried out at 1073 K in He atmosphere is 2.5 x 10^{-3} min^{-1}. The observed reaction rate constant corresponds to the ambient CO partial pressure (P_{CO}) of 3 x 10^{-4} atm. (1 atm = 10^5 Pa). For a P_{CO} value of 3 x 10^{-4} atm and a similar value of P_K, reaction (4) is thermodynamically feasible at all temperatures above 973 K as indicated by the equilibrium stability regions of K(g) and K_2CO_3 (s) in Fig. 9. Two orders of magnitude reduction in the observed reaction rate constant for the gasification reaction (4) is noticed when the reaction temperature is lowered to 873 K. Such a rate corresponds to P_{CO} value of ≈ 10^{-6} atm. As represented in Fig. 9, reaction (5) is still possible at 873 K.

Douglas W Mckee [124] has observed a rapid weight loss, above 1073 K, when a mixture of graphite and Cs_2CO_3 (1:1 wt./wt.%) is heated in helium atmosphere. Such a rapid weight loss was attributed to the carbothermal reduction of Cs_2CO_3 as shown in (6).

$$2\,C + Cs_2CO_3 \rightleftharpoons 2\,Cs + 3\,CO \quad \text{...................................... (6)}$$
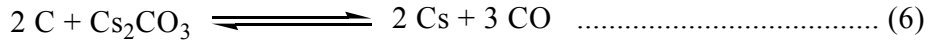
Unlike the carbon gasification reaction with Na_2CO_3, K_2CO_3 and Cs_2CO_3, the reaction with Li_2CO_3 follows a different route (7) and this is because of the relatively greater stability of Li_2O compared to other alkali metal oxides (Na_2O, K_2O or Cs_2O). Also the formation of Li metal is unlikely in the carbothermal reduction reaction under the gasification conditions [124].

$$Li_2CO_3 + C \rightleftharpoons Li_2O + 2\,CO \quad \text{... (7)}$$
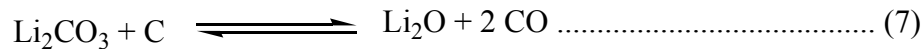
Junichi Hayashi *et al.,* [9] have employed thermal analysis as a tool to understand the nature of interaction between K_2CO_3 (activating agent) and carbon precursor (lignin). The carbon precursor (lignin) obtained from Kraft pulp was subjected to carbonization in N_2 atmosphere in the temperature range of 323 – 1273 K at a heating rate of 10 K/min.

Carbonization is meant for the removal of volatile compounds from the raw material to obtain carbon material with a particular C/H ratio. The reactions that occur during carbonization process are complex in nature. During carbonization process cellulose and lignin (in the case of lingo cellulosic carbon precursors) are transformed into condensed aromatic systems [125]. The carbonization process was monitored by evaluating the weight loss rates as a function of temperature. The lignin chars produced with out the use of activating agents possessed specific surface area values of only 10 – 50 m^2/g. Lignin when activated in the presence of K_2CO_3 at an activation temperature of 1073 K with an impregnation ratio of 1 (K_2CO_3 : lignin (wt./wt.%)) yielded activated carbon material with a specific surface area value of ~ 2000 m^2/g. Activation temperature was found to have a significant effect on the performance of activated carbon. A rapid increase in the S_{BET} as well as Vp values of activated carbon materials was observed when the activation temperature is in the range of 773 – 1073 K. Further increase in the activation temperature lead to the decrease in the S_{BET} and Vp values indicating that K_2CO_3 is effective as activating agent at an activation temperature of about 873 K.

Junichi Hayashi *et al.,* [9] have measured the weight. loss rate behaviour of lignin as well as K_2CO_3 (activating agent) individually in N_2 atmosphere in the temperature range of 323 – 1273 K at a heating rate of 10 K/min. Under identical conditions, the weight. loss rate behaviour of lignin impregnated with K_2CO_3 is also measured and this is termed as experimental curve. In addition, the weigt. loss rate behaviour of lignin impregnated with K_2CO_3 is calculated by the summation of the values obtained from lignin and K_2CO_3 measured individually. The curve thus obtained was termed as calculated or theoretical curve. The assumption made in generating the calculated weight. loss rate curve is that there is no chemical interaction between the lignin and the activating agent. Thus the differences between the experimental and the calculated weight. loss rate curves yield important insights into the chemical interaction as well as the particular weight. losses resulting from the chemical reactivity between the char and the activating agent.

It was noticed that the experimental weight. loss peak at around 673 K shifted to a lower temperature in comparison to the peak position in the calculated or theoretical curve. Such a shift in the weights. loss rate peak towards lower temperature (lower than

673 K) was attributed to the occurrence of dehydrogenation reaction at a relatively low temperature. Such dehydrogenation reactions have not contributed to the enhancement of either S_{BET} or Vp but only indicate that the carbonization behaviour of lignin is altered or influenced by K_2CO_3 below 773 K. Also no convincing path way for the evolution of H_2 during activation in the presence of K_2CO_3 at such a low temperature (in the range 473 – 773 K) is illustrated.

Carbon materials are known to dehydrogenate evolving H_2 in the presence of alkali metals (Li, Na, K, Rb, Cs) at low temperatures [126, 127, 128]. But the important question is that how H_2 evolution can take place in the presence of K_2CO_3 as activating agent under the reaction conditions where there is no possibility for the formation of alkali metal species. The following sequence of reactions offer a convincing pathway for the evolution of H_2 responsible for the observed weight. loss rate peak at lower activation temperatures (< 673 K) in the presence of K_2CO_3 as activating agent.

K_2CO_3 is known to undergo thermal decomposition at a lower temperature in the presence of carbon char as shown in (8).

$$K_2CO_3 \rightleftharpoons K_2O + CO_2 \quad\text{... (8)}$$

The K_2O formed in (8) reacts with the structural or crystalline water evolved in the temperature range of 473 – 623 K from the carbonization mixture to form KOH (9).

$$K_2O + H_2O \longrightarrow KOH \quad\text{.. (9)}$$
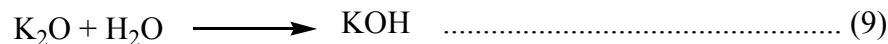
KOH thus formed in (9) reacts with CO_2 formed in (8) as well as with the carbon in the char to evolve H_2 as shown in (10). Reaction (10) is thermodynamically feasible at a temperature as low as 673 K as shown in Fig. 7.

$$4\,KOH + CO_2 + C \longrightarrow 2\,K_2CO_3 + 2\,H_2 \quad\text{..................... (10)}$$
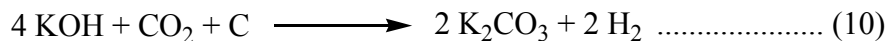
In addition to the shift of the weight. loss rate peak at a activation temperature of ≈ 673 K to a lower temperature, a huge difference in the weight. loss rate behaviour is observed between the experimental and calculated curves at around 1073 K. In fact, a large peak (weight. loss rate) is observed experimentally in sharp contrast to the theoretical or calculated curves where no weight. loss rate peak was present. The recorded weight. loss rate was attributed to the release of CO by the carbothermal reduction of K_2CO_3 by carbon. Thus K_2CO_3 acted differently in two different activation temperature ranges.

Below an activation temperature of 773 K, K_2CO_3 acted as dehydrogenation agent and at an activation temperature of about 873 K, K_2CO_3 was reduced by C releasing CO and there by increasing the specific surface area value and specific pore volume.

Hayashi *et al.*, [129] have produced high specific surface area (2772 m^2/g) activated carbon material with a narrow pore size distribution from waste polyurethane foam using K_2CO_3 activation method. Generally, the activation is a process where in pores are created both in length and width giving raise to a distribution of pore size [125]. Regeneration of polyurethane waste is difficult as it is neither soluble in any solvent nor can be melted by heating there by causing serious threat to ecological balance. Polyurethane foam is a thermosetting polymer with a network structure that finds diverse applications in vehicular and construction fields and there by leading to generation of significant amount of waste. Hayashi *et al.*, [129] have successfully transformed such a waste raw material into a value added activated carbon material using K_2CO_3 activation method.

The generation of high specific surface area value as well as the sharp pore size distribution were attributed to the removal of carbon from the polyurethane char by the carbothermal reduction of K_2CO_3 (1). In addition to lowering of the decomposition temperature of polyurethane component, the presence of K_2CO_3 in the carbonizing mixture, induced structural modification in the polyurethane during activation. K_2CO_3 was found to work effectively as activating agent in two temperature ranges [129]: the one below 773 K where thermal decomposition of the alkali metal carbonate (3) takes place resulting in the alteration in the carbonization behaviour of the carbon precursor and the other temperature range being above 873 K where the process of carbothermal reduction of K_2CO_3 (5) takes over leading to the consumption of carbon in the char. A rapid increase in S_{BET} and V_p were observed at an activation temperature of about 873 K. Presence of K_2CO_3 in the carbonization mixture has lowered the decomposition temperature of the polyurethane foam indicating the structural modification of polyurethane during activation with K_2CO_3. The optimum conditions of activation are: an activation temperature of 1073 K; inert atmosphere offered by N_2 medium; the K_2CO_3 to polyurethane powder ratio (wt./wt.%) is 1:1 and the duration of activation is 1 h. The sorption capacity of the polyurethane based activated carbon for benzene, acetone and

octane vapours were found to be comparable with that of the performance of commercial high surface area activated carbon (2767 m^2/g) and has out performed the sorption ability of the traditional coconut shell based activated carbon (1131 m^2/g).

Low ash content as well as the uniformity in properties (physical and chemical) through out the samples, were the unique advantages of activated carbon produced from polyurethane compared to the carbon materials produced from either coal or lignocellulosic materials [129].

Wei Li *et al.,* [130] have employed K_2CO_3 activation method to produce high specific surface area activated carbon (S_{BET} = 2557 m^2/g, Vp = 1.647 cc/g) using tobacco stems as carbon precursor and micro wave energy as irradiation source rather than conventional heating in electric furnace. Typical activation process comprises of placing a physical mixture of carbonized char from tobacco stems and K_2CO_3 in a quartz reaction chamber with a provision for N_2 gas flow and subjecting the contents to microwave irradiation in a 2.45 GHz in a commercial microwave oven. A micro wave irradiation time of 30 min., micro wave power of 700 W and K_2CO_3 to char (wt./wt. %) ratio of 1.5 were found to be the optimum conditions of activation. After the activation process the resulting material was washed with 50 % HCl for 2 h to remove the metal impurities. The evolution of porosity (1.647 c/g) and generation of high specific surface area value (2557 m^2/g) were attributed to the thermal dissociation of K_2CO_3 as well as the carbothermal reduction of K_2CO_3 and K_2O to yield metallic K. Metallic K thus formed intercalates into the layers of carbon material which upon subsequent removal by HCl washing creates voids in the carbon material.

The K_2CO_3 to char ratio (wt./wt.%) was found to have a significant effect on the textural properties of the activated carbon material. When K_2CO_3 to char ratio increased from 0.5 to 1.5, the iodine number (a measure of the specific surface area value of the carbon material) increased from 1355 to 1834 mg/g and a further increase in the K_2CO_3 to char ratio from 1.5 to 3.0 resulted in a decrease in the iodine number from 1834 to 1350 mg/g. Such a decrease in the specific surface area value with an increase in the amount of activating agent was attributed to pore widening and the subsequent burning off of the carbon material forming the pore wall.

The specific advantages of the process are:

(i)   ecological imbalance caused by tobacco stem waste generation and disposal is solved in a productive way by transforming the waste tobacco stems into technologically useful microporous carbon.

(ii)   Micro wave irradiation has drastically reduced the activation time (only 30 mins. sufficient) saving energy and also reducing the consumption of inert gas (N_2) used as reaction medium, and

(iii)   Micro wave treatment yields good quality carbon materials (uniform structural features and narrow pore size distribution) because of the internal and volumetric heating nature of irradiation unlike the conventional electric furnace heating where in temperature gradient exists between the hot surface of the char particle and the interior region impeding the effective removal of gaseous products and there by resulting in poor quality activated carbon material.

II. 2.1. Role of alkali metal carbonate activation in the production of Activated Carbon Material from Calotropis Gigantea

Industrially, activated carbon materials are produced from either coal or lignocellulosic materials [121]. In addition to several specific advantages like retention of the structural features of the original plant tissue (biotemplating feature), carbon materials produced from botanical sources possess high carbon content. The O/C and H/C ratios are lower in the case of carbon materials produced from plant sources rather than from coal. Char from botanical sources or the raw plant material lose H and O more easily than C when heat treated in inert environment [131]. Thus the carbonization yield is large from lignocellulosic materials.

Indra Neel et al., [132] have produced high surface area, microporous activated carbon with a narrow pore size distribution from the dried stems of Calotropis Gigantea. Calotropis Gigantea is a waste land weed native to India. The effect of alkali metal carbonate (Li_2CO_3, Na_2CO_3 and K_2CO_3) activation on the microstructural, textural and chemical properties of activated carbon is evaluated. The char was obtained by heating a known amount of dried stems of plant in a muffle furnace at 573 K for 30 min as a result

of which volatile matter is eliminated resulting in a carbon rich material. The char thus obtained is ground and sieved through a 200 mesh sieve to obtained fine carbon particles. Useful information on the chemical changes in the original lignocellulosic composition during the initial stages of pyrolysis can be obtained from ^{13}C MAS NMR spectroscopic studies. The ^{13}C nuclei belonging to the aromatic carbons resonate at a frequency range distinctly different from that of the aliphatic carbon making NMR an indispensable tool for the analysis of structural details of the carbon materials. Thus valuable information on the chemical environment of carbon nucleus in condensed aromatic systems can be obtained from NMR spectra.

The ^{13}C MAS NMR spectrum of the char from Calotropis Gigantea was recorded on Bruker Avance 400 spectrometer operating at 100.6 MHz (Magnetic field = 9.4 T). The experiments were carried out using silicon nitride rotors spinning at a frequency of about 5.0 to 6.0 kHz. About 1000 transients were recorded. The chemical shifts were externally referred to tetramethyl silane (TMS). Adamentane was used for setting the reference frequency. The evolution of highly aromatic structure from the pyrolysis of original lignocellulosic material (plant stems) is discernable from the high resolution ^{13}C MAS NMR spectrum of the char shown in Fig. 10. The strong resonance line near 121 ppm from TMS is characteristic of carbon nuclei in the aromatic planes. In addition, two more broad resonance signals at 35 and 200 ppm attributable, respectively, to aliphatic chains of polymethylene type and ketonic carbon groups were observed in the ^{13}C MAS NMR spectrum of the char.

In general, the three main structural components of stems of plant like Calotropis Gigantea are hemicellulose, cellulose and lignin. Among several structural components of the plant, hemicelluloses are more sensitive to temperature and they are the first to decompose in the temperature range of 473 to 533 K during pyrolysis. Cellulose is thermally more stable than hemicellulose and will decompose in the range of 513 – 673 K releasing structural water. In addition rapture of the glycosidic linkages also takes place. Aromatization takes place subsequently. Lignin is the most thermally stable component. Decomposition of lignin takes place in the temperature range of 553 – 823 K resulting in the formation of large amount of aromatics.
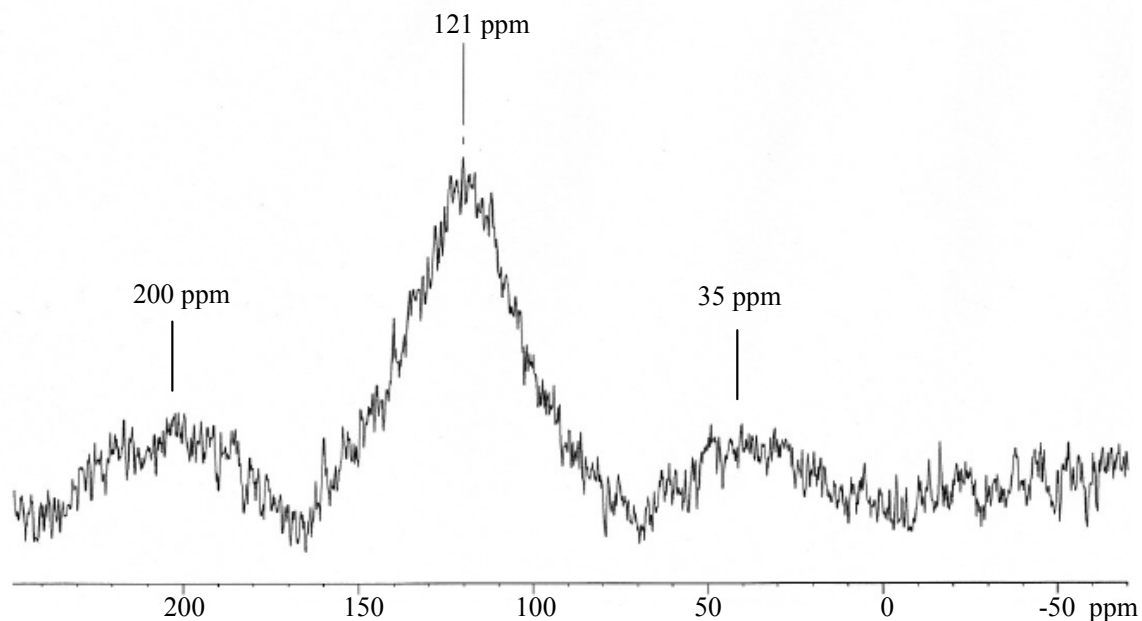
Fig. 10. ^{13}C MAS NMR spectrum of the char (as synthesized) from Calotropis Gigantea [reproduced from ref. 132]

The ^{13}C MAS NMR spectrum of original lignocellulose raw material (rice husk) [133] comprises of resonance signals characteristic of hemicellulose, cellulose and lignin. Typical structural building units of Cellulose and Lignin (guaiacyl unit) are shown in Fig. 11.
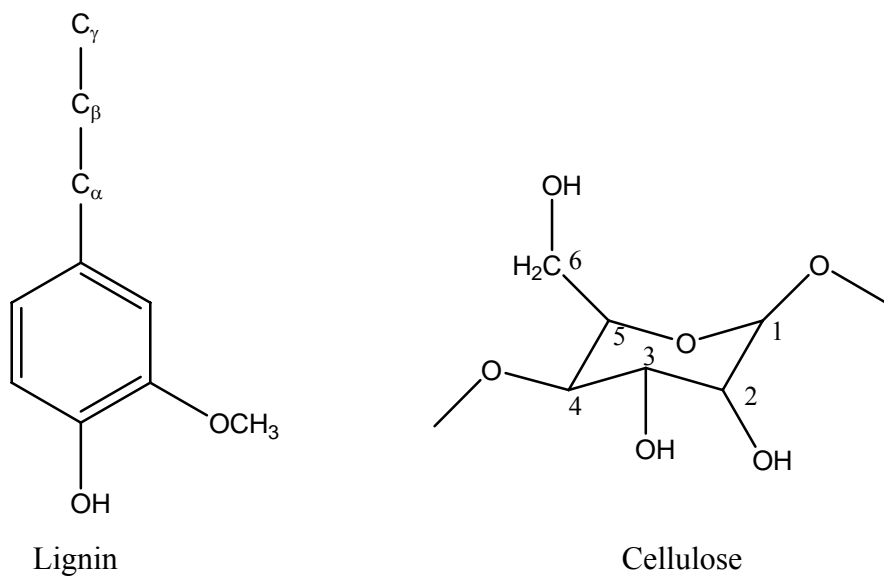
Lignin

Cellulose

Fig. 11. Typical structural building units of Lignin and Cellulose

Typically, for lignin, a resonance line at 56.8 ppm associated with methoxy groups and also another resonance line between 115 and 150 ppm attributable to aromatic carbons are observed. The carbon nuclei from Cellulose structure resonate at the following chemical shift values: C-1 at 105.8 ppm, C–2, 3, 5 at 73.2 and 75.5 ppm, C-4 at 84.4 and 89.3 ppm and C-6 at 63.5 and 65.0 ppm. The carbon nuclei characteristic of hemicellulose structure results in two resonance signals at chemical shift values of 21.8 and 174 ppm respectively corresponding to the methyl and carbonyl carbon nuclei.

Thus the absence of resonance signals characteristic of cellulosic and hemicellulosic structure in the ^{13}C MAS NMR spectrum of the char produced from Calotropis Gigantea (Fig. 10.) indicates the break down of carbohydrate structure (cellulose and hemicellulose) as a result of pyrolysis and also the conversion of aliphatic groups into aromatic system. The broad and strong resonance signal observed at 121 ppm corresponding to condensed aromatic system with a turbostratic graphitic structure is a contribution from the complete thermal decomposition of carbohydrate (cellulose and hemicellulose) structure and partial decomposition of lignin structure and also the subsequent reorientation of carbon containing short lived radical intermediates to hexagonal layered structure of aromatic carbon. The undecomposed component of lignin also contributes to the intensity of the signal at 121 ppm. In fact, chars were supposed to comprise of interwoven network of carbon "ribbons" containing hexagonally arrayed carbon layers – a turbostratic.

The char obtained is subjected to activation with varying amounts of K_2CO_3. The K_2CO_3 to char (wt./wt.%) ratio was varied from 1, 2, 3, 4 and 5 in N_2 at a temperature of 1073 K for 8 h. After activation, the temperature of the furnace is lowered to room temperature. When the activated material is brought out of the furnace, the material started to burn with glowing confirming the formation of metallic K by the reduction of K_2CO_3 by C.   In air or O_2 at 1 atm, the alkali metals are known to burn [99]. The material is ground instantaneously and treated with Conc. HCl to remove the metallic compounds. The resulting material is filtered and washed with excess distilled water to remove traces of chloride.

^{13}C NMR spectra for the activated carbon samples, obtained by K_2CO_3 activation at 1073 K, could not be recorded because of the problem with the tuning process. Such a problem in the tuning of the radio wave frequency is an indirect evidence for the enhancement in the electrical conductivity of the activated carbon samples. Thus, upon activation with K_2CO_3 at high temperature (1073 K) in N_2 atmosphere, the carbon materials became electrically conductive making the MAS experiments difficult. The problem can be surmounted by mixing the conductive carbon sample with an insulating media such as Kaolin. The detuning of the NMR probe caused by the improvement in the electrical conductivity of the well carbonized samples can thus be eliminated.

Details of phase structure and the process of graphitization of carbon materials are obtained from XRD studies. XRD patterns of carbon materials were recorded using Shimadzu XD-D1 X-ray diffractometer operated at a scan range of 0.05° with CuKα radiation (λ = 1.5418 Å) and a Ni filter. The diffraction profiles were obtained in the scan range (2θ) of 5 - 80°. The XRD patterns of carbon materials (char as well as activated carbon materials) are shown in Fig. 12. The XRD pattern of the char comprises of two broad diffraction peaks centered at 2θ values of 10 and 22°. The broad diffraction peak at a 2θ value of 22° is characteristic of the presence of lignin component. The broadness of the two diffraction peaks mentioned earlier indicates the amorphous nature of the lignin in the char. The decomposition temperature of lignin is in the range of 553 - 823 K. As the char is produced at 573 K, under the synthesis conditions, not all lignin decomposes. As a result the inherent lignin structure is observed in the char

While evaluating the crystallinity of the of cellulose and lignin blends from XRD studies, Timothy G. Rials *et al.,* [11] have observed a broad diffraction peak at a 2θ value of 21.7° in the case of organosolv lignin (OSL). The diffraction peak was attributed to the presence of lignin component in amorphous phase. In addition to a diffraction peak at a 2θ value of 21.7°, the authors have also observed a small diffraction peak at a lower 2θ value, namely, 14.8°. No origin was attributed to the diffraction signal observed at low 2θ value of 14.8°.

Sanjay Sarkar *et al.,* [13] have observed similar XRD pattern for the lignin collected from the paper industry and such a peak pattern was attributed to amorphous lignin structure.

Chars from lignocellulosic materials were known to comprise of an interwoven network of carbon "ribbons" containing hexagonally arrayed carbon layers – a turbostratic graphitic structure. Precursors containing hexagonally arrayed carbon, as those found in lignin, would readily reform to stable graphitic arrays. In the case of cellulose such structural advantage is missing [98].

Above a 2θ value of 27° several sharp and intense diffraction peaks are observed in the XRD profile from the char and they are a result of silica and other typical mineral matter present in the plant tissues which remain intimately bound with carbon material in the char. Treatment of the char with NaOH (10 wt.% solution) followed by HCl treatment (conc.) removed significant amount of mineral matter. NaOH treatment is effective in removing silica where as HCl treatment is effective in the removal of alkali (Na, K), alkaline (Ca, Mg) and transition (Fe) metals which are inevitable in the chars from lignocellulosic materials. The sharp diffraction peaks characteristic of such mineral matter were completely absent in the char sample produced after NaOH and HCl treatment. The effectiveness of NaOH and HCl treatment in the removal of mineral matter is also confirmed from the analysis of ash content of the original char, char treated with NaOH followed by HCl and activated carbon material obtained from K_2CO_3 activation (char:K_2CO_3 = 1:3 (wt./wt.%). The ash content was determined by adopting ASTM standard procedure bearing the designation D2866-94. The ash content decreased from 12.7 to 4 wt.% upon treatment with base and acid in succession. Activation with K_2CO_3 followed by adddtional acid washing has further reduced the ash content from 4 to 1.8 wt.%. Kiyoshi Okada *et al.,* [121] have observed the usefulness of HCl treatment in the decrease of ash content in the activated carbon material produced from news paper waste
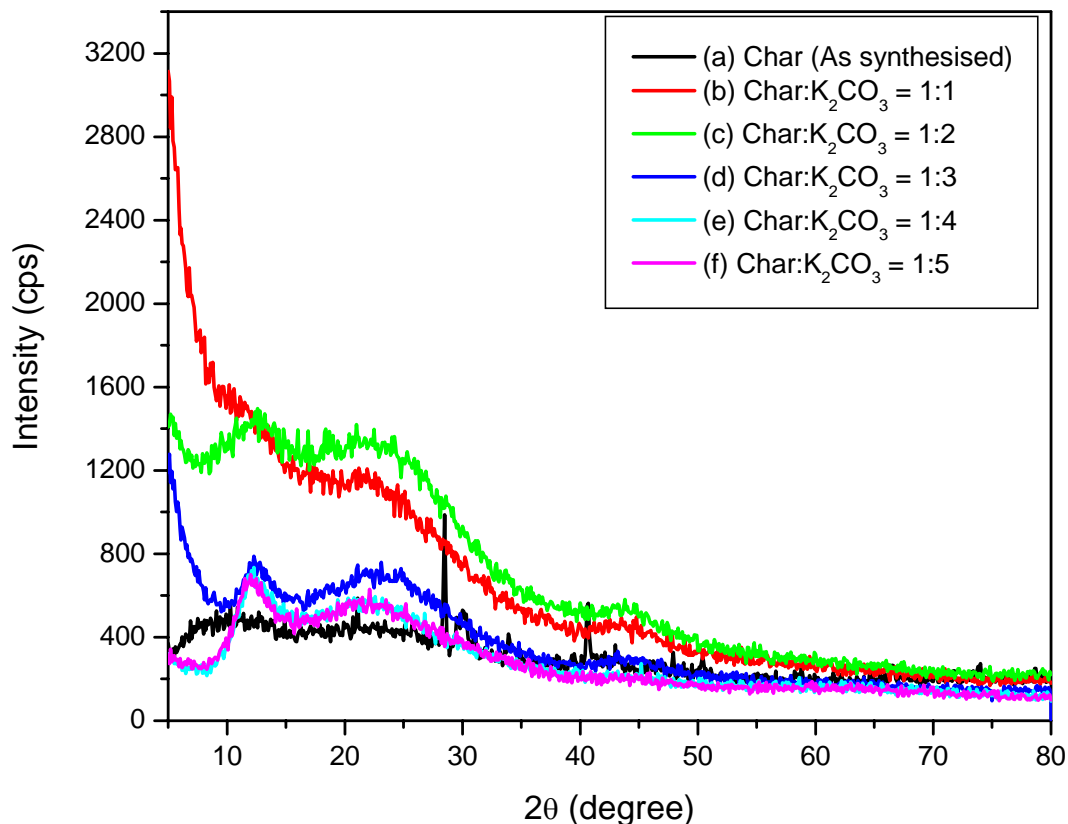
Fig. 12. XRD pattern of carbon materials prepared from Calotropis Gigantea, (a) as synthesized (char), activated carbon with a Char to K_2CO_3 ratio (wt./wt.%) of (b) 1:1, (c) 1:2, (d) 1:3, (e) 1:4 and (f) 1:5 [reproduced from ref. 132.]

Significant changes in the XRD profiles were observed upon activation of the char with K_2CO_3. Upon activation, in addition to the retention of the inherent lignin structure, as evident from the retention of two broad peaks centered around 2θ values of 12 and 22°, a new diffraction peak originated at a 2θ value of 43.5 which is attributable to (10) diffraction of turbostratic carbon containing small hexagonal layer units of carbon. Satoshi Kubo et al., [134] have observed the formation of such trubostratic carbon structure upon carbonization of hard wood acetic acid lignin derived from Betula platyphylla sukachev.

Viboon Sriharoenchaikul et al., [135] have observed a diffraction peak at 2θ value of 43° in the case of pyrolyzed char produced from Physic Nut (Jatropha Curcas L.) and attributed the same to the formation of graphitic basal planes.

Beyond a char to K_2CO_3 ratio of 1:3, the intensity of the above mentioned peak centered at 2θ value of 43.5^0 decreased steadily indicating the partial collapse of the turbostratic graphitic structure leading to disordered carbon structure with hexagonal carbon layers misoriented to one another.

N_2 sorption studies provide information on the textural properties (specific surface area, pore volume, and the distribution of pores depending on the size) of carbon materials produced. The sorptometric analysis on the char (assynthesised material from Calotropis Gigantea) as well as the activated carbon materials were carried out on Sorptometic 1990 Carbo Erba sorptometer using N_2 as adsorbent at 77 K (-196 °C). Prior to the analysis, the carbon samples were out gassed at 523 K for 12 h. The N_2 adsorption – desorption isotherms of the char as well as carbon materials activated with different amounts of activating agent (K_2CO_3) were shown in Fig. 13. The specific surface area values are derived from the isotherm using BET (Brunauer-Emmet-Teller) method. Details of texture properties of the carbon materials produced are given in Table 3. The amount (volume) of N_2 adsorbed is the highest (Fig. 13. (d)) for the carbon material obtained when the K_2CO_3 to char ratio (wt./wt.%) ratio of 3 implying the highest specific surface area value (1296 m^2/g) (Table 3) for this material. Thus the optimum ratio of activating agent::char is 3 (wt./wt.%). Beyond the above mentioned raio of actiating agent : Char, the SSA as well as the pore volume only decreased.

Close inspection of the isotherms gives details of the type and nature of pores present in the carbon materials. Irrespective of the amount of the activating agent, all the activated carbon materials exhibited type I isotherms, according to Brunauer, Deming, Deming and Teller (BDDT) classification [136].

Such type I isotherms are characteristic of micorporous materials having pore diameter < 2 nm. According to IUPAC, porous materials can be classified into three types depending on the pore size (pore diameter). Micorporous materials possess a pore size of less than 2 nm. Among micorpores, those pores with size less than 0.7 nm are termed as ultra micorpores and those pores with sizes ranging between 0.7 and 2 nm are called as super micropores. Mesopores are those having pore sizes in the range of 2 to 50 nm. Materials with pore sizes greater than 50 nm are termed as macroporous materials [130].
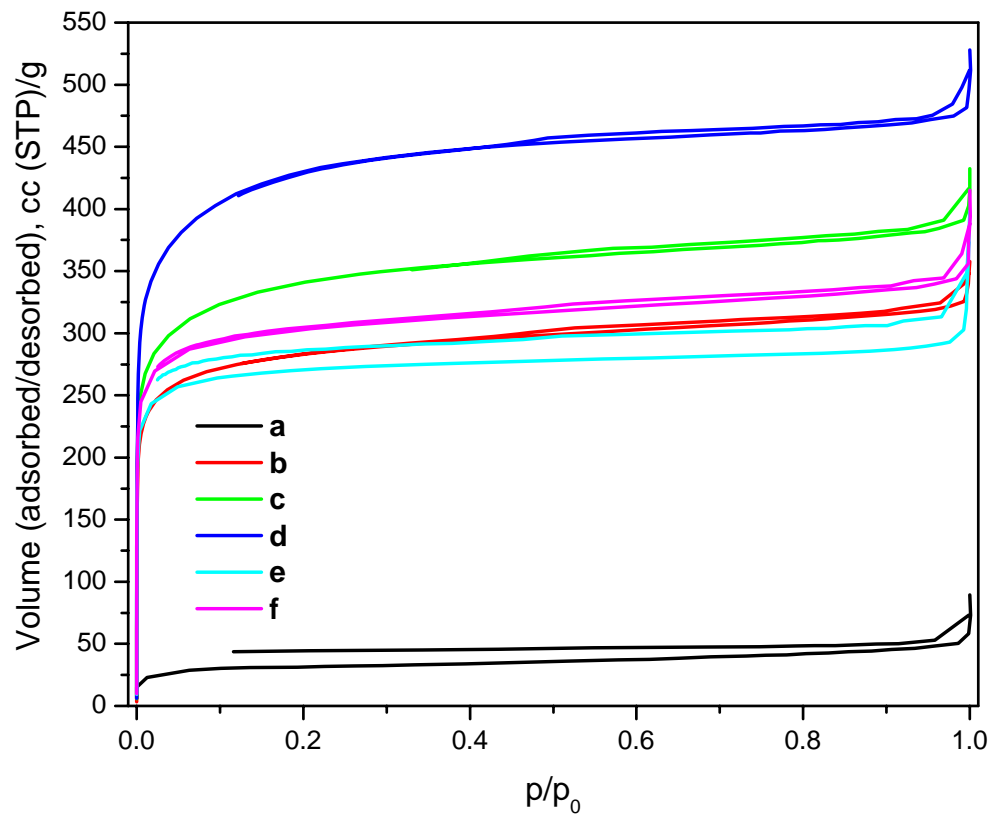
Fig. 13. N_2 adsorption-desorption isotherms of carbon materials prepared from Calotropis Gigantea, (a) as synthesized (char), activated carbon with a Char to K_2CO_3 ratio (wt./wt.%) of (b) 1:1, (c) 1:2, (d) 1:3, (e) 1:4 and (f) 1:5 (reproduced from ref. 132)

Table 3. Effect of amount of activating agent (K_2CO_3) on the specific surface area and pore volume values of carbon materials produced from Calotropis Gigantea

S. No.	Sample	K_2CO_3 : C (wt./wt.%)	Specific Surface Area (m^2/g)	Specific Pore Volume (cm^3/g)
1	Char (as synthesised)	0	97	0.08
2	Activated Carbon1	1	892	0.50
3	Activated Carbon2	2	1083	0.59
4	Activated Carbon3	3	1296	0.73
5	Activated Carbon4	4	765	0.45
6	Activated Carbon5	5	922	0.53

Evaluation of the pore size distribution (PSD) is of paramount importance in the characterization of microporous materials. The PSD of the char as well as the activated carbon materials produced from different K_2CO_3 impregnation ratios using Horvath-Kawazoe method are shown in Fig. 14. Owing to the computational simplicity, Horvath-Kawazoe (HK) method is preferred compared to the density functional theory. The impregnation ratio is found to have a profound effect on the PSD of the activated carbon materials. With an increase in the impregnation ratio upto a K_2CO_3 to char ratio of 3, the micro pore structure (pore radius between 2 to 4 Å) as well as the mesopore volume (pore radius between 10 to 15 Å), formed by the widening of the micropores, increased resulting in an increase in the total pore volume. Beyond a K_2CO_3 to char ratio of 3, the intensity of micropore volume as well as the mesopore volume decreased due to blocking of the pores. Such pore blockage by both partial collapse of the pore wall as well as by the decomposed products of the activating agent is more prounounced in the case of activated carbon produced with a K_2CO_3 : char (wt./wt.%) ratio of 4 (Fig. 14. (e)).

Up to a K_2CO_3 to char (wt./wt.%) ratio of 3, there is a tremendous increment in the amount of N_2 adsorbed indicating an increase in pore volume and specific surface area of the carbon material as a result of evolution of pores as well as widening of the existing pores. A peculiar behaviour is observed in the textural properties of the carbon material obtained at a char to K_2CO_3 ratio of 1:4 indicating a sort of transition being taking place at this stage.

Even though, all the carbon materials produced from activation with different amounts of K_2CO_3 exhibited type I isotherms indicating that all the carbon materials are microporous in nature, there are significant differences in the shapes of isotherms offering valuable information. Firstly, the isotherm (Fig.13. (e)) is parallel or horizontal to the relative pressure (p/p_0) axis (X-axis) implying that the activated carbon material obtained from a char to K_2CO_3 (wt./wt.%) ratio of 1:4 is exclusively microporous. Major uptake occurred at a low relatively pressure (less than 0.1). This is an indication of the formation of highly microporous material with a narrow pore size distribution. Gregg and Sing [137] have attributed such complete filling of pores at very low relative pressure in the case of microporous materials to the strong interaction potential between the

Fig. 14. Pore size distribution curves, based on Horvath-Kawazoe method, of carbon materials prepared from Calotropis Gigantea, (a) as synthesized (char), activated carbon with a Char to K_2CO_3 ratio (wt./wt.%) of (b) 1:1, (c) 1:2, (d) 1:3, (e) 1:4 and (f) 1:5 (reproduced from ref. 132.)
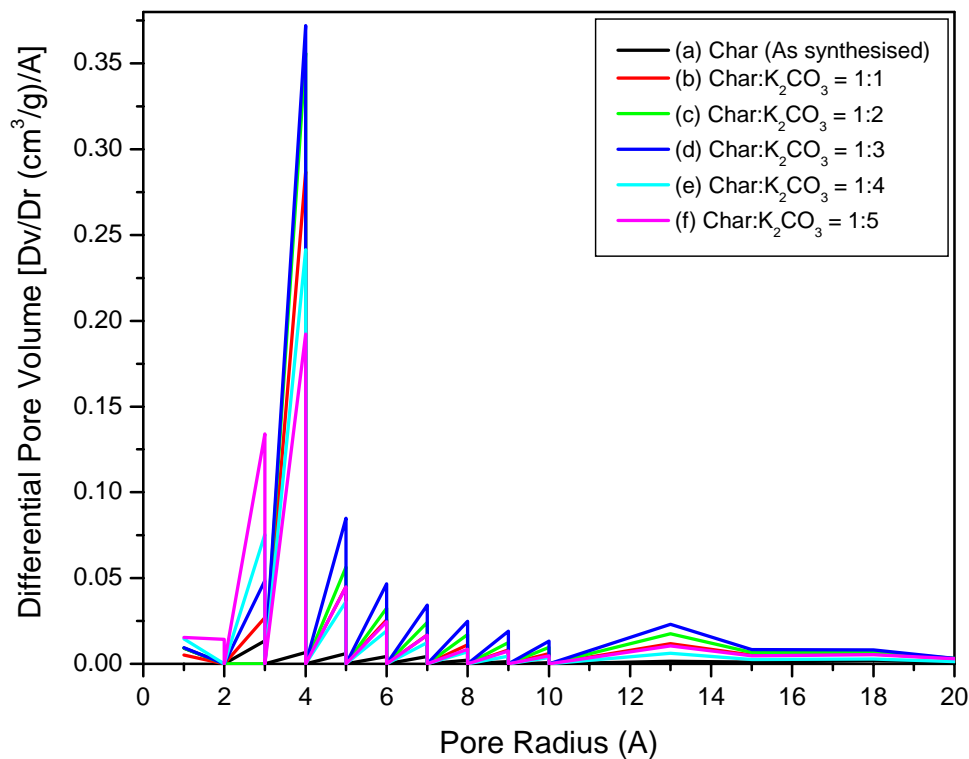
adsorbent and adsorbate. Also the initial steep region was abruptly followed by a plateau. This indicates that the adsorption is stopped owing to the close proximity of the pore wall preventing the formation of multi-layers . Thus mesopores and macropores are absent in the case of activated carbon produced with a K_2CO_3: :char ratio of 4.

The exclusive microporous nature and also the decrease in the micro and mesopore volumes in the above mentioned case were observed in the pore size distribution (PSD) curve shown in Fig. 14. (e). In addition there is a pronounced decrease in the specific surface area value of the carbon material activated upon increasing the char to K_2CO_3 ratio from 1:3 to 1:4 (SSA decreased from 1296 to 765

m^2/g) indicating blockage of micorpores as well as the mesopores. Except the case of sample, with activation with a char to K_2CO_3 activation of 1:4, (Fig. 14. (e)), other isotherm curves (Fig. 13. (b), (c), (d) and (f)) exhibited appreciable slope in the isotherm in the high pressure region. Such a marginal increase in adsorbed volume in the relative pressure range of 0.35 – 0.95 with an increase in the char to K_2CO_3 ratio (wt./wt.%) from 1:1 to 1:3 can be attributed to the formation of mesopores as a result of the pore widening. Formation of such mesopores (an increase in pore volume in the range of 20 – 30 Å (pore diameter)) is observed in the PSD curves (Figs. 14. (b), (c), (d) and (f)).

The elemental analysis of the char, char treated with NaOH followed by HCl as well as char activated with K_2CO_3 (char:K_2CO_3 (wt./wt.%) = 1:3) was carried out on CHNS/O analyzer (Perkin Elmer Instrument, Series II) and the results are summarized in Table 4. Acetanilide was used as reference for calibrating the elemental analyzer.

Simple treatment of the char with NaOH (10 wt.% solution) and HCl in succession has improved the carbon content (wt.%) from 73.13 to 77.62 which is attributed to the elimination of mineral matter. Activation with K_2CO_3 has further increased the carbon content from 77.62 to 80.04 % and also the oxygen content decreased from 14.6 to 13.6 %. as expected. It is interesting to note an increase in the hydrogen content from 2.63 to 3.5 wt.% upon activation which is not expected. Upon activation, oxygen and hydrogen are striped off from char structure. The increase in hydrogen upon activation is not because of activation step (reaction) but because of the subsequent treatment of the activatead carbon composite (carbon material with the decomposed products of activated carbon, mainly K) with HCl and further washing with water. In fact, during the K_2CO_3 activation process surface species such as C-O-K are formed which upon treatment with HCl and subsequent washing with water gets transformed to C-O-H groups which contribute to an increase in the hydrogen content in the case of activated carbon sample relative to either the original char or to the base and acid treated char.

II. 2.1. A. Effect of the nature of cation of the alkali metal carbonate on the textural properties of Activated carbon Materials:

To evaluate the effect of the cation of the activating agent on the textural properties of activated carbon, the char obtained from Calotropis gigantea is subjected to activation

with Li_2CO_3, Na_2CO_3 and K_2CO_3 at a temperature of 1073 K for 8 h in N_2 temperature. The char : activating agent ratio was 1:1 (wt./wt.). The original char as well as the activated carbon materials were subjected to sorptometric analysis using N_2 gas as adsorbent at 77 K. The N_2 adsorption-desorption isotherms collected over the activated carbon materials obtained from activation with Li_2CO_3, Na_2CO_3 and K_2CO_3 are depicted in Fig. 15.

Table 4. Chemical composition of carbon materials from Calotropis Gigantea

Element (wt. %)	Carbon Materials from Calogropis Gigantea		
	Char (As synthesized)	Base and Acid treated (NaOH and HCl) treated	Activated with K_2CO_3 (Char:K_2CO_3 = 1:3)
Carbon	73.13	77.62	80.04
Hydrogen	2.61	2.63	3.50
Nitrogen	0.81	0.82	0.67
Sulphur	0.36	0.33	0.36
Total	76.91	81.40	84.57
Ash content	12.7	4.0	1.8
Oxygen*	10.39	14.6	13.63

* By difference from the total amount of other constituents

Table 5. Effect of nature of cation of the activating agent on the textural properties of activated carbon

S. No.	Activating agent	Ionic radii of the cation (Å)[a]	E^0 (V)[b, c]	Textural properties of Carbon Materials	
				Specific Surface Area (m^2/g)	Specific Pore Volume (cc/g)
1	Li_2CO_3	0.60	-3.0	480	0.263
2	Na_2CO_3	0.96	-2.7	811	0.395
3	K_2CO_3	1.33	-2.9	892	0.497

a. & b. from ref. [99] p.197

$$M^+ (aq) + e \rightleftharpoons M (s)$$

.

c. The standard redox potential of activated carbon is + 0.24 V [138]
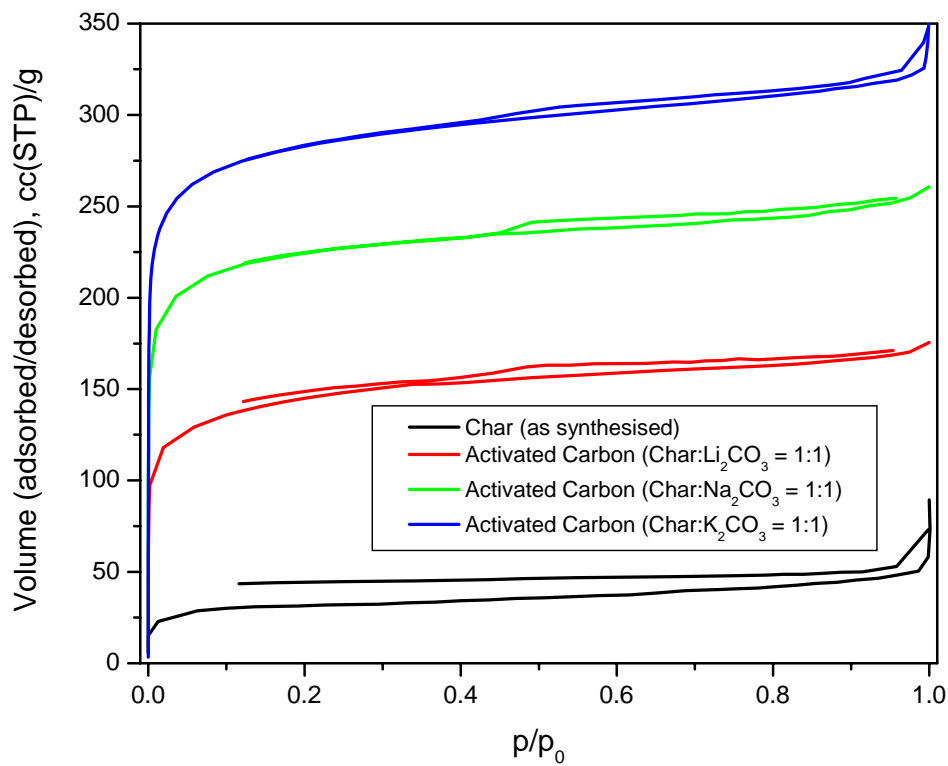
Fig. 15. N_2 adsorption-desorption isotherms of carbon materials prepared from Calotropis Gigantea, (a) as synthesized (char) and activated carbon with a char to activating agent ratio (wt./wt.%) of 1:1, (b) Li_2CO_3 activation (c) Na_2CO_3 activation and (d) K_2CO_3 activation (reproduced from ref. 3.)

There is a steady raise in the volume of the adsorbate adsorbed on the activated arbon material as the activating agent is changed from Li_2CO_3 to K_2CO_3 through Na_2CO_3. The specific surface area of the activated carbon produced was found to be dependent on the radii of the cation of the activating agent as shown in Table 5.

II. 2.1. B. Effect of K_2CO_3 activation on the chemical environment and the concentration of unpaired electrons (spin density of electron) in carbon materials from Calotropis Gigantea

Electron paramagnetic (spin) resonance (EPR or ESR) spectroscopy is a sensitive technique to examine and investigate the electronic structure of carbon materials. EPR

studies on carbon materials provide information on the chemical environment of the unpaired electrons present in the carbon matrix [139].

As early as 1953, the phenomenon of EPR was discovered in carbon materials, particularly in graphite. The same phenomenon was found in the case of coals and chars in 1954. The research on the origin, broadening and unsymmetry of the ESR line of carbon materials has been an unending fight for researchers [140].

The EPR spectra on the char, char treated with base (NaOH) and acid (HCl) and the char activated with K_2CO_3 (char : K_2CO_3 = 1:3 (wt./wt.%)), shown in Fig. 16., were recorded on a Varian E-112, X band spectrometer at room temperature using the free radical, DPPH (diphenyl picryl hydrazyl radical) as external reference to evaluate the g factor value as well as the concentration of the unpaired electrons in each of the carbon samples. The g factor is a dimensionless constant and is equal to 2.002319 for unbound electron (free electron). From the EPR spectra shown in Fig. 1, the g-factor values, peak to peak separation, ΔH in Gauss, and the spin concentration values were evaluated and are summarized in Table 6. The spin concentration values were determined by following the procedure described in reference [142].
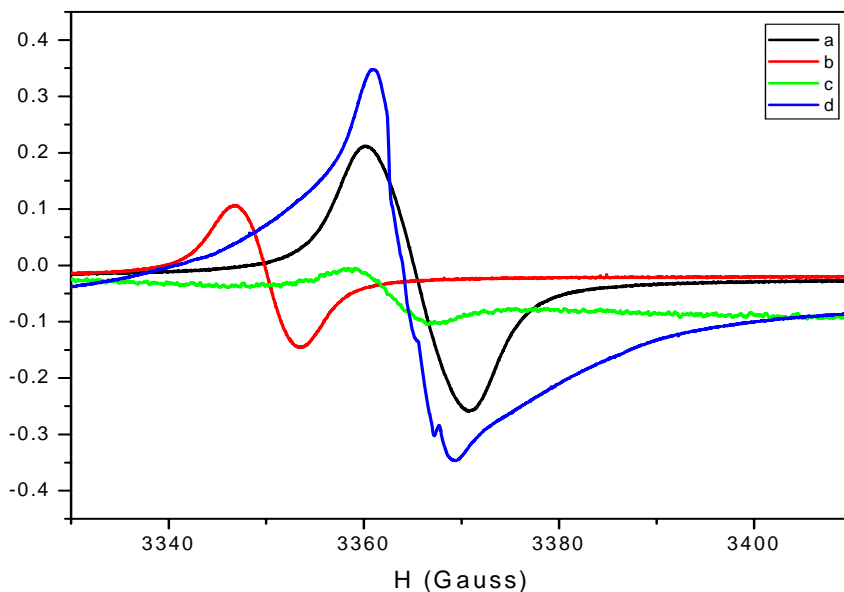
Fig. 16. EPR spectra of (a) char from Calotropis Gigantea, (b) char treated with NaOH followed by HCl, (c) char activated with K_2CO_3 (char:K_2CO_3 (wt./wt.%) =1:3) and (d) DPPH (diphenyl picryl hydrazyl radical) [reproduced from ref. 141]

Table 6. g-factor, peak-to-peak separation (ΔH in Gauss) and concentration of unpaired electrons in the carbon materials produced from Calotropis Gigantea

S. No.	Carbon Material	g-factor value	ΔH (in Gauss) Peak to peak separation	Spin Concentration per gram of carbon material
1	Char (as synthesized)	2.00092	11.0	0.73×10^{19}
2	Char (base and acid treated)	1.99980	6.0	0.33×10^{19}
3	Char activated with K_2CO_3 (char:K_2CO_3 = 1:3, wt./wt.%)	2.00058	9.5	0.15×10^{16}

Important revelations from the data derived from the EPR spectra shown in Fig.16. and summarized in Table 6 are:

(i) The g factor values of the original char, char treated with base and acid as well as the char activated with K_2CO_3 are close to the g value of the free electron (2.002312) with in the error of our experiments (± 0.002). Singer and Wagoner [143] have observed a g factor value close to that of free electron g value in the case of polycrytaline graphite doped with K. Vilas Ganpat Pol *et al.,* [144] have observed a g factor value of 2.00277 and a peak width (peak to peak separation) of 40 G in the case of Carbon Spherules produced by the carbonization of mesitylene. Such a narrow resonance signal was attributed to non-graphitized carbon black [145]. Manivannan *et al.,* have attributed the EPR signal from coconut shell based as well as wood based activated carbon materials with a g value of 2.0028(3) to the presence of dangling bonds of disordered carbon materials [146]. Chauvert *et al.,* [147] have observed g-factor values of 2.012 and 2.018 in the case of multiwalled carbon nanotubes and graphite respectively. Zhuo *et al.,* [148] have observed g-factor values of 2.000 and 2.004 in the case of multiwalled carbon nanotubes and graphite respectively.

(ii) The peak to peak separation was found to be higher in the case of original char (ΔH = 11.0 Gauss) compared to either the char treated with base and acid or the char activated with K_2CO_3. Such a broadness in the EPR signal is attributed to the presence of SiO_2 in the original char as revealed from XRD analysis. The decrease in ΔH value upon treatment with base and acid is an indication of the removal of silica from the char,

highlighting the effectiveness of the process in getting rid of silica which is usually and inherently bound intimately in the carbon matrix. As early as 1968, Singer and Wagoner [143] have made similar observation of broadening of the EPR signal resulting from graphite because of the presence of impurities like silica. Impurities such as SiO_2, SiC, Si and Ge deposited on polycrystalline graphite were found to form surface complexes and there by acting as effective agents for spin-lattice relaxation causing the broadening of the EPR signal resulting from graphite. Mrozowski has attributed to the peak broadening to some changes in the structure of carbon material [140]. From the data given in Table 6., it is observed that upon activation with K_2CO_3, the ΔH value increased from 6.0 to 9.5 G indicating the presence of traces of K in the carbon material after activation. Chen *et al.*, [139] have observed g factor values of 2.0 and 2.003 and ΔH values of 2.0 and 1.0 G in the case of purified and shortened single walled carbon nanotubes.

(iii) The concentration of unpaired electrons in the char produced from Calotropis Gigantia was found to be of the order of 0.74×10^{19}/g. The origin of such spins is attributed to the generation of dangling bonds formed as result of the extensive devolatilization from the defragmentation of the hemicellulose, cellulose and lignin structure during the preparation of the char in the muffle furnace at 573 K. Paramagnetic centers were found to be associated with the dangling bonds formed during the carbonization of carbon materials [133].

The spin concentration of the graphon black and acetylene black [149] was found to be 1.1×10^{19} and 3.8 and 10^{19} spin/g respectively which are the same order of the as that of the spin concentration value observed in the case of the original char given in Table 6. Upon treatment of the char with base and acid, the spin concentration decreased from 0.74×10^{19} to 0.34×10^{19} spin/g. Nearly a three orders of magnitude reduction in spin concentration is observed upon activation of char with K_2CO_3 (0.15×10^{16} sping/g). Such a drastic decrease in spin concentration upon activation with K_2CO_3 is because of the saturation of the dangling bonds with K metal, formed during the carbothermal reduction of K_2CO_3, resulting in the formation of surface C-K bonds which subsequently transform to C-H bonds upon final treatment with conc. HCl. Such a transformation is also confirmed from the increase in the hydrogen content (2.63 to 3.5 wt.%) of the carbon sample activated with K_2CO_3 and subsequently treated with conc. HCl (Table 4).

Manivannan *et al.,* [146] have found the spin concentration values of activated carbon materials, namely, GX203 (from coconut shell precursor), P1400 (from wood precursor) and Med50 (from coconut shell precursor) to be 1.8 x 10^{17}, 5.8 x 10^{17} and 1.8 x 10^{16} spins/g respectively.

II. 3. Transition Metal Salts as Activating Agents

Adsorption properties of carbon materials are enhanced upon chemical activation [150]. Carbonization and activation are the two important stages in the manufacturie of activated carbon. The essential reaction taking place during carbonization is the elimination of non-carbon elements (O and H are stripped off from the carbon precursor). The residual carbon atoms are polylmerized into sheets of condensed aromatic system which are often relatively irregular and disordered. Because of the misalignment of sheets of condensed aromatic systems relative to each other, interstices or voids are formed in the char. But the voids are often blocked by deposition of tar. As a result, the incipient pores will be rendered inaccessible. The process of activation is, thus, inevitable to generate porosity. Pore structure in the char can be developed either by physical or chemical activation [151].

In general, the chemical species used for activation are normally dehydrating agents. They influence the pyrolytic decomposition of carbon precursor. Even though, $ZnCl_2$ is extensitvely used as activating agent very little is known on the activation mechanism in presence of $ZnCl_2$.

II. 3.1. Activation with $ZnCl_2$

The ability of $ZnCl_2$ to activate (generate porosity) carbon precursors is based on its dehydrating function. During the process of activation, $ZnCl_2$ eliminates hydrogen and oxygen atoms of carbon materials as water rather than as oxygenated organic compounds, thus leading to the generation of porosity as well as enhancing the carbon content [150].

Zhonghua Hu *et al.,* [150] have produced activated carbon material (specific surface area = 1465 m^2/g) by activating Elutrilithe (a waste from coal) with $ZnCl_2$. Since by nature $ZnCl_2$ is dehydrating agent, it can alter the pyrolysis behaviour of carbon precursor. $ZnCl_2$ gets intercalated into the carbon matrix by impregnation. Upon pyrolysis, the impregnated $ZnCl_2$ causes dehydration of the carbon precursor leading to charring and aromatization along with the creation of pores. During the process of activation, liquid $ZnCl_2$ is formed above the melting point of $ZnCl_2$ (556 K). Liquid $ZnCl_2$ thus formed is mobile. Further increase in the temperature of activation, beyond the boiling point of $ZnCl_2$ (1003 K), interaction between carbon atoms and Zn species takes place resulting in a significant widening of the interlayers of carbon creating pores in the carbon matrix. During such severe interaction with carbon, $ZnCl_2$ aids removal of water from carbon structure by stripping off hydrogen and oxygen of the carbon precursor.

Caturla *et al.,* [151] have studied the effect of $ZnCl_2$ in the activation of peach stone. The amount of Zn introduced into the precursor during the impregnation was found to be the prime factor governing the textural properties (specific surface area and micropore size distribution) of the carbon material. A combination of chemical activation with $ZnCl_2$ and physical activation with CO_2 was found to yield carbon material with a high specific surface area value of 3000 m^2/g at 60 – 70 % burn off. Upon impregnation with $ZnCl_2$, at first, the cellulose component is known to decompose followed by dehydration reaction during carbonization step. As a result of carbonization, charring followed by aromatization of carbon skeleton as well as evolution of porosity takes place.

Ahmadpour *et al.,* [153] have evaluated the process of $ZnCl_2$ activation of bituminous coal. The impregnation ratio of activating agent ($ZnCl_2$) to carbon precursor was identified to be the most important parameter. Too high a carbonization temperature is found to destroy the carbon structure in the case of $ZnCl_2$ contrary to KOH activation. The effect of washing (usually with HCl) was found to have profound influence on the evolution of porosity which is more so when high concentration of activating agent ($ZnCl_2$) was employed. During washing step, the $ZnCl_2$ remaining in the carbon matrix is removed which too contributes to the evolution of porosity. In other words, $ZnCl_2$, or any chemical activator in general, acts as template for the creation of microporosity in

addition to chemically reacting with carbon in the char [154]. When the activating agent to char (carbon precursor) ratio is high, significant amount of $ZnCl_2$ is deposited on the external surface of the carbon matrix. As a result, localized decomposition of organic matter takes place, leading to the generation of wider and larger pores (meso and macroporosity).

Reynaldo Nacco *et al.,* [155] have found $ZnCl_2$ to be the best chemical activator relative to either K_2CO_3 or H_3PO_4 for producing activated carbon from Backery Yeast (Saccharomyces Cerevisiae). No activation was observed with H_3PO_4 where as the yield of the activated carbon was low with K_2CO_3. Using $ZnCl_2,$ a specific surface area value of 739 m^2/g was obtained at a carbonization temperature of 973 K and an activation period of 1 h.

Lopez-Gonzalez *et al.,* [65] have produced activated carbon from Olive stones using either $ZnCl_2$ or CO_2 as activating agents. $ZnCl_2$ was found to be a better activating agent compared to CO_2 in terms of the specific surface area value (2084 m^2/g), total pore volume (0.5 cc/g) and methylene adsorption. $ZnCl_2$ produced activated carbon material with better textural and adsorptive properties compared to CO_2 activation. Physical activation by CO_2 was based on the following gasification reaction:

$$C + CO_2 \rightleftharpoons 2\ CO \qquad \Delta H = -\ 136\ kJmol^{-1}$$
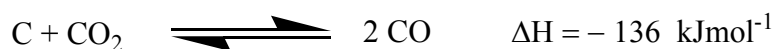
The above reaction is endothermic implying the easiness of controlling the process of gasification and inturn leading to exclusive micropore formation. But low yield of carbon as well as the requirement of longer periods of activation is the stumbling block in this method of activation. On the contrary $ZnCl_2$ activation needs shorter activation time and results in higher yields. But control of microporosity is still a challenge in the activation with $ZnCl_2$.

Rafael Kandiyoti *et al.,* [156] have evaluated the effect of heating rate on the pyrolysis behaviour (tar formation) of Linby bituminous coal in the presence of $ZnCl_2$. Slow heating rate (nearly 5 °C/min) facilitated the reduction of tar formation (from 29.8 to 12.7 %) and there by enhancing the char yield. Hussein et al., [157] have observed the transformation of micropores to mesopores with an increase in the amount of ZnCl2 in the activation of oil palm shells.

Jale Yanik *et al.,* [158] have obtained a 10.5 vol.% increase in the pore volume of the lignite upon activation with $ZnCl_2$. Lignite coke with desired values of porosity and compressive strength (for metallurgical applications) were derived by the addition of 6 wt.% of $ZnCl_2$ to lignite.

Namasivayam *et al.,* [159] have produced activated carbon material from coir pith using $ZnCl_2$ as activating agent. The $ZnCl_2$ to cabon precursor impregnation ratio was varied from 0.125, 0.25, 0.5 and 1.0. With an increase in the $ZnCl_2$ impregnation ratio, the specific surface area values, carbon yield, bulk density, ash content, decolouring power and the iodine number were found to increase.

Olivares Marin *et al.,* [11] have employed $ZnCl_2$ as activating agent to produce activated carbon from Cherry stones. As the impregnation ratio ($ZnCl_2$: Char, wt./wt.%) varied from 1, 2, 3 and 4, the specific surface area values obtainable are 567, 1086, 1566 and 1971 m^2/g respectively. Thus a percentage increase, S_{BET}, of 250 was observed upon varying the impregnation ratio. No change in the FT-IR spectral features were observed indicating impregnation amount ($ZnCl_2$) has no role to play in the surface chemistry or modification of surface functional groups.

Diana C. S. Azevedo *et al.,* [52] have produced activated carbon from coconut shell by $ZnCl_2$ activation followed by activation with CO_2. The advantages derivable from $ZnCl_2$ activation are the well developed porosity (micro and meso pores), high carbon yield and low activation time. The carbon material showed potential for the sorption of methane gas (122 mg of methane/g of carbon). The storage/delivery value for the coconut shell based carbon is 80 v/v. Even though the storage to delivery ratio of the above mentioned sorbent is lower compared to the commercial activated carbon materials, namely, LFC 54 (155/135 (V/V)) and A20 (155/140 (V/V)), significant improvement can be achieved by modifying the activation procedures.

Mehmet Ugurlu *et al.,* [75] have adopted $ZnCl_2$ activation process for producing activated cabron materail from Olive stone. The S_{BET} values of the carbon materials from Olive stone were found to be dependent on the amount of activating agent employed for activation process As $ZnCl_2$ concentration increased from 10, 20 and 30 % (wt./wt.%) the S_{BET} values varied from 58, 790 and 167 m^2/g. The performance of the olive stone derived carbon was compared with that of the commercial activated carbon (with S_{BET} =

1438 m^2/g) for the removal of Remazol Red B dye. The sorption capacities of Olive stone derived carbon were found to be 7.28, 8.53 and 9.33 mg/g at 288, 298 and 308 K respectively. Under identical conditions the sorption capacities for the commercial activated carbon were found to be 6.73, 144.92 and 102.04 mg/g at 288, 298 and 308 K respectively.

II. 3.2. Role of Zinc chloride activation in the production of Activated Carbon Material from Calotropis Gigantea:

Indra Neel *et al.,* [160] have produced activated carbon from Calotropis Gigantea using $ZnCl_2$ as activating agent. Char (as synthesized) from Calotropis Gigantea is produced by heating the dried stems of the plant in muffle furnace at 573 K. The coal obtained is ground, sieved and treated with conc. HCl to remove alkali and alkaline metal impurities. The char is further treated with base (NaOH) to remove silica which is inherently present. The process of activation with $ZnCl_2$ is carried out at 1073 K in N_2 atmosphere for 8 h with varying amounts of activating agent to char (wt./wt. %) ratio, namely, 1, 2, 3, 4 and 5. $ZnCl_2$ is added to the char in solid state by physical impregnation. Textural and structural properties and parameters of the activated carbon materials were found to be influenced by the amount of the activating agent employed for the activation as revealed from the Sorptometric, XRD and Confocal Raman studies.

N_2 adsorption-desorption isotherms recorded on the char (as synthesized) as well as the activated carbon materials obtained with different impregnation ratios of activating agent to the char (1, 2, 3, 4 and 5 wt./wt. %) are shown in Fig. 17. Irrespective of the amount of the activating agent, all the activated carbon materials presented type I isotherms typical of microporous materials. The specific surface area values, total pore volume as well as the average pore diameter details deduced from the isotherms are summarized in Table 7. The specific surface area values of the carbon materials produced gradually increased with an increase in the $ZnCl_2$ to char (wt./wt.%) ratio of 4 and beyond which no increase in the S_{BET} value is observed indicating that the optimum value of $ZnCl_2$:Char ratio is 4.
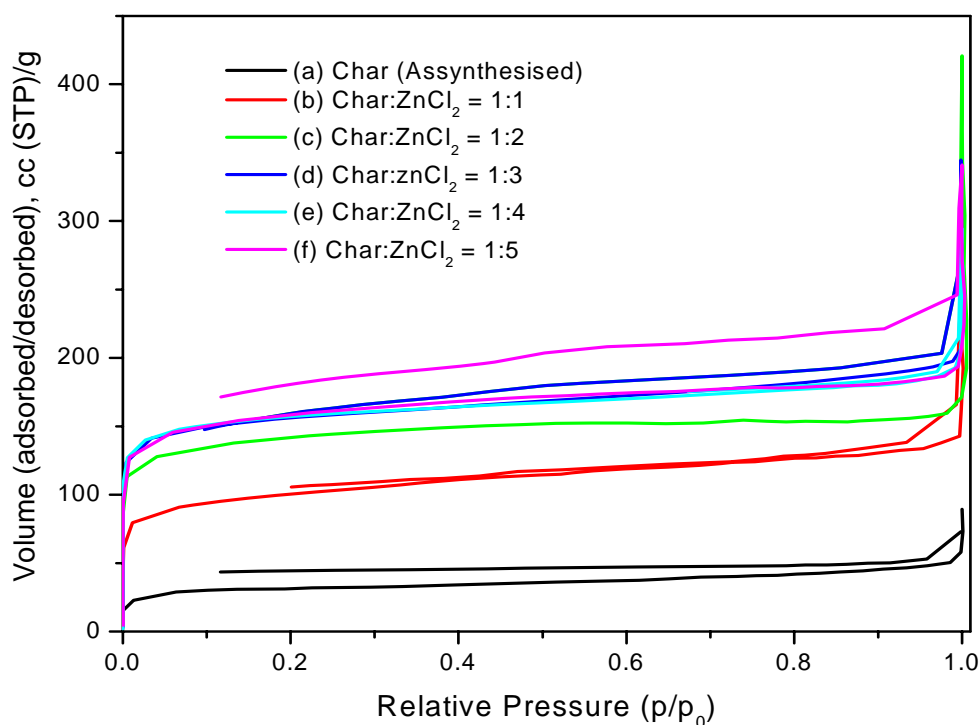
Fig. 17. N_2 adsorption-desorption isotherms of carbon materials prepared from Calotropis Gigantea, (a) as synthesized (char), activated carbon with a Char to $ZnCl_2$ ratio (wt./wt.%) of (b) 1:1, (c) 1:2, (d) 1:3, (e) 1:4 and (f) 1:5 (reproduced from ref. 160)

Table 7. Effect of amount of activating agent ($ZnCl_2$) on the textural properties of carbon materials produced from Calotropis Gigantea

S. No.	Sample	$ZnCl_2$: C (wt./wt.%)	S_{BET} (m²/g)	V_P (cm³/g)	Mean Pore Diameter[ii] (nm)
1	Char	0	97	0.08	3.3
2	[1]AC1	1	356	0.21	2.36
3	AC2	2	493	0.25	2.03
4	AC3	3	564	0.30	2.13
5	AC4	4	573	0.29	2.02
6	AC5	5	553	0.29	2.1

i. AC – Activated carbon; ii. Mean Pore Diameter, d = 4V/A (in nm) ; where V is the total pore volume and A is the specific surface area

Crystallographic parameters of the activated carbon structures produced by $ZnCl_2$ activation of Calotropis Gigantea were obtained from X-ray diffraction studies. Powder X-ray diffraction patterns were recorded on a Rigaku Miniflex II desk top X-ray diffractometer at 30 kV and 15 mA using CuK_α radiation (λ = 1.5405 nm) at a step size of 0.01°.

X-ray diffractograms of the char as well as the activated carbon materials produced with different impregnation ratios to char are shown in Fig. 18. Three typical broad diffraction peaks centered around 2θ values of 25, 44 and 80° are visible in the activated carbons generated with the activating agent to char impregnation ratios of 1, 2, 3, 4 and 5. The two broad peaks centered around the 2θ values of 25 and 44 are attributed (002) and (10) diffraction peaks of turbostratic carbon structure [161]. The origin of the broad peak around 2θ value of 80° is not yet clearly known.

The (00l) line is because of interlayer scattering where as the (hk) line is because of intra layer scattering. Thus the extent of graphitization is revealed by the appearance of general (hkl) reflections [144, 162, 163].

The occurance of broad diffraction bands centered around 2θ values of 25 and 44 indicate better layer alignment as well as an increased regularity in crystal structure [164].

The interlayer spacing values, d_{002}, and the crystallite size values along the c (L_c) and a (L_a) axis of the turbostratic graphitic carbon were deduced from the X-ray diffractograms shown in Fig. 18. are summarized in Table 8. The interlayer spacing, d_{002}, is calculated from the Bragg equation as shown below:

$$d = n\lambda/2Sin\theta$$

where λ is the wave length of the radiation ($CuK\alpha$) used = 0.15405 nm, θ is the diffraction angle for the peak position. Using Scherrer equation (shown below), the crystallite size along the c-axis, L_c and the size of the large planes, L_a, were determined from the full width at half maximum of the diffraction peaks centered at 2θ values of 25 and 44 which were respectively indexed to the (002) and (10) diffraction planes of carbon structure.
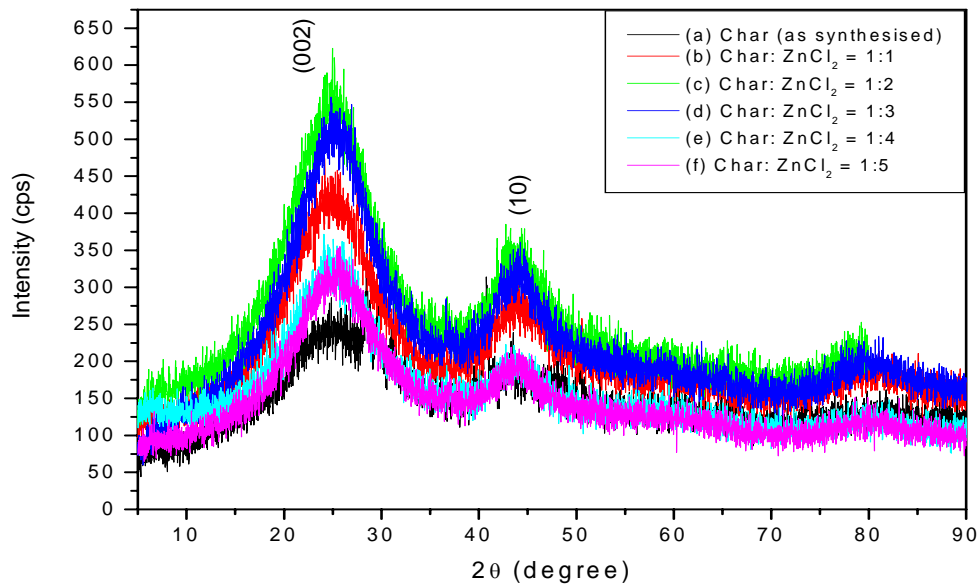
Fig. 18. XRD pattern of carbon materials prepared from Calotropis Gigantea, (a) as synthesized (char), activated carbon with a Char to ZnCl$_2$ ratio (wt./wt.%) of (b) 1:1, (c) 1:2, (d) 1:3, (e) 1:4 and (f) 1:5 [reproduced from ref. 160]

$L = K\lambda/B\cos\theta$ where $L = L_c$ or L_a

B is the half-width of the peak in radians and K is the shape factor. The shape factor K depends on the lattice dimension. The K values of 0.9 and 1.84 were used respectively for calculating L_c and L_a values. The wave length (λ) of CuKα radiation is 0.15405 nm.

Table 8. Effect of amount of activating agent (ZnCl$_2$) on the structural properties of carbon materials produced from Calotropis Gigantea

S. No.	Sample	ZnCl$_2$: C (wt./wt.%)	d$_{002}$ (nm)	L$_c$ (nm)	L$_a$ (nm)
1	[i]AC1	1	0.356	1.04	3.94
2	AC2	2	0.356	1.02	3.50
3	AC3	3	0.353	1.03	3.96
4	AC4	4	0.356	0.91	3.72
5	AC5	5	0.350	0.94	3.80

i. AC – Activated carbon

The interlayer spacing values, d_{002}, almost remained unchanged with impregnation ratio of $ZnCl_2$ to char. The interlayer spacing values, d_{002}, summarized in Table 8 are in the range of 0.35 to 0.356 nm. The above mentioned values were greater than 0.335 nm, which is the typical value of the interlayer spacing for pure graphitic carbon structure. L_C values for different activated carbon materials, summarized in Table 8, are of the order of 1 nm. A decreasing trend in the L_c value is observed with an increase in the amount of the activating agent. The L_c value is the smallest for the activated carbon with the highest S_{BET} value. The L_a values varied in the range of 3.5 to 3.96 nm. For typical graphitic carbon structure, the L_c and L_a values are respectively 0.06708 nm and 0.2461 nm. The magnitude of L_C and La values of the activated carbon materials from Calotropis Gigantea (obtained by $ZnCl_2$ activation) indicate that the carbon material contained roughly about 2 cell length along the c-direction and about 14 − 16 cell lengths along the a − direction.

Raman Scattering Studies on Carbon Materials:

Tuinstra *et al.*, [165] have made an earliest attempt to characterize carbon materials by Raman spectroscopy. Several carbon materials, namely, single crystals of graphite, stress annealed pyrolytic graphite, commercial graphite, activated charcoal, lampblack and vitreous carbon were examined by Raman spectroscopy. Single crystals of graphite yielded a single Raman signal centered around 1575 cm^{-1} which was termed as graphitic or G band attributable to the E_{2g2} Raman active vibration mode (doubly degenerate deformation vibration of the hexagonal ring with D^4_{6h} crystal symmetry). Excepting single crystals of graphite all other carbon materials showed an additional signal at 1355 cm^{-1} which was termed as D band characteristic of disordered carbon attributable to the A_{1g} mode (due to the finite crystal size A_{1g} mode of the lattice becomes Raman active). An inverse proportionality relationship was observed between the crystallite size and the intensity of the Raman signal. Thus the intensity of the Raman bands gives an idea of the crystallite size.

Nakamizo *et al.,* [166] have gained insight into the complex microstrural nature of carbonaceous compounds from Raman spectroscopic studies. The relationship between Raman spectra and the chemical structure of carbon materials (natural graphite, pyrolytic graphite, carbon black, glassy carbon, coal, sputtered carbon and white carbon) was reported. An increase in the Raman intensity ratio (I_{1360}/I_{1580}) as well as the half band width was observed going from graphite to carbon black through glassy carbon. Raman spectroscopy is a non-distructive characterization tool. Raman spectra provide information on the structure as well as the phase details of carbon materials. Graphitic carbon as well as amorphous carbon materials is strong Raman scatterers [167]. Raman scattering technique is a tool for studying the disorder in activated carbon materials [168]. Raman scattering is found to be more sensitive to the precursor carbon material rather than the specific surface area of the activated carbon material. Raman scattering provides an authentic evidence for the presence of local two-demensional graphene structures. Important information on the microstructure of the carbon material can be obtained from the analysis of Raman spectra. In addition to structural details, one can understand the process of graphitization from Raman spectra of carbon materials [169].

Information on the crystallographic disorder of carbon materials can be obtained from Raman spectroscopic studies [146]. Information on the crystalline structure of carbon materials could be obtained by the analysis of the band position, band width and also the Raman intensity ratio. The Raman intensity ratio ($R = I_{1360}/I_{1580}$) was found to be inversely related to the crystallite size – L_a [170].

Natural graphite possesses a hexagonal lattice. Theoretically only one line is expected at 1575 cm^{-1}. Analogous to natural graphite, in the case of stress annealed pyrolytic graphite also a single signal at 1575 cm^{-1} is observed. In addition to a signal at 1575 cm^{-1}, another signal at 1360 cm^{-1} is observed in the case of glassy carbon as well as poly crystalline graphite. The Raman line at 1360 cm^{-1} was attributed to the disorganized regions near the crystal edges and lattice defects such as edge dislocation and lattice vacancies [171]. A measure of the concentration of the lattice defects in graphitic structure is obtained from the Raman intensity ratio, ($R = I_{1360}/I_{1580}$), the ratio of observed intensity of signal at 1360 cm^{-1} to that at 1580 cm^{-1}. Nakamizo *et al.,* [172] have studied the effect of grinding on the change in the crystal structure of natural graphite. The

generation of disorder as well as defects was noticed from the Raman spectroscopic studies. As a result of grinding, in addition to the single signal at 1580 cm^{-1}, natural graphite exhibited two more signals centered around 1360 and 1620 cm^{-1} which were attributed to the presence of disordered carbon with defects in the structure.

Unlike several reports on the Raman spectral analysis of carbon materials focussing on the first order spectral features (mainly G and D band features), Sato *et al.,* [173] have focused their studies on the grey areas in the second order Raman spectral region, 2400 – 3000 cm^{-1}, to gain understanding on the effect of heat treatment on the structure of carbon materials produced from copper containing furfuryl alcohol and graphite fluoride. Three typical bands were observed (in the second order spectral region) at 2700, 2950 and 3,250 cm^{-1} corresponding to the overtone of the 1360 cm^{-1} band, a combination of the 1580 and 1360 cm^{-1} band and a second order feature common to graphite respectively.

Terrence P Mernagh *et al.,* [174] have produced graphon black by heat treating Spheron 6 carbon at 3273 K. Under the conditions of preparation, the surface oxygen groups were removed leading to an increase in the layer ordering. The Raman spectrum of graphon carbon black exhibited three signals at 1360, 1580 and 2700 cm^{-1}. The D band at 1360 cm^{-1}, attributable to the non-planar micro structure distortions, was found to be sensitive to the excitation source. The D band position changed from 1378 to 1330 cm^{-1} as the excitation source changed from Ar^{+} (457.9 nm) to Kr^{+} (647.1 nm).

The structure of graphite comprises of layers of carbon atoms. With in each layer, the carbon atoms are arranged in a two dimensional network of regular hexagons. The C-C bond in a graphitic plane is 0.142 nm characteristic of hexagonal aromatic carbon structure. The distance between each of the adjacent layers is 0.335 nm [22]. Graphite crystals are susceptible to disorder along the c-axis. Such a disorder is because of the weak interaction between adjacent layers in the graphitic lattice. On the contrary, a high degree of order is maintained with in the individual layers containing hexagonal arrangement of carbon atoms. Presence of such a high degree of order is because of the strong C-C bonding with in each of the graphitic layers. Such a peculiar disordered and ordered arrangement of carbon atoms with in the same material results in a condition known as turbostratic stacking where in random relative orientation of successive layers

of carbon atoms is present [22]. Raman Spectroscopy is an important tool in characterizing such disordered graphitic carbon materials.

Typical Raman spectra of some noncrystalline graphitic carbon materials, namely, glassy carbon, diamond – like carbon, coke and char coal are shown in Fig. 20. a. The term graphitic means carbon atoms which are three coordinated and are bound by sp^2 type bonding orbitals and not to do with the stacking of layers along c direction.

What is glassy carbon?

The structural model of glassy carbon is schematically represented in Fig. 19. Glassy carbon is produced by the thermal degradation followed by the controlled carbonization of natural or artificial cellulose. Various phenol-based or furfuryl alcohol – phenol copolymers also yield glassy carbon materials upon thermal degradation followed by carbonization. Glassy carbon is a hard, smooth and shiny non-graphitizable carbon of low open porosity. Glassy carbon contains high closed porosity which is revealed by the low specific surface area (0.1 – 1 m^2/g) and low density (1.4 – 1.5 g/cm^3). As the glassy carbon cannot be machined, the objects of glassy carbon are to be shaped before being subjected to heat treatment.
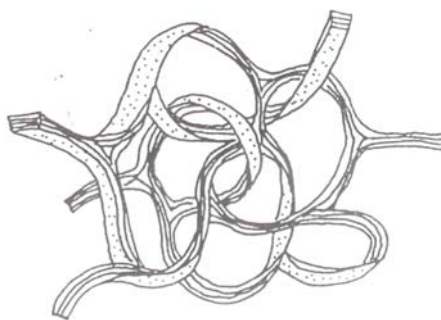

Fig. 19. Schematic representation of the structural model for glassy carbon (reproduced from ref. 114)

The most striking difference between the glassy carbon and artificial graphite is the extremely low permeability of glassy carbon to gases owing to closed voids or porosity.
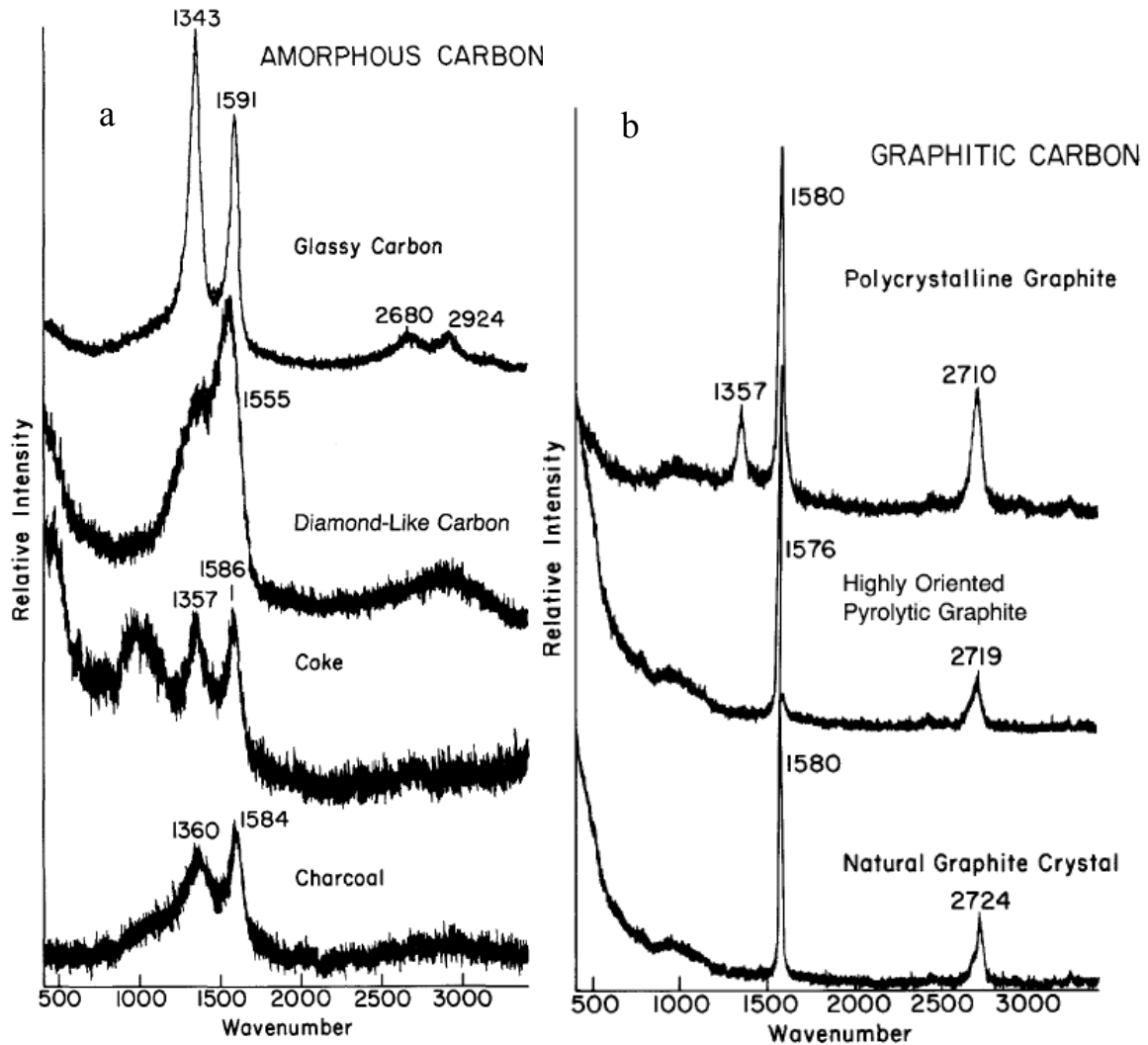
Raman spectra of various non-crystalline carbon materials are shown in Fig. 20. (a). Presence of a pair of bands around 1357 and 1580 cm^{-1} is characteristic of disordered polycrystalline or non crystalline graphite carbon materials. The band near 1357 cm^{-1} is

designated as D band where as the band at 1580 cm^{-1} is designated as G band. Depending on the structure of the carbon material the line width as well as the I_D/I_G (Raman intensity ratio) varies. In the case of glassy carbon, the Raman lines were narrow unlike the broad bands seen in the spectra of highly disordered carbon like char coal and coke. The band at 2700 cm^{-1} (split as doublet in the case of glassy carbon) is a result of the second order phonon. The first order Raman lines (at around 1357 and 1580 cm^{-1}) are related to the structural ordering with in the carbon sheets (individual layers of carbon with hexagonal arrangement of carbon atoms). The second order Raman lines (at 2680, 2700 and 2924 cm^{-1}) are related to the disorder in the stacking of carbon layers along c-axis. The presence of disorder with in the carbon layer can be located by the broadening of the G band.

Raman spectra of polycrystalline graphite, highly oriented pyrolytic graphite and natural graphite crystal (single crystal) are shown in Fig. 20 (b). The Raman spectrum of natural graphite crystal showed two characteristic features:, a sharp intense band at 1580 cm^{-1} and another slightly broader and lower intensity band in the range of 2710 – 2724 cm^{-1}.

The band at 1580 cm^{-1} is attributed to the E_{2g2} C-C stretching mode. The signal in the range of 2710 – 2724 cm^{-1} was attributed to the two phonon (second order phonon) band. Similar features (an intense sharp band at 1576 cm^{-1} and a broad band of relatively lower intensity at 2719 cm^{-1}) were observed in the case of highly oriented pyrolytic graphite. In the case of polycrystalline graphite, in addition to two signals at 1580 and 2710 cm^{-1}, a slightly broader band with lower intensity is observed at 1357 cm^{-1}. Such a band at 1357 cm^{-1} results only from well crystallized graphites with small partical size. Rao *et al.,* [169] have observed two distinct bands located at around 1360 and 1580 cm^{-1} in the Raman spectrum of activated carbon fiber. The peak around 1580 cm^{-1} was attributed to the E_{2g2} Raman-allowed graphitic (G) peak associated with zone centered phonon. In the presence of disorder, the selection rules for Raman –active modes are relaxed. As a result non-zone centered peaks such as those observed in at 1360 cm^{-1} (D, disorder, line) because of the presence of disordered carbon are observed. Upon heat treatment of the activated carbon fiber, Rao *et al.,* [169] have observed a decrease in the intensity of the disorder induced D band relative to the G peak at 1580 cm^{-1}. In addition,

the half width at half maximum (HWHM) of the G band too decreased upon heat treatment indicating graphitic ordering and suppression of disorder upon heat treatment at high temperatures.

Fig. 20. Raman Spectra of (a) various non-crystalline, mainly graphitic, carbons and (b) crystalline graphites (reproduced from ref. 22)

Fung *et al.,* [168] have observed two bands near 1360 and 1620 cm^{-1} in the Raman spectrum of activated carbon fibers. The band at 1360 cm^{-1} was attributed to the disorder induced peak where as the other band at 1610 cm^{-1} was attributed to the presence

of graphitic carbon resulting from the E_{2g2} Raman-active mode of graphite. The later peak is generally termed as Breit-Wigner-Fano peak. The Raman intensity ratio's $R(I_{1360}/I_{1600})$ for activated carbon fibers, namely, FRL10, FRL15, FRL20, FRS12, FRS15, FRS20, ACP10, ACP15, ACP 20, ACP30 were found to be 1.89, 1.90, 1.92, 1.67, 1.69, 1.70, 1.69, 1.81, 1.70 and 1.84 respectively.

Manivannan *et al.,* [146] have observed two lines in the Raman spectra of activated carbon materials, namely, GX203 (coconut shell), P1400 (wood) and Med50 (coconut shell). The Raman intensity ratios R (I_{1360}/I_{1600}) were found to be 1.5, 1.4 and 1.7 for the above mentioned carbon materials. Li *et al.,* [175] have prepared ultrafine carbon powder from carbonaceous sol-gel by super critical fluid drying. The Raman spectrum of the ultrafine carbon powder contained two characteristic signals at 1372 cm^{-1} (D line) and 1602 cm^{-1} (G line). The D and G lines are a result of the A_{1g} and E_{2g} modes respectively. Upon heat treatment of the carbon material at 2873 K, the maximum intensity positions of the D and G lines shifted from 1372 and 1602 cm^{-1} to 1348 and 1580 cm^{-1}. Such a shift of the D and G bands to lower wave number values is a result of the increase in the micro crystalline size upon heat treatment. Also a narrowing of the D band was observed upon heat treatment of the ultrafine carbon powder which too was attributed to the increase in the micro crystalline size of the carbon powders [175].

Hee Jin Jeong *et al.,* [176] have produced vertically aligned carbon nanotubes (CNT's) using C_2H_2 as carbon source using thermal chemical vapour deposition. Si substrate coated with Ni placed parallel to Pd was used as dual catalyst. Tungsten wire filament was employed. The CNT's grown at three different temperatures, namely, 823,873 and 1023 K were analyzed by Raman Spectroscopy to know the effect of temperature on the defect concentration as well as on the extent of graphitization. Two distinct bands at 1290 cm^{-1} (D band) and 1602 cm^{-1} (G band) were observed in the CNT's grown at 823,873 and 1023 K. But the stricking difference in the features of the Raman Spectrum is that with an increase in the temperature of CNT growth the two bands at 1290 and 1602 cm^{-1} became narrower and the area under both the bands decreased indicating a decrease in the defect in the wall of CNT's with an increase in growth temperature. In addition, the intensity of the G band is larger in the case of CNT's grown

at high temperature (1023 K) indicating the formation of a complete hexagonal CNT structure.

Jieshan Qiu *et al.,* [177] have produced highly graphitized carbon with ball like morphology and high carbon content (99.5 wt.%) from a mixture of coal powder (Anthracite) and coal tar using 5 wt.% Ni catalyst. The degree of graphitization was evaluated from the UV- Raman studies. The UV – Raman spectrum of the carbon microballs contained two specific and remarkable Raman signals at 1582 cm^{-1} and 1400 cm^{-1}. The signal at 1582 cm^{-1} was attributed to C-C bond stretching mode characteristic of graphitic carbon (G band). The band at 1400 cm^{-1} could not be attributed to any known carbon features. The intensity of the signal at 1350 cm^{-1} typical of disordered carbon (D band from defects and disorder in carbon structure) was almost negligible giving a I_D/I_G (Raman Intensity Ratio) value of 0.25 implying the highly graphitized nature of the carbon microballs with large graphitic crystallites.

Vilas Ganpat Pol *et al.,* [144] have produced non-graphitic carbon from mesitylene with spherical morphology possessing carbon content greater than 99 wt.% and a specific surface area value of 8 m^2/g. The micro – Raman spectrum of the carbon material showed two bands centered around 1340 and 1596 cm^{-1} corresponding to the disordered and graphitic carbons respectively. The Raman intensity ratio (I_{1340}/I_{1596}) was found to be 0.8 indicating that the carbon material possesses amorphous carbon structure with high content of lattice edges or plane defects.

Indra Neel *et al.,* [178], using Confocal Raman Spectroscopic studies, have analysed the microstructural changes and the extent of crystallographic disorder (concentration of lattice defects in the graphitic structure) in the activated carbon materials produced from Calotropis Gigantia by employing ZnCl$_2$ as activating agent. The Raman spectra, shown in Fig. 21., resulting from activated carbon materials produced with varying the impregnation ratios of the activating agent (ZnCl$_2$) to the char (wt./wt.%), namely, 1, 2, 3, 4 and 5, were recorded on Confocal Raman instrument (CRM 200) using Ar ion laser (514.5 nm) as irradiation source.

Irrespective of the amount of the activating agent, all the carbon materials, showed two first order Raman lines. Those lines that appear in the region of 1200 – 1600 cm^{-1} are termed as first order Raman lines. On the contrary ,the Raman lines that appear

in higher region, typically in the range of 2400 – 3300 cm^{-1} are termed as second order Raman lines. The information derived from the features of first order Raman lines is different from the information deduced from the feature of the second order Raman lines and both of them are important to access the structure order or disorder in the carbon structure whether it be amorphous or graphitic. First order Raman lines indicate only the structural order or disorder with in the carbon sheet or layer, i.e., carbon plane along a-axis. First order Raman lines are silent about the stacking order or disorder in carbon structure. On the contrary, second order lines hold information on the structural (stracking) disorder along the crystallographic c-axis [179].

The two first order lines centered around 1590 and 1348 cm^{-1} are attributed to the graphitic and disordered carbon structure. The term "graphitic" means carbon atoms which are three coordinated and are bound by sp^2 type bonding orbitals. The term "graphitic" has nothing to do with the stacking of layers along c - direction. The disorder in the carbon sheet may be because of the non-planar microstructure distortions or because of the disorganized regions near the crystal edges. Lattice defects such as edge dislocation and lattice vacancies too contribute to the band at 1348 cm^{-1}.
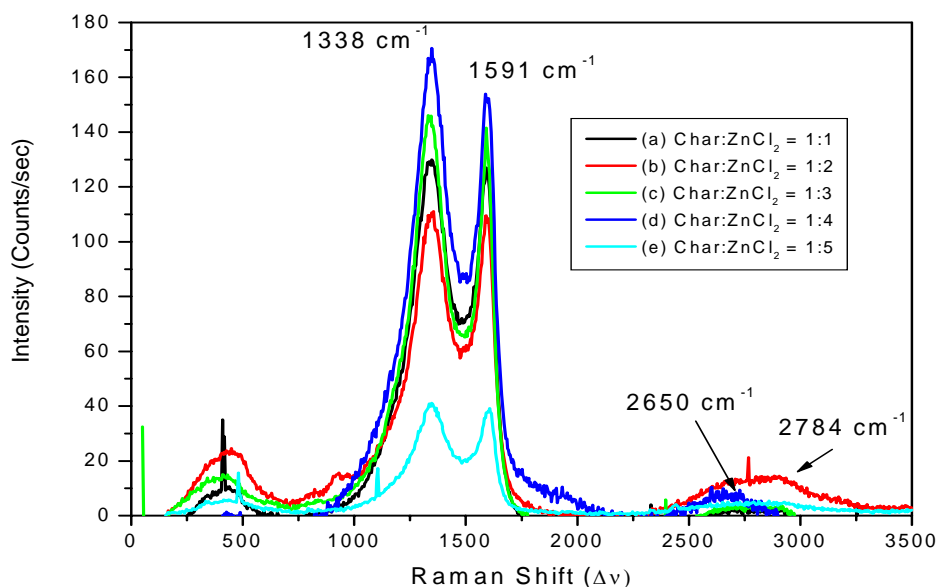
Fig. 21. Confocal Raman spectra of activated carbon materials prepared from Calotropis Gigantea with a Char to ZnCl$_2$ ratio (wt./wt.%) of (a) 1:1, (b) 1:2, (c) 1:3, (d) 1:4 and (e) 1:5 [reproduced from ref. 178]

Table 9. Structural parameters of the activated carbon materials from Calotropis Gignatea activated with $ZnCl_2$ deduced from Raman Spectra

S. No.	Sample	$ZnCl_2$: C (wt./wt.%)	Peak Intensity Frequency, v_x, cm^{-1}		$R = I_D/I_G$	L_a (nm) = 4.4/R (From Raman)	L_a (nm) (from XRD)
			G band	D band			
1	[1]AC1	1	1591	1348	1.40	3.14	3.94
2	AC2	2	1591	1355	1.42	3.09	3.50
3	AC3	3	1591	1331	1.33	3.30	3.96
4	AC4	4	1587	1348	1.48	2.97	3.72
5	AC5	5	1606	1348	1.53	2.87	3.80

In general the band around 1348 cm^{-1} attributable to disordered carbon structure with in the carbon sheet is termed as D band and the Raman signal around 1580 cm^{-1} attributable to the graphitic ordering (with in the layer of carbon) is designated as G band. The G band is because of the E_{2g} Raman active mode arising from the C-C stretching where as the D band results from the A_{1g} Raman mode. Important information extracted from the Raman spectra in Fig. 21. are summarized in Table 9. The Raman intensity ratio which is a measure of the extent of disorder (quantity of defects and vacancies and dislocations) is found to decrease initially upto the activating agent to char impregnation ratio of 3 beyond which the R value increased. The disorder induced into the carbon structure is increased beyond a $ZnCl_2$ to char (wt./wt.%) ratio of 3. An inverse proportionality relation is observed between the value of R and the stack width L_a (crystallite size along a-axis). The position of the D band (peak intensity and position) as well as the relative intensity of D band is found to be structure sensitive. An increase in the frequency value of the D band was correlated to the decrease in the crystallite size (L_a) and vice verse. A strong correlation between the structural parameters deduced from XRD studies (Table 8) as well as Raman studies (Table 9) was observed as the two afore mentioned techniques are mutually complimentary to each other. Interestingly, the L_a values ($L_a = 44/R$ in Å) deduced from the relative intensity of the D band of the activated

carbon materials correlated well with the L_a values obtained from XRD studies using Scherrer equation (Table 8). This emphasises that XRD and Raman studies are equally informative on the crystallographic disorder in carbon structure. But it should be noted that the measurement of line width from the XRD is more accurate than the measurement of the integrated peak intensity values deduced from the Raman spectra. As a result the La values derived from XRD are more reliable than those deduced from Raman spectra. In addition, the integrated intensity values from Raman spectra are sensitive to the choice of the base line. As a result, the Raman intensity ratio's (R) shown in Table 9 are uncertain upto ± 7 %.

Details of the surface morphology of the actaivated carbon material from Calotropis Gigantea using $ZnCl_2$ activation ($ZnCl_2$ to Char (wt./wt.%) = 3) was obtained from High resolution scanning electron microscopy (HR SEM) studies. HR SEM image of activated carbon material using FEL, Model: Quanta 200 scanning electron microscope at a magnification of 3000 x and at a scanning voltage of 30 kV is shown in Fig.22.
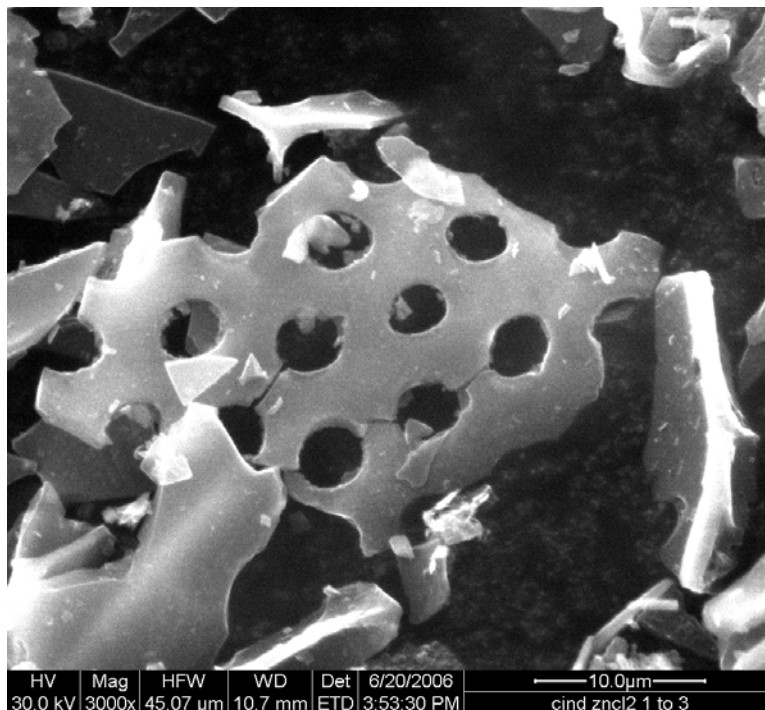
Fig. 22. SEM image of Activated Carbon from Calotropis Gigantia activated with $ZnCl_2$ (wt/wt. % ratio of Char:$ZnCl_2$ is 1:3) (reproduced from ref. 160)

Well aligned uniform cylindrical pores of diameter (size) 2.4 μm are observed on the carbon surface as shown in Fig. 22.

Recently several research groups have exploited the method of $ZnCl_2$ activation to activate carbon precursors like Rice husk [180], Corn cob [181], Coffee residue [182], Tectona Grandis sawdust [183], Apricot stone [184], Cherry stones [14], Sugar beet bagasse [185], Coconut coir pith [186] and Tamarind wood [187]. The above mentioned studies highlight the usefulness of $ZnCl_2$ activation in the production of activated carbon from diverse carbon precursors.

Apart from alkalimetal hydroxides, alkali metal carbonates and transition metal salts, activating agents belonging to the class of alkaline earth metal salts [188, 189] , and mineral acids, such as, H_3PO_4 [190 - 213], HNO_3 [214 -222], and H_2SO_4 [223 - 225], have been extensively exploited for the chemical activation of carbon materials. Even though less advantageous, physical activation methods based on steam [43, 221 – 232], air [233 – 238] and CO_2 [64, 65, 67, 94, 135, 239 – 264] as activating agents have proven to be useful for the activation of caron materials.

Carbon Materials (as catalyst support) for Electrochemical Applications

III. 1. Challenges in Development of Fuel Cell Anode Electrocatalyts

Fuel cells are electrochemical devices comprising of an electrolyte in contact with an anode (where oxidation of fuel takes place) and a cathode (where reduction of oxygen takes place). In a fuel cell, the chemical energy of the fuel is directly converted to the electrical energy through a chemical reaction [265]. In addition to the electrodes (anode where oxidation of fuel takes place and cathode where reduction of oxygen takes place), membrane, gas-diffusion layer and bipolar plates are the other important components of a fuel cell.

Fuel cells are efficient and environmentally acceptable energy conversion devices. Electric current is generated in the fuel cell by the direct electrochemical oxidation of either hydrogen (proton exchange membrane fuel cell, PEM) or MeOH (Direct Methanol Fuel Cell, DMFC) or any other hydrocarbons which act as fuel. The electrochemical processes that yield energy are free from pollution. Water formed during the operation of the device is beneficial in space travel and submarines. Applications of fuel cells are diverse ranging from stationary (individual homes or district schemes) or mobile [transportation (cars, buses), mobile phones and lap top computers] [266].

Direct methanol fuel cells (DMFC's) are considered as potential and promising low-temperature green power sources for automobiles, residence and portable electronic devices. Insufficient activity and durability are among several other problems involved in the commercial applications of these fuel cells. Pt in nanodimensions is the only effective catalyst that promotes the adsoption/dissociation of MeOH in acid medium. Several attempts have been made to improve Pt utilization, activity and durability in DMFC technology. Some of the approaches include alloying Pt with other transition

metals (Ru, Os, W), promoting Pt with metal oxides, optimizing the composition, structure, size and shape of Pt based nanoparticles [267].

Carbon materials are interesting candidates for supporting Pt particles. The supporting carbon material influences the electrochemical properties of Pt-based electrocatalysts. In fact the nature of carbon material (oxygen surface functional groups, electronic conductivity, pore structure, morphology, electro-chemically accessible surface area) determine the electrochemical performance of electrode catalysts. Electronic conductivity, surface area, microstructure, macromorphology, corrosion resistance and cost are some important properties that determine the suitability of a carbon material for electrode applications.

Carbon black, Vulcan XC-72 has been the most widely used support material for Pt. Any breakthrough in the commercialization of DMFC's is possible only by significant improvements either in the active Pt metal as well as the support carbon material.

Platinum group metals (PGM's) were most widely used for electrode applications. There are two major problems involved in this. One is CO poisoning [5] (Phosphoric acid fuel cells can with stand upto 2 % CO in the fuel stream. But Proton exchange membrane fuel cells can only withstand ppm levels of CO). The second problem is the high cost restricting the rapid and wide spread commercialization of fuel cells. Reduction in the cost of catalyst is one of the key objectives of fuel cell research.

There are two approaches in which one can solve the above two problems. One approach is to find suitable alternative (partial or complete) to the active component i.e., Pt and the second approach is to find suitable alternative to Vulcan XC 72 which is the best carbon support material commercially used todate. To over come the problem of CO poisoning several attempts in the direction designing CO tolerant anode electrocatalysts have been made. Au, in nano regime, is one of the best known and active catalyst for CO oxidation particularly and interestingly at low temperatures. It means alloying Au with Pt can result in a bifunctional catalyst where Au assists the removal of CO and Pt facilitates with more ease and spontaneity the main fuel cell reaction as the poisoned sites (Pt sites where CO is chemisorbed strongly) are being regenerated by the presence of Au. Pt has also been alloyed with, oxophilic metals, either Ru or Mo or Sn. Ru acts as a promoter

for CO oxidation. The function of Ru was explained in terms of either bifunctional mechanism (Ru promotes CO oxidation of the strongly bound CO on Pt by supplying oxygen source Ru-OH$_{ads}$) or by the ligand field effect (the energy level of the PtRu alloy catalyst is changed in such a way that the binding strength of CO on Pt site is weakened and correspondingly the oxidation over potential is reduced). Yicheng Liu *et al.,* [268] showed an example of achieving improved performance of the electrocatalyst compared to the standard E-TEK catalyst (Pt-Ru/Vulcan XC-72 R) simply by changing the method of preparation of the catalyst using reverse micellar method showing another avenue to generate improved performance in the MeOH oxidation electrocatalysts [268].

Samant *et al.,* [269] in an example generated a catalyst more active than 10 wt.% Pt/Vulcan XC 72 R just by changing the support i.e., by replacing Vulcan XC 72 R with mesoporous carbon produced by sol-gel method.

Even though systems based on PtRu (ternary systems like PtRuOs, PtRuW, PtRuMo and quaternary systems like PtRuSnW or PtRuOsIr) supported on carbon are regarded as the state-of-the art materials for electrocatalysts, improvement is anticipated in the generation of effective and inexpensive electrocatalysts for the electroxidation of MeOH for practical DMFC applications [270].

The electroxidation reaction of methanol at the anode can be represented as follows [271]:

$$CH_3OH + H_2O \longrightarrow CO_2 + 6\ H^+ + 6\ e^- \qquad E^0 = 0.02\ V$$
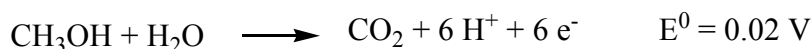
III. 2. Activated Carbon Materials from the Limonea Acidissima Shells for DMFC applications

Activated carbon materials from natural sources have been widely exploited for sorption and catalytic applications. So far no attempt has been made in literature to exploit the carbon materials derived from natural souces for high end applications, particularly for fabrication of electrodes for fuel cell applications. Viswanathan *et al.,* [178] have exploited that carbon material produced from Limonea Acidissima shells as support for Pt for the electroxidation of MeOH for Fuel cell electrode applications.

III. 2.1. Carbon Material from Limonea Ascidissima Shell by KOH Activation

Limonea Acidissima (Wood Apple) Shells were conceived for the first time as a source for activated carbon. The fruit, Limonia Acidissima, is native to India and other Asian countries. Limonia Acidissima is also called as Feronia Elephantum, Feronia Limonia, Hesperethusa Crenulata, Schinus Limonia, Wood apple, Elephant Apple and Curd fruit. The shells of Limonia Acidissima (wood apple) have features bearing close resemblance tho coconut shells. Activated carbon from Limonea Acidissima is produced by the method of KOH activation.

Typical method of synthesis of carbon material involve soaking of known amount (50 g) of dried shells of Limonea Acidissima in 100 ml of 50 wt.% KOH solution for 2 h. Excess KOH solution is then decanted. The shells soaked in KOH solution were then dried in air oven at 150 °C followed by subjecting the same to themochemical activation in N_2 atmosphere at 800 °C for 2 h. The char thus obtained was subsequently treatead with conc. HNO_3 with the char to conc. HNO_3 ratio (wt./wt.%) being 1:5. There are two advantages in treating the char with HNO_3. One advantage being the effective removal of traces of activating agent and its decomposed products and the other advantage is the generation of oxygen rich surface functional groups.

The activated carbon material produced was systematically characterized by various physico chemical techniques. Textural properties of the carbon material were obtained from sorptometric studies (BET sorptometry). XRD and Confocal Raman spectroscopic studies provided details of crystal structure, crystallite size and the extent of defects and disorder in the carbon material. High resolution scanning electron microscopic studies and the accompanying energy dispersive spectroscopic studies revealed the surface morphology as well as the elemental composition of the carbon material produced. The details of the concentration of the unpaired electrons (spin concentration) were obtained from Electron Paramagnetic Resonance Spectroscopic studies. The richness of oxygen surface functional groups generated upon HNO_3 treatment is viewed though FT – IR studies. After thorough characterization of the carbon material (designated as C_{WA} – WA meaning wood apple), the same is successfully exploited as support for Pt for carrying out the electro oxidation reaction of methanol

(MeOH) which is of technological significance bearing importance in the commercial exploitation of direct methanol fuel cells.

N$_2$ adsorption – desorption isotherm resulting from the activated carbon from Limonea Acidissima is shown in Fig. 23. The corresponding pore size distribution curve (BJH) is also shown as the insert of Fig. 23.
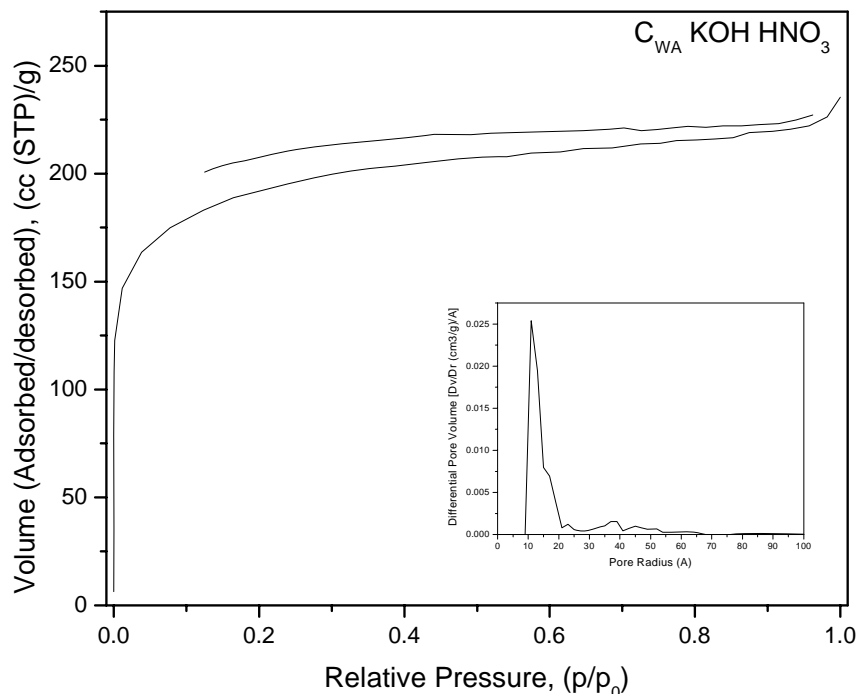

Fig. 23. N$_2$ adsorption-desorption isotherms of carbon materials prepared from Limonea Acidissima; the corresponding pore size distribution of the activated carbon material is shown in the insert (reproduced from ref. 178]

The isotherm shown in Fig. 23. is of type I characteristic of a microporous material. The pore size distribution indicates that the pore dimensions are lower than 2 nm in the activated carbon material. Thus the activated carbon material obtained by KOH activation of the shells of Limonea acidissima is of micorporous nature. The textural properties of the activated carbon material deduced from the N$_2$ adsortion-desorption isotherm shown in Fig. 23. are summarized in Table 10.

Textural properties of activated carbon material from Limonea Acidissima

S. No.	Sample	S_{BET} (m^2/g)	V_P (cm^3/g)	Mean Pore Diameter[i] (nm)
1	Activated carbon, C$_{WA}$	698	0.35	2.0

i. Mean Pore Diameter, d = 4V/A (in nm)

The X-ray diffraction curve resulting from the activated carbon material from Limonea Acidissima is shown in Fig. 24. Two broad diffraction peaks centered around 2θ values of 24 and 43° which are respectively attributed to the reflections from the (002) and (10) diffraction peaks of carbon material.

The values of average crystallite sizes along the c-axis (stacking axis) and the a – axis were determined using Debye – Scherrer equation. The shape factor, k, values of 0.89 and 1.84 were employed for the calculation of L_c and L_a values respectively. The diffraction angles as well as the full width at half maxima values corresponding to the diffraction planes of (002) and (10) were employed for the calculation of L_c and L_a values respectively. The L_c and L_a values were found to be of the order of 1.1 nm and 3.656 nm respectively. The values of c and a for typical graphitic carbon structure are 0.0670 nm and 0.2461 nm respectively [272, 273].
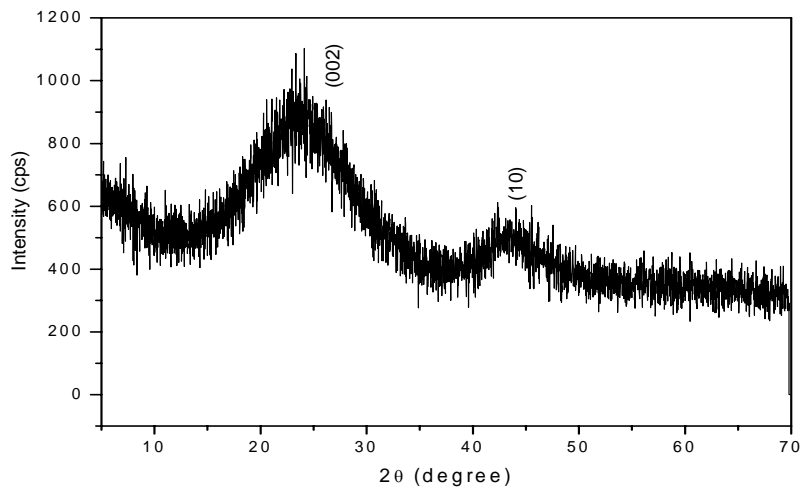
Fig. 24. XRD pattern of carbon material prepared from Limonea Acidissima using KOH activation method

The magnitude of L_C and La values of the activated carbon materials from Limonea Acidissima (obtained by KOH activation) indicate that the carbon material contained roughly about 2 cell length along the c-direction and nearly 15 cell lengths along the a – direction. The structural parameters deduced from the X-ray diffraction pattern shown in Fig. 24 were summarized in Table 11.

Table 11. Crystallographic structural details of activated carbon material from Limonea Acidissima using KOH activation method

S. No.	Sample	d_{002} (nm)	*L_c (nm)	*L_a (nm)
1	Activated Carbon, C_{WA}	0.377	1.1	3.656

* For graphitic structure the values of c and a are 0.0671 and 0.2461 nm

Details of structural disorder as well as the crystallographic parameter of the activated carbon material produced by the KOH activation of the shells of Limonia Acidissima were obtained from the Confocal Raman spectrum shown in Fig. 25. Two characteristic Raman peaks centered around 1348 and 1591 cm-1 were observed in the confocal Raman spectrum. The two afore mentioned bands designated as D (disordered) and G (graphitic) bands were attributed to the A_{1g} and E_{2g} Raman active C-C vibration modes with in the graphitic layer. The Raman peaks at 1348 and 1591 cm^{-1} were called as first order Raman peaks. Such peaks hold information only about the ordering of carbon atoms with in the layer or sheet of carbon but remain silent about the way the sheets or layers are stacked one over other in the c-direction. The details of the structural parameter of the activated carbon material deduced from the confocal Raman spectrum in Fig. 25. are summarized in Table 12.

The ration of intensity of Raman spectral peaks (I_D/I_G) which is the ratio of the integrated intensities of the D and G bands is a measure of the extent of disorder with in a carbon layer. The R value for the activated carbon material from Limonia Acidissima was

found to be 1.408 which is typical of disorder carbon materials like glassy carbon. The average crystallite size along the a - direction, L_a, can also be obtained from the value of
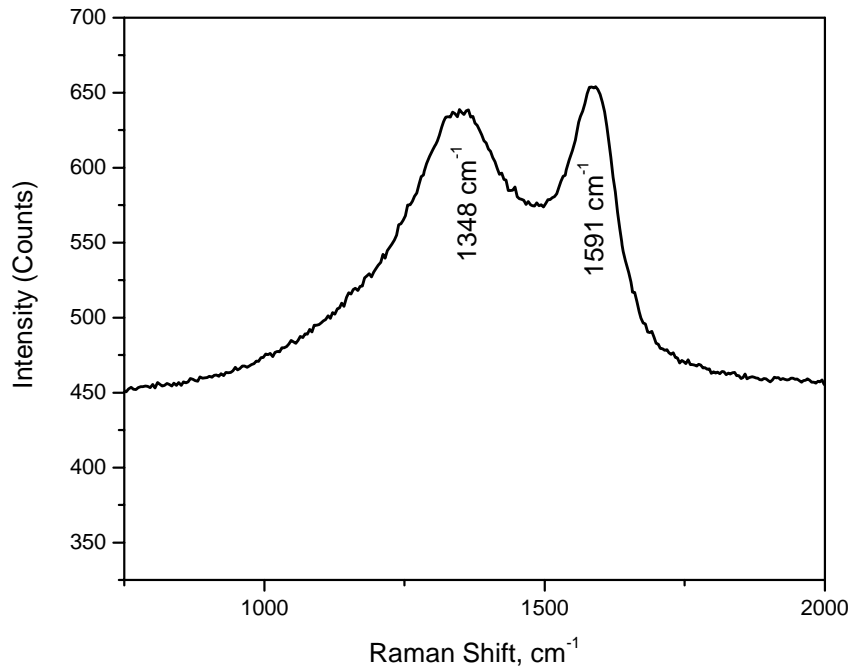

Fig. 25. Confocal Raman spectrum of activated carbon produced from Limonea Acidissima by KOH activation

Table 12. Structural parameters of the activated carbon material from Limonea Acidissima deduced from the confocal Raman spectroscopic studies

S. No.	Sample	Peak Intensity Frequency, v_x, cm^{-1}		$R = I_D/I_G$	L_a (nm) = 4.4/R (From Raman)	L_a (nm) (from XRD)
		G band	D band			
1	C_{WA}	1591	1348	1.408	3.125	3.656

Raman Intensity Ratio, R. The L_a value deduced from confocal Raman spectrum, 3.125 nm, is found to be in good agreement with that of the L_a value obtained from wide angle X-ray diffraction (L_a = 3.656 nm). The slight variation ($\approx$ 5 Å) in the L_a value obtained Confocal Raman spectrum and X-ray diffraction pattern is attributed to the ± 7 % error involved in the calculation of the integrated intensity values under the D band G band.

Since line width from XRD is more accurately determined compared to the integrated intensity values under the D and G in the confocal Raman spectrum, the L_a value obtained from wide angle X-ray studies is more reliable.
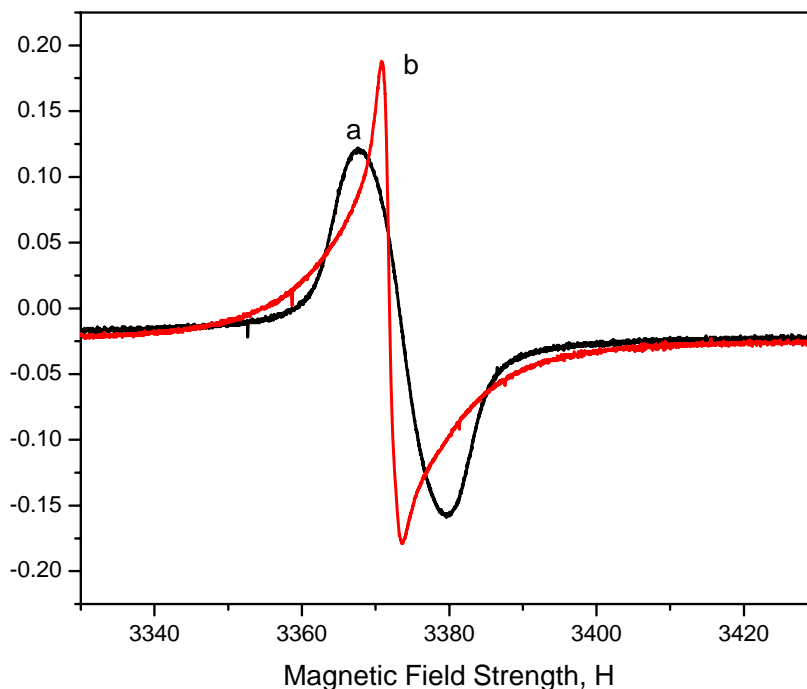

Fig. 26. EPR spectrum of activated carbon from (a) Limonea Acidissima by KOH activation and (b) DPPH (reference)

The Electron Paramagnetic Resonance (EPR) spectrum of activated carbon from Limonea Acidissima is shown in Fig. 26. The EPR spectrum was recorded on a X-band EPR spectromter operated at a microwave frequency of 9.2 GHz at room temperature using diphenyl picryl hydrazyl radical as external reference. The g value of the resonance signal from the activated carbon is 2.03095 which is close to the free electron g – value. The origin of the EPR signal is attributed to the presence of dangling bonds in the carbon structure. The concentration of unpaired spins was found to be 0.13×10^{19} spins/g of the carbon material.

Details of the surface morphology as well as the elemental composition of the activated carbon material were obtained using High Resolution Scanning Electron

Microscopy (HR SEM, FEL, Model: Quanta 200) equipped with Energy dispersive X-ray analysis facility (also called as Energy dispersive spectroscopy). scanning electron microscope at a magnification of 4000 x and 10, 000 x and at a scanning voltage of 30 kV.

(a)

(b)

(c)

(d)
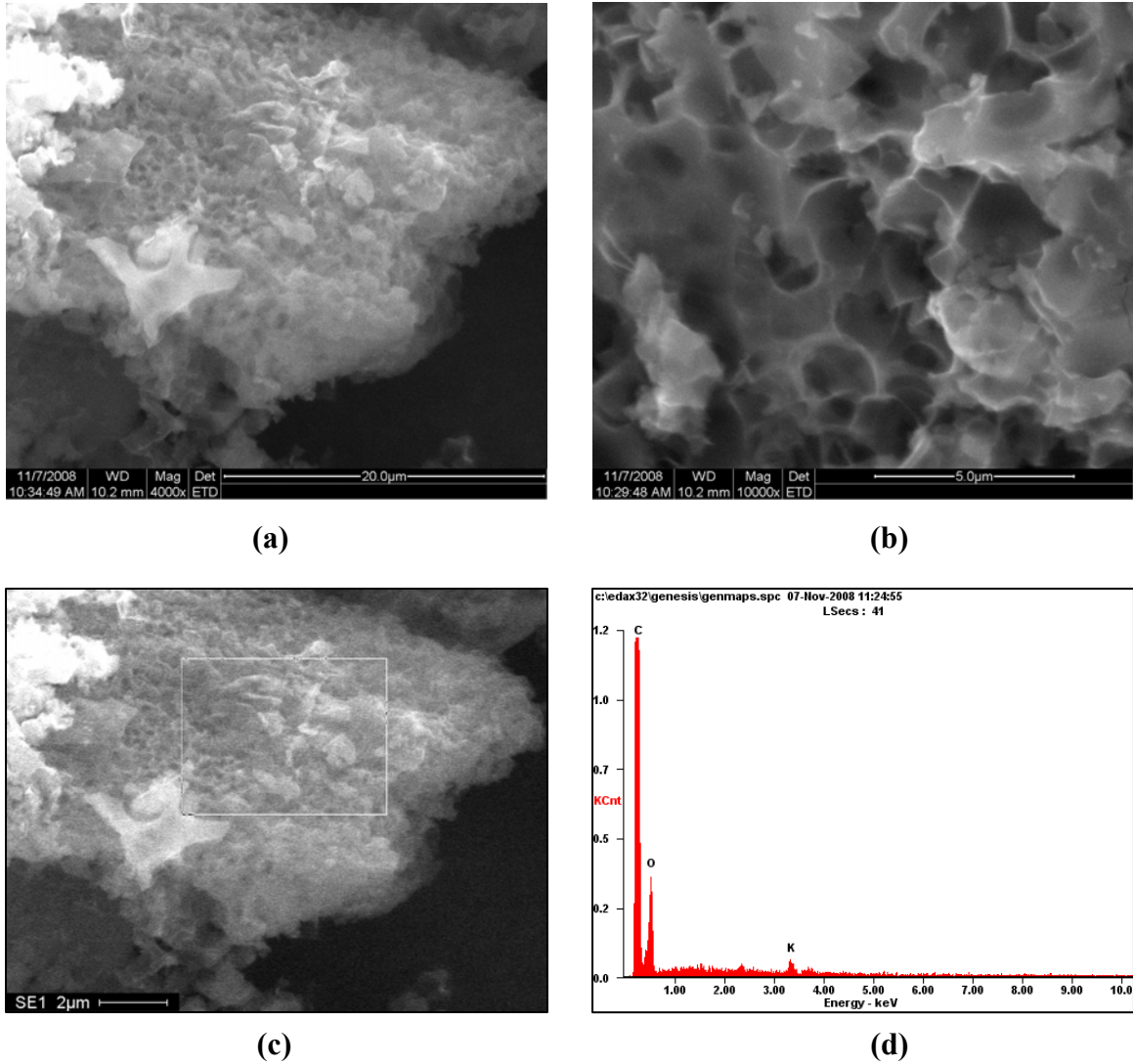
Fig. 27. SEM images and EDAX spectrum from the activated carbon material from Limonea Acidissima using KOH activation; at a magnification of (a) 4000 x, (b) 10, 000 x, (c) selected region for elemental analysis and (d) energy dispersive X-ray analysis spectrum

Highly heterogeneous and rough surface with continuous pore net work is viewed on the surface of the activated carbon produced from Limonea Acidissima. The pore network is clearly viewed at higher magnification (10, 000 x).

The chemical composition of the activated carbon material is determined using Energy dispersive X-ray analysis and the details are summarized in Table 13. A high corbon content of 74.84 wt.% is derivable from KOH activation of the shells of Limonea Acidissima. Inspite of treatment with HNO3, 0.45 wt.% K is inevitably present in the activated carbon.

Table 13. The elemental composition of the activated carbon material from Limonea Acidissima from EDAX

S. No.	Element	Wt. %	At. %
1	Carbon	74.84	80.02
2	Oxygen	24.70	19.83
3	Potassium	0.45	0.15

Fourier transform infrared (FT-IR) spectroscopy provides evidence for the presence of specific functional groups on the surface of carbon material. The FT – IR spectrum of activated carbon from Limonea Acidissima, C_{WA}, was recorded on Shimadzu photometer. The spectral range of analysis is $450 – 4000$ cm^{-1} with a resolution of 4 cm^{-1}. The spectrum was obtained in transmission mode at 20 scans. Pressed KBr pellets were prepared by grinding 200 mg of carbon samples with 0.5 g of KBr.

Several characteristics bands were observed in the FT – IR spectrum shown in Fig. 28. and each of the bands has been assigned to specific functional group based on the previous assignments made in literature. The details of band assignments to functional groups are shown in Table 14.
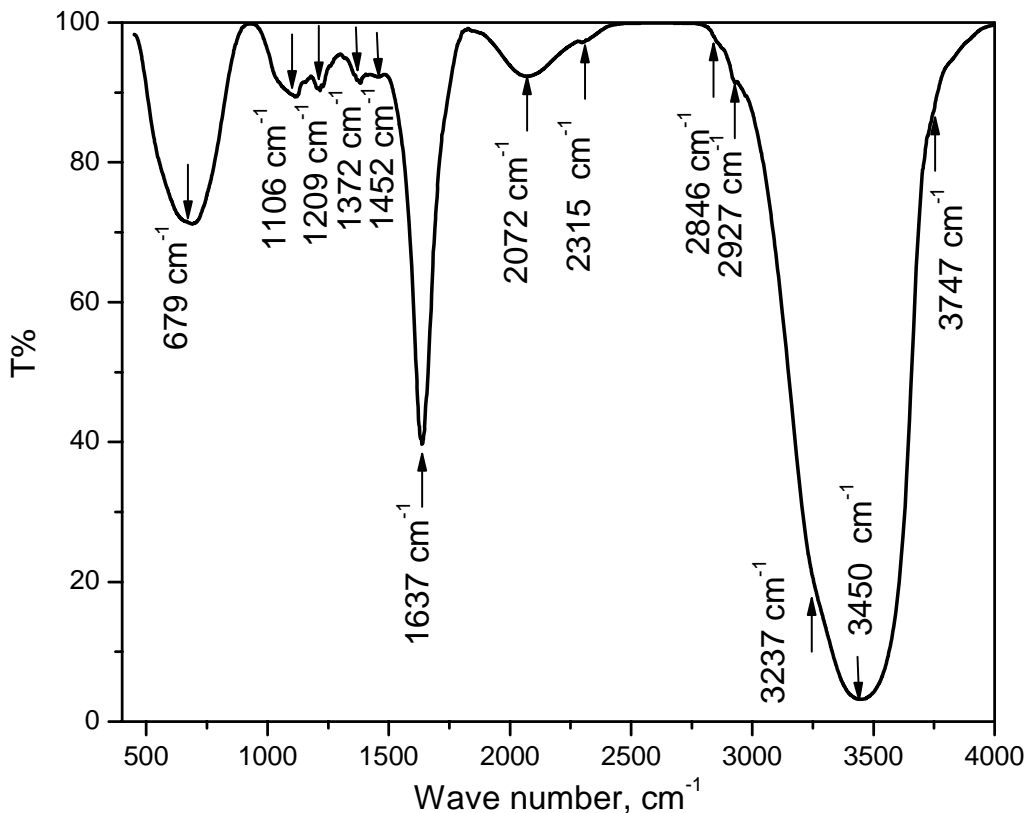
Fig. 28. FT – IR spectrum of activated carbon produced from Limonea Acidissima Shells using KOH activation

Even though a cluster of functional groups are present on the carbon surface, the prominent among them are a sharp and intense band centered around 1637 cm^{-1} which is attributed to the carbonyl (C=O) stretching vibration of quinone. The carbon surface is oxidized by treatment with Conc. HNO_3 leading to the generation of such Quinone type carbon functional groups which bear significance in the redox chemistry of carbon materials. Such carbonyl functional groups are known to be pronounced in the case of oxidized carbon materials rather than the original parent carbon material. In addition, a broad and intense band is observed in the range of 3200 – 3600 cm^{-1}, centered at 3450 cm^{-1} attributable to the O-H stretching vibration of surface hydroxylic groups as well as to the adsorbed water. The asymmetry of this band (a shoulder at lower wave number, 3237 cm^{-1}) indicates the presence of strong hydrogen bonding interactions.

Table 14. Assignment of FT – IR bands to specific oxygen containing surface functional groups of the activated carbon material

S. No.	Band position ν, cm^{-1}	Assignment	Reference
1	3747	Isolated –OH groups	[198, 205]
2	3450	O-H stretching vibration of surface hydroxyl groups and adsorbed water. Asymmetry (shoulder like feature at 3237 cm^{-1}) indicated presence of hydrogen bonding interaction	[198, 274, 275, 252, 225, 276, 277, 202, 2]
3	2927	Aliphatic, asymmetric C-H stretching vibration of methylene group	[198, 225, 202]
4	2846	Aliphatic, symmetric C-H stretching vibration of methylene group	[198, 225, 202]
5	2315	Ketone group	[278]
6	1637	C=O (carbonyl) stretching vibration in quinone	[274, 275, 252, 277, 182, 279, 220]
7	1452	In plane bending vibration of C-H of methylene group	[198, 205, 225, 202, 164]
8	1372	In plane bending vibration of C-H in methyl group	[198, 205, 225, 202, 164]
9	1000 - 1300	C-O stretching in phenols, alcohols, acids, ethers and esters	[198, 252, 277, 202, 210]
10	679	Out of plane deformation vibration of C-H groups located at the edges of aromatic planes	[275]

III. 2.2. Application of acativated carbon material from the shells of Limonea Acidissima for the fabrication of anode electrode catalyst for DMFC's

In general, high specific surface area carbon material is employed as support for Pt for fuel cell electrode applications. The choice of the support is connected with the possibility of dispersing the stable metal crystallites with favourable electronic and metal support interaction [280].

Reduction of the expensive Pt metal loading, enhancement of the long term stability of the electrode, improving the CO tolerance of the electrode, reduction of MeOH cross over through the polymer electrolyte membrane, improving the oxygen reduction kinetics, searching for non-noble metal based electrodes and designing of low cost and effective membrane are the typical challenges in the field of direct MeOH fuel cell research [281].

Lack of efficient and inexpensive electrocatalyst for MeOH oxidation is a challenge for the large scale utility of direct methanol fuel cells. Viswanathan *et al.*, [178] have devoted their efforts in designing cost effective and highly active electrocatalysts by developing new porous carbon material supports for Pt, as alternative to Vulcan XC 72, with suitable porosity and surface area which showed a substantial decrease in the loading of the active component (Pt) by increasing the Pt utilization in addition to being tolerant to CO poisoning.

To evaluate the suitability of the carbon material as support for Pt for the electro chemical oxidation of MeOH for DMFC applications, Pt supported carbon catalysts have been prepared by impregnating hexachloroplatinic acid in carbon material followed by reduction of Pt^{4+} to $Pt(0)$ in hydrogen atmosphere at 450 ºC for 2 h. Catalysts with different wt.% loadings, namely, 5, 10, 15 and 20 wt. %, of active component (Pt) on the carbon support were prepared by adding requisite amount of H_2PtCl_6 solution (7.7 mM, 1.0 g H_2PtCl_6. $6H_2O$ dissolved in 250 ml distilled water) to carbon support (C_{WA} and Vulcan XC 72 R)

X-ray diffraction studies on the carbon supported Pt catalysts provided details on the crystal structure, crystallite size and the lattice constant values of Pt metal loaded on

carbon support. The X-ray diffractograms of 5, 10, 15 and 20 wt.% Pt on carbon material obtained from the shells of Limonea Acidissima (wood apple) were shown in Fig. 29. Diffraction peaks characteristic of Pt metal with a face centered cubic structure are observed and the peaks are all indexed (111), (200), (220), (311) and (222) (JCPDS file No. 87-0647).
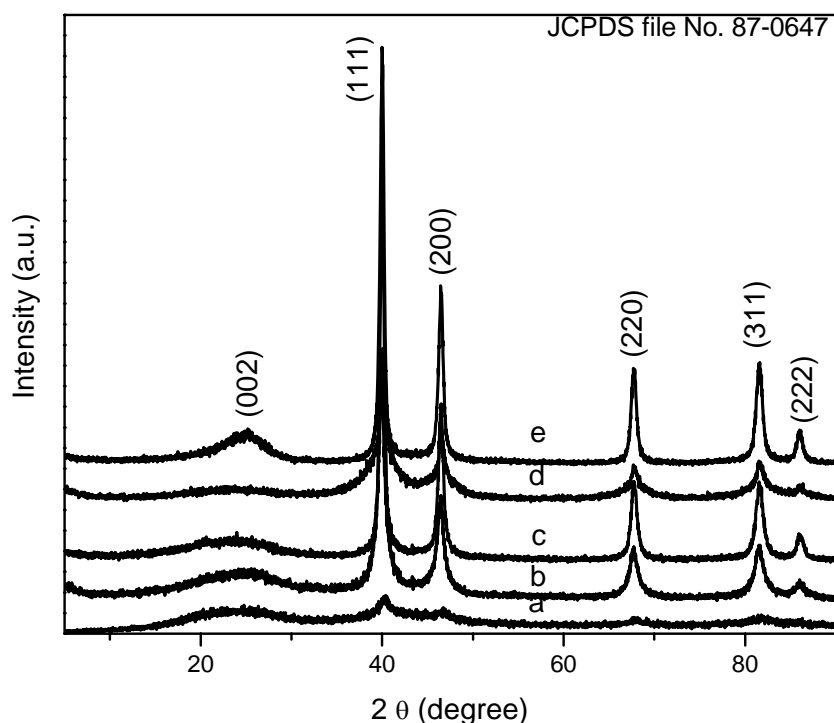

Fig. 29. X-ray diffraction patterns of (a) 5 wt.% Pt/C_{WA} (b) 10 wt.% Pt/C_{WA} (c) 15 wt.% Pt/C_{WA} and (d) 20 wt.% Pt/C_{WA} and (e) 20 wt.% Pt/Vulcan XC 72 R

Table 15. Crystallite size and lattice constant of Pt/CWA catalysts

Catalyst	Crystallite size (nm)	Lattice constant, a, (nm)
5 wt. % Pt/CWA	5.0	0.3897
10 wt. % Pt/CWA	10.2	0.3909
15 wt. % Pt/CWA	13.5	0.3907
20 wt. % Pt/CWA	10.4	0.3904
20 wt.% Pt/Vulcan XC 72	13.1	0.3909

The crystallite size and the lattice parameter values of Pt metal in the case of each of the catalysts is calculated and are summarized in Table 15. The broad diffraction peak centered around a 2θ value of 25 corresponds to the reflection from the (002) plane of carbon support. The crystallite size of Pt in different catalysts was calculated by using Debye-Scherrer equation [282]. The lattice constant value of around 0.39 nm correlated well with the FCC structure of Pt metal supported on carbon materials [283, JCPDS file No. 87-0647]. The mentioned value is in good agreement with that of the lattice constant value of pure Pt metal (0.3923 nm) [284].

The reflection from (220) plane of Pt metal is considered for the calculation of crystallite size as it is away from the region of the broad diffraction peak (from (002) plane) of carbon support. The crystallite size of Pt is found to be dependent on the Pt loading and also on the nature of the carbon support. With the same amount of Pt loading (20 wt.%), the crystallite size of Pt on carbon produced from Limonea acidissima shell is smaller (10.4 nm) than that of the crystallite size of Pt on Vulcan XC 72 R (13.1 nm) indicating better dispersion of Pt on the former support due to the richness of oxygen surface functional groups. Also the Pt crystallite size was found to be the least in the case of 5 wt.% Pt supported on carbon material from Limonea Acidissima indicating better dispersion of Pt particles on the support at lower Pt loadings. A strong correlation was found between the Pt crystallite size and the electooxidation activity of supported Pt catalysts.

In addition to the structural properties, crystallite size of the Pt dispersed on carbon, the textural properties of the electro catalyst (Pt/C_{WA}) too have an effect on the electrocatalytic activity of the supported catalysts. The textural properties (specific surface area, total pore volume, mean pore diameter) of the Pt/C_{WA} catalysts are investigated by sorptometry. The N_2 adsorption-desortion isotherms of carbon supported Pt catalysts with varying amounts of Pt loading (5, 10, 15 and 20 wt.%), recorded on a Micromeritics model ASAP2020 porosimeter, are shown in Fig. 30. All the catalysts exhibited typical type I isotherms characteristic of micorporous solids. This indicates that the pore texture of the support is retained and no collapse of pore texture has taken place upon impregnating Pt on to the support upto a loading of 20 wt.%.
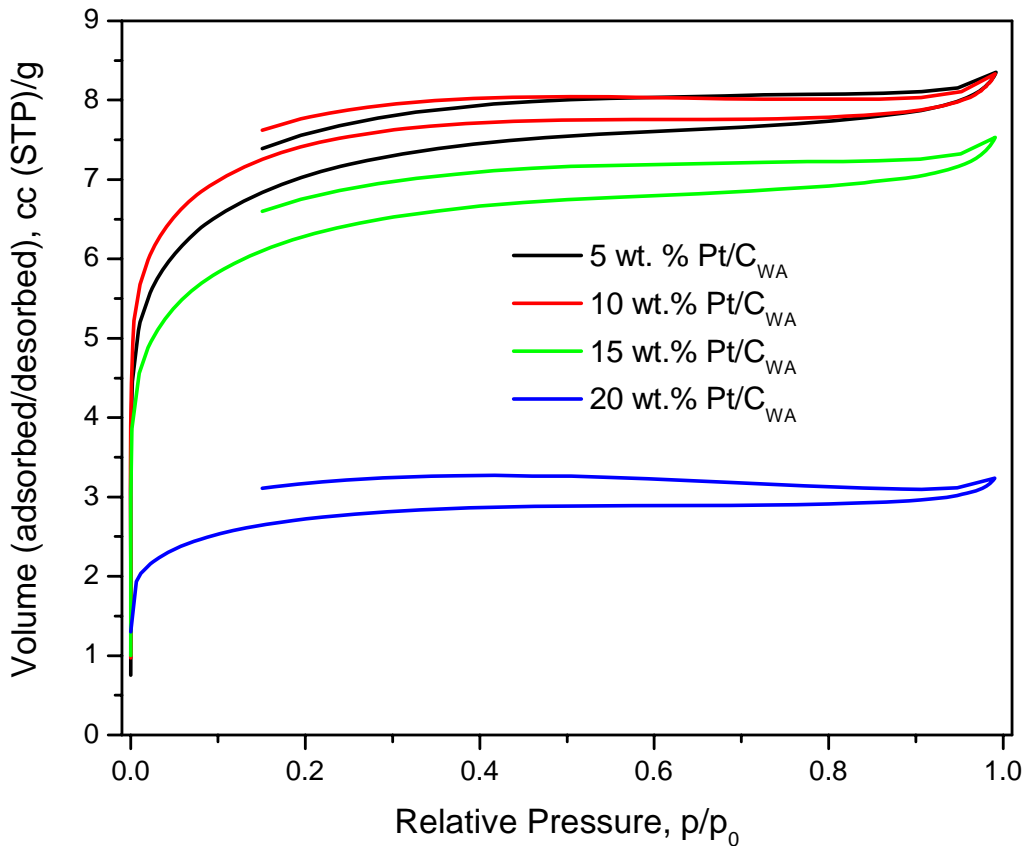
Fig. 30. N₂ adsorption-desorption isotherms of Pt/CWA electro catalysts (a) 5 wt.% Pt/C$_{WA}$, (b) 10 wt.% Pt/C$_{WA}$ (c) 15 wt.% Pt/C$_{WA}$ and (d) 20 wt. % Pt/C$_{WA}$

Another important observation is that the volume of N₂ (adsorbate) adsorbed, decreased drastically as the wt. % loading of Pt increased from 10 wt. % to 20 wt.% through 15 wt. % Pt over C$_{WA}$ support. 10 wt. % Pt/C$_{WA}$ showed similar sorption capacity of the adsorbate as that of 5 wt.% Pt/C$_{WA}$ even though it is expected to show lower sorption for N₂ compared to 5 wt.% Pt/C$_{WA}$. The observed discrepancy is because of the fact that, in the case of 5 wt. % Pt/C$_{WA}$ catalyst, the small crystallites of Pt (5.0 nm) were very finely dispered over the whole of the carbon support surface. Even though the dispersion of the nanocrystallites of Pt is advantageous, these small crystallites partially block the accessibility of the micropores to the adsorbate (N₂) and this phenomenon is more severe in the case of 5 wt.% Pt/C$_{WA}$. The non accessibility of the micropores to the adsorbate is also evident from the micro surface area value of 5 wt.% Pt/C$_{WA}$ (267 m^2/g) which is lower than that of the micropore surface area of 10 wt. % Pt./C$_{WA}$ (318 m^2/g).

110

The micorpore values were deduced from t-plots. Even though no quantitative estimation of the dispersion of Pt over carbon support is made, an appropriate guess can be made about the extent of dispersion from the relative crystallite sizes of Pt in the case of 10 wt.% Pt/CWA (10.2) and 5 wt.% Pt/CWA (5.0 nm). The details of textural properties and parameters deduced from the isotherms shown in Fig. 30. are summarized in Table 16.

Table 16. Textural properties of carbon supported Pt catalysts

| S. No.	Electro catalyst	S_{BET} (m^2/g)	$^iS_{Micropore}$ (m^2/g)	$^{ii}V_P$ (cm^3/g)	Mean Pore Diameter^{iii} (nm)
1	5 wt. % Pt/C$_{WA}$	505	267	0.289	2.28
2	10 wt. % Pt/C$_{WA}$	526	318	0.288	2.19
3	15 wt. % Pt/C$_{WA}$	451	233	0.261	2.31
4	20 wt. % Pt/C$_{WA}$	195	102	0.119	2.44

i. Micropore area deduced from t-plot
ii. Total pore volue
iii. Mean pore diameter, d = 4V/A (in nm)
where V is the total pore volume and A is the BET specific surface area

The electro catalytic activity of the carbon supported Pt catalysts for the MeOH electroxidation in half cell mode was investigated by cyclic voltammetry. The stability of the fabricated electrodes was evaluated by chronoamperometry. Cyclic voltammetric studies were carried out on a BAS Epsilon potentiast using modified glassy carbon (Bioanalytical system, USA) as the working electrode, Ag/AgCl (saturated KCl) as the reference electrode and a platinum foil (1.5 cm^2) as an auxiliary electrode. 0.5 M H$_2$SO$_4$ was employed as supporting electrolyte. The electrochemical measurements were carried out in a conventional three-electrode glass cell. The MeOH oxidation reaction was carried out with 1 M CH$_3$OH in acid medium.

The cyclic voltammograms recorded with electrodes fabricated using 5 wt. %, 10 wt.%, 15 wt.% and 20 wt.% Pt supported on carbon material from Limonea Acidissima

are depicted in Fig. 31. For comparison the cyclic voltammetric response from the electrode fabricated with 20 wt.% Pt supported Vulcan XC 72 R is also shown in Fig. 31. The feature common to all the cyclic voltammograms is that one anodic peak is observed in the forward scan and in the reverse scan to another anodic scan is observed. The anodic peak in the forward scan is attributed to oxidation of MeOH [285, 286, 287, 288, 289, 290]. The anodic peak in the reverse scan is attributed to the removal of the incompletely oxidized carbonaceous species (mostly in the form of linearly bonded Pt=C=O) formed in the forward scan [285].
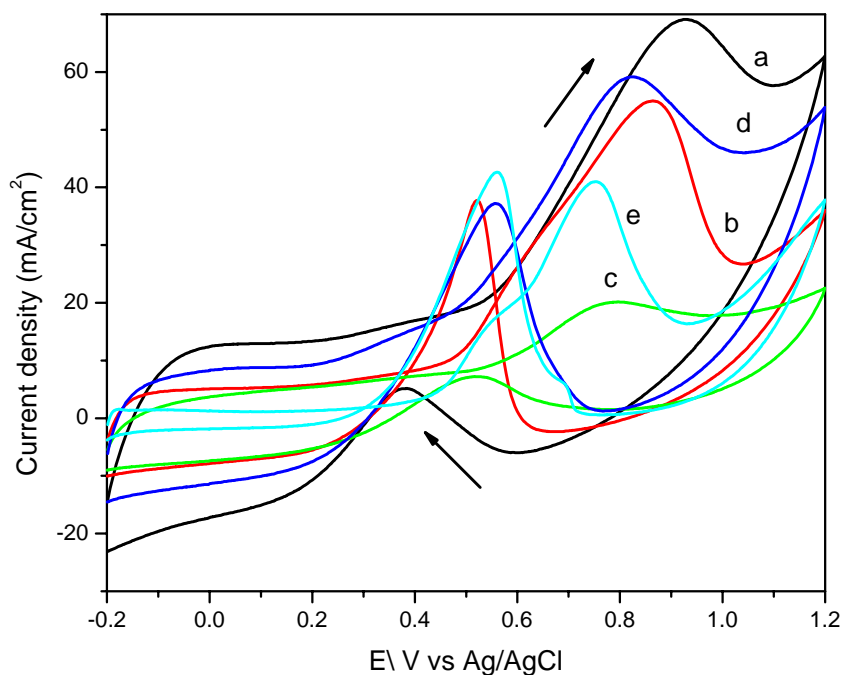
Fig. 31. Cyclic Voltammetric response of (a) GC/C_{WA} - 5 wt.% Pt - Nafion electrode (b) GC/C_{WA} - 10 wt.% Pt - Nafion electrode (c) GC/C_{WA} - 15 wt.% Pt - Nafion electrode and (d) GC/C_{WA} - 20 wt.% Pt - Nafion electrode and (e) GC/Vulcan XC 72 R - 20 wt.% Pt - Nafion electrode in 0.5 M H_2SO_4 and 1 M MeOH, at a scan rate of 25 mV/sec between -0.2 to 1.2 V Vs Ag/AgCl

The critical parameter that determines the usefulness of an electrode is the onset potential. Less positive value of the onset potential is preferred. Lower onset (less

positive potential) potential value implies the requirement of lower energy of the MeOH oxidation reaction to take place [291]. The onset potential value is related to the breaking of the C-H bond of MeOH which is the primary step involved in the mechanism of electroxidation of MeOH [267]. The onset potential values for the electroxidation of MeOH deduced from the cyclic voltammograms obtained over different electrode, along with peak potential and current values corresponding to the MeOH oxidation (anodic peak in the forward sweep) as well as the oxidation of intermediate species formed during the oxidation of MeOH (anodic peak in the reverse sweep) are summarized in Table 17. Zhaoling Liu *et al.,* [286] have reported the onset potential vaues of 0.27 and 0.28 respectively on Pt/Vulcan carbon and Pt/CNT's for the electrooxidation of MeOH in 1 M H_2SO_4 and 2 M MeOH at a scan rate of 50 mV/sec

Table 17. Effect of Pt loading as well as the nature of carbon support on the electro catalytic activity of MeOH electrooxidation - Comparison of electrocatalytic activity of Pt/C_{WA} and Pt/Vulcan XC 72 R

| S. No.	Electrode	Onset Potential, V	i_f/i_b	Activity*			
				Forward sweep		Reverse sweep	
				I (mA/cm^2)	E (V)	I (mA/cm^2)	E (V)
1	GC/C_{WA}-5 % Pt-Nafion	0.21	14.4	69.0	0.92	4.97	0.37
2	GC/C_{WA}-10 % Pt-Nafion	0.18	1.45	55.0	0.86	37.6	0.52
3	GC/C_{WA}-15 % Pt-Nafion	0.30	2.76	20.0	0.79	7.2	0.51
4	GC/C_{WA}-20 % Pt-Nafion	0.18	1.60	58.9	0.82	37.28	0.51
5	GC/Vulcan XC 72 R-20 % Pt-Nafion	0.25	0.96	40.9	0.75	42.6	0.56

*Activity evaluated 0.5 M H_2SO_4 and 1 M MeOH, at a scan rate of 25 mV/sec between -0.2 to 1.2 V Vs Ag/AgCl

The onset potential being little lower (0.21 V) than that observed with the commercial vulcan carbon (0.25 V), 5 wt.% Pt/C_{WA}, catalyst showed higher current

density which is an indication of higher electrochemical catalytic activity. Such a high current values derivable from the modest wt.% loadings of Pt is an indication of the effective utilization of Pt over the C_{WA} support. The improved performance of the electrocatalyst, 5 wt.% Pt/C_{WA}, is attributed to the high electro catalytic activity of the Pt nano crystallites (5.0 nm) finely dispersed over the carbon support. The fine dispersion is facilitated by the lower amont of Pt loading, high specific surface area of the support as well as the hydrophilic (oxophilic) quinone surface functional groups present on the carbon support surface. The ratio of the anodic peak current densities in the forward (i_f) and reverse (i_b) scans too gives a measure of the catalytic performance. A higher i_f/i_b ratio indicates superior oxidation activity of methanol during the anodic scan and less accumulation of carbonaceous species on the nanocatalyst surface and thus an indication of better CO tolerance. The i_f/i_b value in the case of 5 wt.% Pt/C_{WA} catalyst is 14.4 which is an order of magnitude higher than that of either 20 wt.% Pt/C_{WA} or 20 wt.% Pt/Vulcan XC 72. The i_f/i_b value of the electrocatalyst produced from commercial fuel cell grade culvan XC 72 carbon was found to be 0.96. At all the loadings of Pt, the electrodes fabricated using CWA carbon materials showed an i_f/i_b value greater than 0.96 (resulting from Vulcan XC 72 R based catalyst). For comparison, the i_f/i_b value for 20 wt. % PtRu/C catalyst of commercial Johnson Matthey sample is 1.33.[292]. Zhibin Lei *et al.,* [293] have observed the i_f/i_b values of 2.22, 1.47, 1.33, and 1.11on 20 wt.% Pt supported on nitrogen containing ordered mesoporous carbon heat treated at 873, 973, 1123 and 1173 K. The above mentioned catalysts were precpared by wet chemical reduction method. For comparison the performance of 20 wt. % Pt/Vulcan XC 72 R has also been evaluated under identical conditions and a i_f/i_b value of 0.89 was observed which is close to the value shown in Table 17 in the studies carried out by Viswanathan *et al.,* [178].

The effect of scan rate on the electrochemical performance (current out put) of different electrodes, namely, 5, 10, 15 and 20 wt. % $Pt/C_{WA}/GC$ at the scan rates of 5, 10, 15, 20 and 25 mV/sec in 0.5 M H_2SO_4 and 1 M MeOH between – 0.2 to 1.2 V Vs Ag/AgCl is evaluated and the result is shown in Fig. 32 (a – d). For comparison the current response to variation in scan rate for the electrode fabricated using Vulcan XC 72 R as support with 20 wt.% Pt loading was also shown in Fig. 32 (e). It was observed that the peak current density values due to the MeOH oxidation increased as the scan rate

increased from 5 to 25 mV/sec irrespective of the nature of the catalyst. A small increment in the peak potential with an increase in the scan rate is also observed.
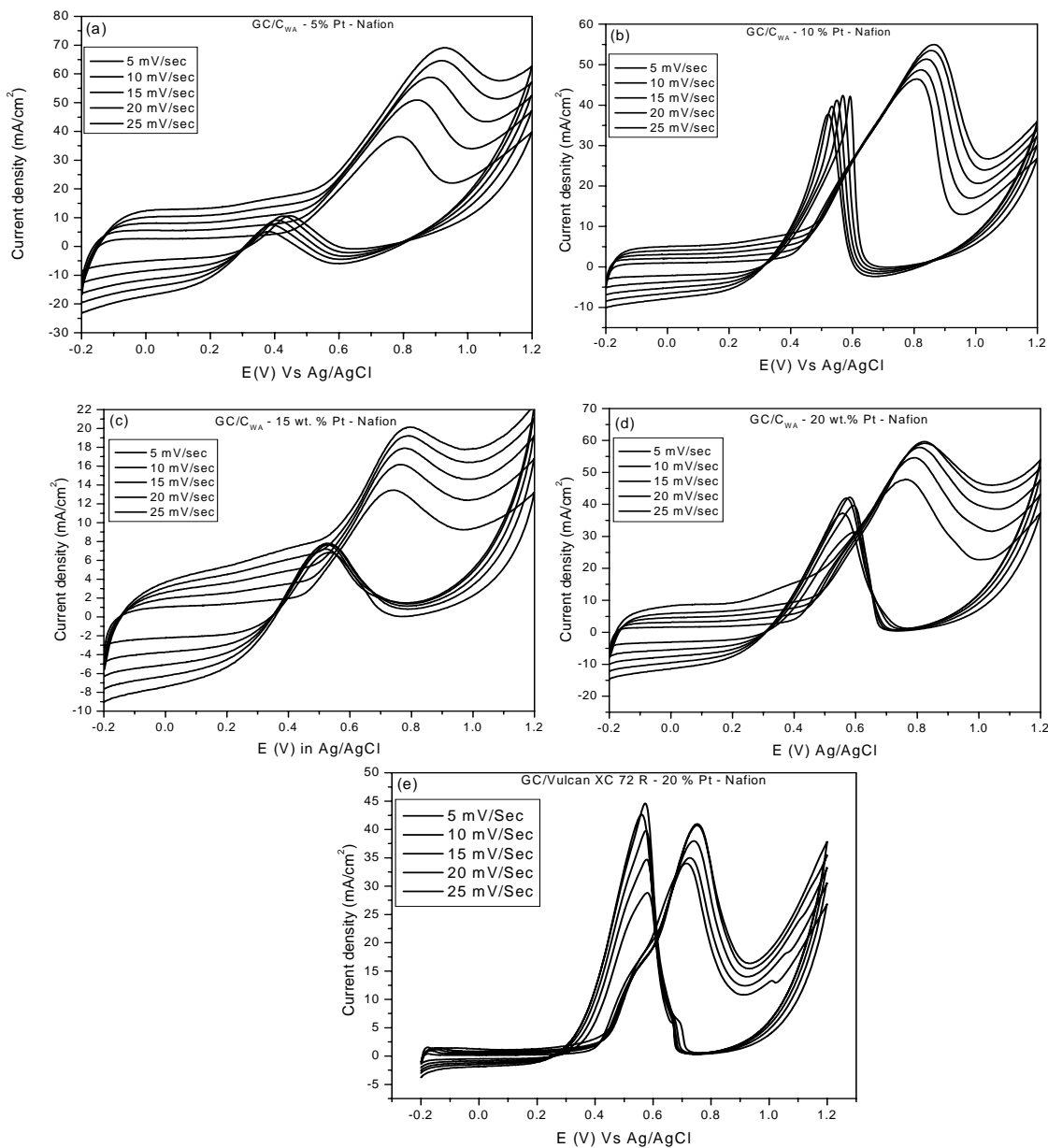
Fig. 32. Cyclic Voltammetric response of (a) GC/Pt C_{WA} 5 wt.%- Nafion electrode, (b) GC/Pt C_{WA} 10 wt.%- Nafion electrode, (c) GC/Pt C_{WA} 15 wt.%- Nafion electrode, (d) GC/Pt C_{WA} 20 wt.%- Nafion electrode and (e) GC/Pt Vulcan XC 72 20 wt.% - Nafion electrode in 0.5 M H_2SO_4 and 1 M MeOH, at different scan rates (5, 10, 15, 20 and 25 mV/sec) between -0.2 to 1.2 V Vs Ag/AgCl

The peak currents were found to be linearly proportional to the square root of scan rates as shown in Fig. 33. in all the cases. Such a linear proportionality relationship between the current response and square root of scan rate indicates that the electrooxidation process of MeOH is controlled by diffusion to the catalysts employed [294, 259].
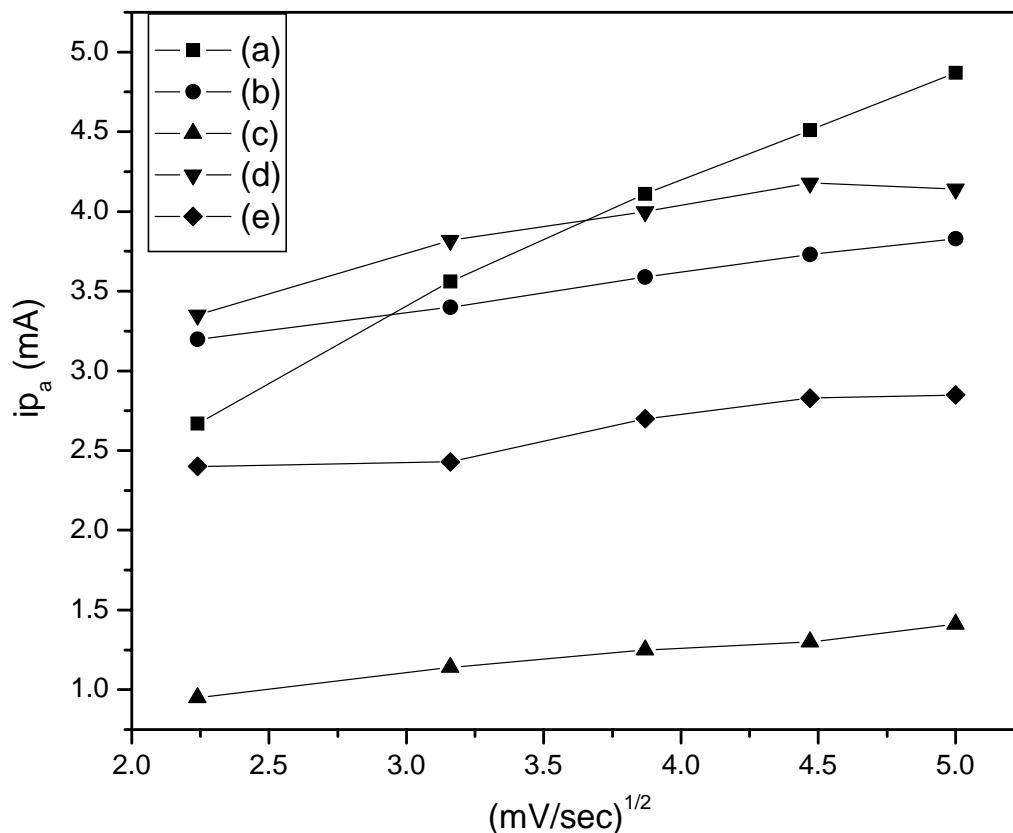
Fig. 33. Dependence of peak currents on the square roots of scan rates for (a) GC/Pt C_{WA} 5 wt.%- Nafion electrode, (b) GC/Pt C_{WA} 10 wt.%- Nafion electrode, (c) GC/Pt C_{WA} 15 wt.%- Nafion electrode, (d) GC/Pt C_{WA} 20 wt.%- Nafion electrode and (e) GC/Pt Vulcan XC 72 20 wt.% - Nafion electrode in 0.5 M H_2SO_4 and 1 M MeOH, at different scan rates (5, 10, 15, 20 and 25 mV/sec) between -0.2 to 1.2 V Vs Ag/AgCl

The long term stability of the fabricated electrodes was evaluated by chronoamperometric studies carried out for a duration of 3 h with the electrode being polarized at + 0.6 V Vs Ag/AgCl in 0.5 M H_2SO_4 and 1 M MeOH. The current density

116

Vs time plots derived from the electrodes based on 5, 10, 15 and 20 wt.% Pt/C$_{WA}$ are shown in Fig. 34. The initial and final (after 3 h duration) current densities values derived from the electrodes fabricated from 5, 10, 15 and 20 wt. % Pt/C$_{WA}$ electocatalysts are summarized in Table 18. The percentage decrease of the activity of the afore mentioned electrodes after 3 h is also given in Table 18.
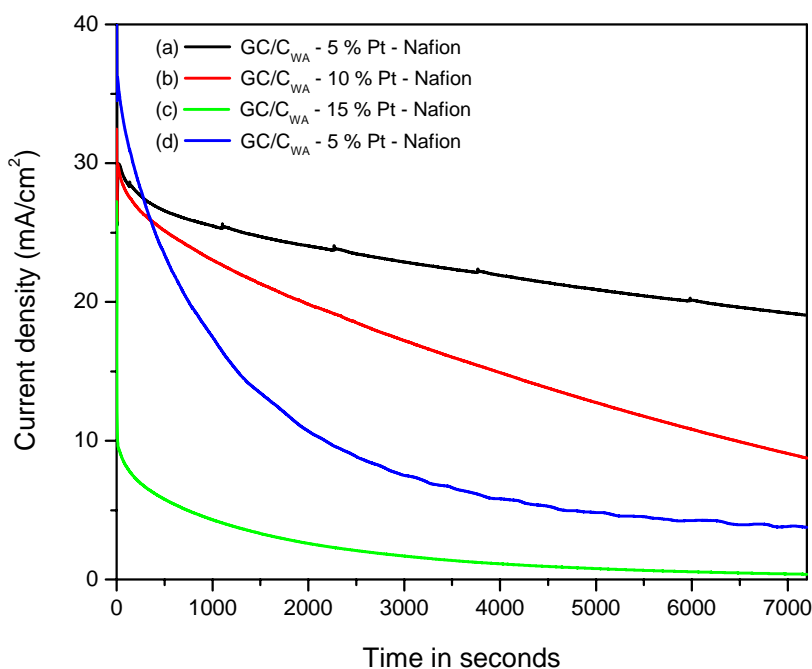
Fig. 34. Chromoamperometric response of (a) GC/C$_{WA}$ - 5 wt.% Pt - Nafion electrode (b) GC/C$_{WA}$ - 10 wt.% Pt - Nafion electrode (c) GC/C$_{WA}$ - 15 wt.% Pt - Nafion electrode and (d) GC/C$_{WA}$ - 20 wt.% Pt – Nafion electrode polarized at + 0.6 V Vs Ag/AgCl in 0.5 M H$_2$SO$_4$/ 1 M MeOH for 3 hours

Among the electrodes studied, the 15 wt. % Pt/C$_{WA}$ catalyst based electrode showed least stability with a 96 percentage decrease of initial activity at the end of 3h. Such a poor performance is the result of the higher crystallite size (13.5 nm) of Pt formed in the case of 15 wt.% Pt/C$_{WA}$ catalyst. In sharp contrast, as expected, the electrode fabricated using 5 wt.% Pt/CWA possessing the smallest Pt crystallites (5.0 nm) as well as high i$_f$/i$_b$ ratio showed highest stability. Only 24 % loss in the initial activity is observed even at the end of 3 h in the case of the GC/C$_{WA}$ – 5% Pt – Nafion electrode.

Thus it is clear from the above mentioned result that the stability of the electrode is based on the smaller crystallite size of Pt as well as the high CO tolerance (high i_f/i_b ratio value).

Table 18. Evaluation of the stability of C_{WA} based electrodes for the electrooxidation of MeOH in half cell mode

S. No.	Electrode	Activity*		% Decrease in activity
		Initial (I), mAcm^{-2}	Final (I), mAcm^{-2}	after 3 hs at + 0.6 V
1	GC/C_{WA}-5 % Pt-Nafion	25.2	19.1	24
2	GC/C_{WA}-10 % Pt-Nafion	29.7	19.0	36
3	GC/C_{WA}-15 % Pt-Nafion	10.0	0.4	96
4	GC/C_{WA}-20 % Pt-Nafion	36.1	3.7	89

*Activity evaluated in 0.5 M H_2SO_4 and 1 M CH_3OH for 3 h with the electrode being polarized at + 0.6 V Vs Ag/AgCl

The activated carbon material produced from Limonea Acidissima by KOH activation is a promising support for Pt for the electroxidation of MeOH. The excellent performance of 5 wt. % Pt/C_{WA} is attributed to the increase in the extent of utilization of Pt metal. Thus the use of carbon material from Limonea acidissima as support for Pt offered the promise of effective utilization of Pt, high electrooxidation (MeOH) actaivity, high CO tolerance and long term stability.

SECTION IV

Carbon Materials (as adsorbent) for Adsorptive Desulphurization

Removal of organo sulphur compounds from diesel is an issue of concern from scientific, social, economic and environmental view points. Any break through achieved in desulphurization technology will have its impact on human well being. Burning of fuel (gasoline or diesel) with S contents beyond permissible limits causes ill effects on human health. Current world demands zero sulphur fuel. Production of clean fuel has always been the goal of petroleum refining industry. But refinery itself is engulfed now in the vicious circle of a host of problems that include environmental legislation, crude oil variation, product demand, economic imbalances, energy uptake, safety and process efficiency. It should not be mistaken that conventional HDS can be a panacea to the recurring problem of S specification in the transportation fuels. Newer technologies, if found promising, should be given place and adopted.

Hydroprocessing is one of the most important steps in the petroleum refining industry. Hydroprocessing refers to a variety of catalytic processes aimed at the removal of S, N, O and aromatic compounds present in the gasoline and diesel feed stocks. $\gamma - Al_2O_3$ supported sulfided NiMo oxide is the best known commercial catalyst for hydrodenitrogenation (HDN) where as the sulfided CoMo oxide supported on $\gamma - Al_2O_3$ in the industrial catalyst for hydrodesulphuriztion. As the name of the processes suggest, the catalyst should possess strong hydrogenation function as hydrogenation is the prime reaction in both HDN and HDS processes.

Sulphur in the oil streams is removed as H_2S from the petroleum streams in the process of hydrodesulphurization (HDS) under severe conditions of reaction temperature and hydrogen pressure [296].

Even though the oxides of sulfided CoMo and NiMo supported on $\gamma - Al_2O_3$ showed excellent performance for HDS and HDN reactions respectively, the afore mentioned catalysts need to be sulfided a priori to achieve the active site formation. The sulphidation process is usually carried out by exposing the catalyst to the sulphur containing feed itself. There are several ways in which the sulfided CoMo and NiMo based catalysts loses the activity. Factors that cause the loss of activity are: sintering of the active phases, decomposition of the active phases, covering of the active sites by reactants or products, coking, formation of deposits of metal sulfides. Owing to the afore mentioned problems, in addition to the necessity of H_2 as well as the severity of the operation conditions, there is an urgent need for the development of alternate methods of desulphurization with efficiency towards the removal of refractory compounds.

4, 6 dimethyl dibenzothiophene (4, 6 DMDBT) with alkyl groups close to 'S' atom is highly refractory compound to be desulphurized. 'S' species in such 'sterically' inaccessible environment are too difficult to be removed. Two parallel reaction path ways, namely, the direct desulphurization as well as the path involving the hydrogenation step followed by desulphurization, are possible for the desulphurization of 4, 6 DMDBT on commercial oxide catalyst (either NiMoS/Al or CoMoS/Al) as depicted in Fig. 35.
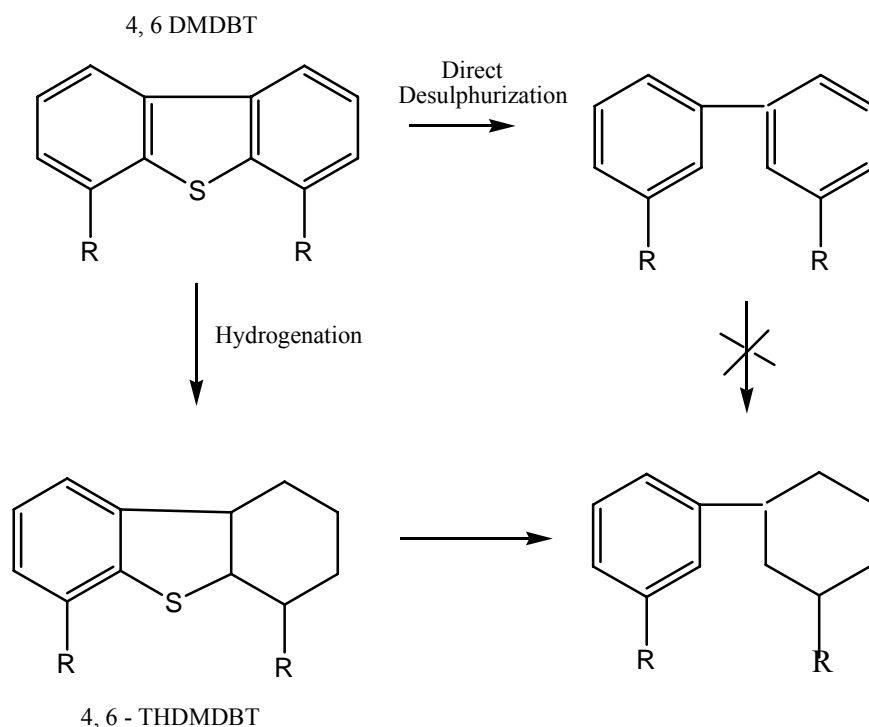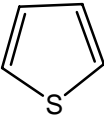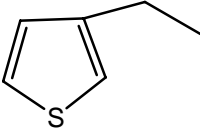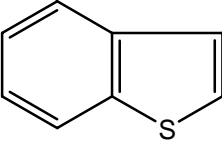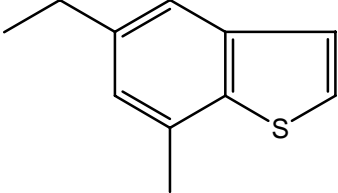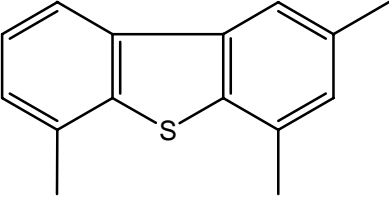
Fig. 35. Hydrodesulphurization of 4, 6 – DMDBT (R – CH$_3$) involving direct route and hydrogenation route (reproduced from ref. 297)

Direct desulphurization of 4, 6 DMDBT yields dimethyl phenyl where as the hydrogenation route initially yields dihydrobenzothiophene which is subsequently desulphurized to form methyl cyclohexyl toluene (MCHT). It was found that around 80 % of the HDS of 4, 6 – DMDBT proceeds via the hydrogenation route where in the adsorbed 4, 6 – DMDBT is first hydrogenated and then the hydrogenated compound is desulphurized [297].

Typical S containing compounds present in petroleum fractions are shown in Table 19 [298].

Table 19. Some S containing compounds present in petroleum fractions

S. No.	S Compounds
1	R-SH (Thiol, Mercaptan), R-S-R' (Sulfide), R-S-S-R' (Disulfide)
2	Thiophene Substituted Thiophene
3	Benzothiophene Substituted Benzothiophene
4	Substituted dibenzothiophene

Michele Breysse *et al.*, [299] have proposed the following reaction mechanism for the hydro desulphurization of substituted dibenzo thiophene which is classified as refractory compound (difficult to get desulphurized).

The origin of refractory behaviour in compounds such as highly substituted dibenzothiophenes, 4, 6 DMDBT in particular, is related to the steric hindrance encountered for the breaking of the C-S bond. The desulphurization of 2, 6 DMDBT

proceeds by two routes is shown in Fig. 36. As depicted in Fig. 36, the partial hydrogenation reaction of 4, 6 DMDBT is a common as well as primary reaction for either hydrogenation (HYD) route or direct desulphurization (DDS) route. After the formation of partially hydrogenated products, the C-S bond is cleaved in the DDS route with out any further hydrogenation. Unlike the DDS route, in the path through hydrogenation (HYD route), complete hydrogenation of atleast one of the aromatic rings is inevitable for the C-S bond to cleave.
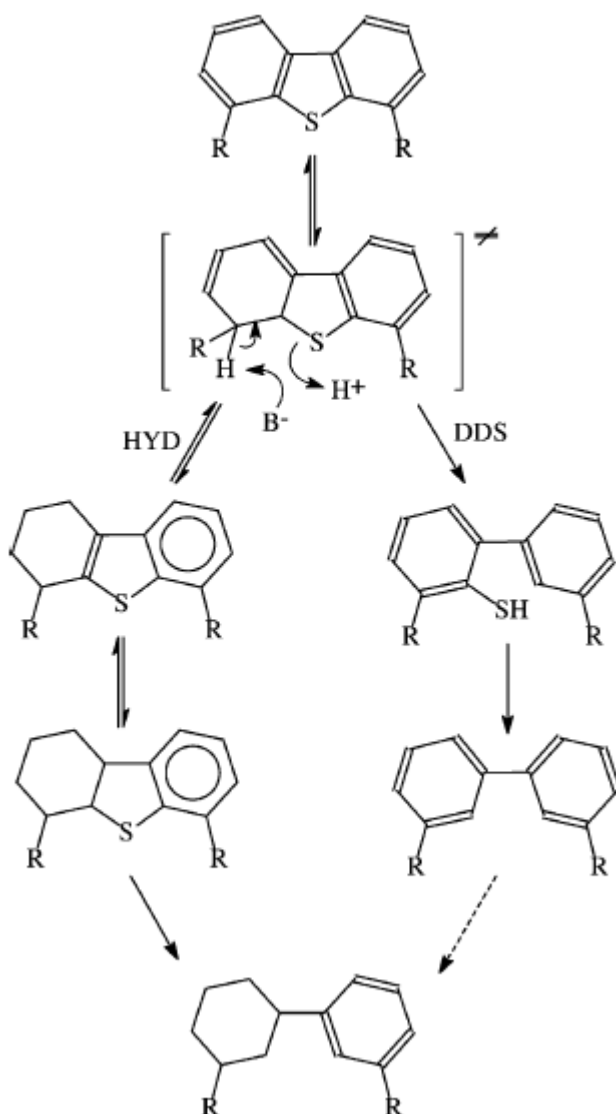

Fig. 36. Mechanism of desulphurization of substituted dibenzo thiophene (reproduced from 299)

The presence of substituents at 4 and 6 positions of DBT hinder the β – elimination step which is necessary for the desulphurization to take place. To over come the problem of desulphurization of refractory compounds various strategies of desulphurization are being developed [300-309].

Stringent regulations are being imposed on the permissible limits of S in transportation fuel. In India, the sulphur speciation is made stringent. Bharat IV norm, implying the regulation of 50 ppm sulfur by 2010, is being imposed in the selected metropolitan cities of India. Bharat III norm indicating the specification of 350 ppm of S in the diesel fuel will be implemented in places other than metropolitan cities in India. From 2000, onwards, the HDS units in many refineries are being revamped to meet the new norms. In US from 2006 onwards, the maximum permissible limit of S in the diesel fuel is reduced to 15 ppmw. Presence of refractory sulphur compounds like, 4, 6 dimethyl dibenzothiophene, necessitates the severe operational conditions. In most of the diesel fuels, 4, 6 DMDBT, the most difficult S containing compound to be desulphurized, is present in > 100 ppm. In view of the increasing process severity of diesel, HDS units to meet the upcoming stringent specifications of permissible S content, alternate methods of desulphurization are being explored. The process of oxidative desulphurization is selective in converting refractory sulphur compounds to sulfones. But the major disadvantages with the process of oxidative desulphurization are:

(i)   the oxidant used for the oxidative desulphurization is expensive and

(ii)   the separation of sulfones is an energy intensive process.

Adsorptive desulphurization is an energy efficient process yielding clean fuel free from S under modest process conditions. Zeolite based adsorbents are not a viable option as such a process necessitates the requirement of hydrogen for producing fuels meeting the Euro III/IV norms. Carbon materials being multifunctional in terms of structural, textural and surface properties, they can be tuned to match the requirement for the adsorption of S containing compounds including refractory compounds.

Viswanathan *et al.*, [310] have developed the process for the desulphurization of SR diesel, with an initial S content of 737 ppm, from Cauvery Basin Refinery (CBR) Distillation Unit based on Adsorption. Removal of S compounds, refractory compounds

in particular, is achieved under modest conditions of temperature (room temperature) and pressure (atmospheric pressure) in sharp contrast to the conventional hydrodesulphurization process where in the operation conditions are severe. The process is based on selective adsorption of organo sulphur compounds onto the tailored carbon surfaces which are employed as adsorbents. In addition to the removal of appreciable amounts of S from the SR diesel feed (430 – 450 ppm S removed from ml-diesel/g adsorbent), a simple process for the regeneration of the adsorbent bed is developed. Solvent based regeneration was found to be the best method yielding fresh carbon surface for further adsorption of S compounds. The regenerated bed was found to be as efficient as the fresh carbon sorbent bed. Among the cluster of activated carbon materials tested, tailored carbon materials generated from the Adsorbent carbon (Adsorbent Carbons Pvt. Ltd., Tuticorn, India), Calgon Carbon (Tianjin Co., Ltd.,) and Nuchar Carbon (MeadWestvaco, Covington, VA) were found to yield promising results for the removal of S compounds from SR diesel.

The physicochemical properties of SR diesel from Cauvery Basin Refinery are summarized in Table 20.

Table 20. Physicochemical Chracteristics of SR diesel from CBR distillation unit

S. No.	Property	Value
1	Total Sulphur content (in ppm)	737
2	Flash Point (°C)	93
3	Aniline Point (°C)	81
4	Viscosity (at 40 °C in cSt)	4.04
5	Pour Point (°C)	+6
6	Density (g/cc)	0.8553
7	Diesel Index	60
8	Cetane Index	53

Adsorptive Desulphurization

Several commercially available activated carbon materials of varying physical and chemical properties were tested as adsorbents for the removal of organo sulphur

compounds from SR diesel from Cauvery Basin Refinery Distillation unit. Among them, adsorbent carbon (A) was purchased from Adsorbent Carbons Pvt. Ltd., Tuticorn. Calgon carbon (B) was purchased from Calgon Carbon (Tianjin) Co. Ltd., Activated carbons, IG 18 x 40, IG 12 x 40 and IG 8 x 30 were purchased from Indo German Carbon Ltd., Kerala. Activated carbons, AC 4 x 8, AC 6 x 12, AC 12 x 30 were purchased from Active Carbon Pvt. Ltd., Hyderabad.

Process of Sulphur Adsorption

A simple, inexpensive and efficient process for desulphurisation is designed. The potential of the above mentioned carbon materials were tested. In a typical experiment the glass column of length 50 cm and internal diameter 1.5 cm is packed with 5.0 g of sorbent carbon column with glass beads on either sides. Deisel is fed on to the sorbent bed in the column through a burette at the slowest flow rate possible. The first 20 ml product collected at the bottom of the column (out let) was analyzed for S. From the S content remaining in the product and subtracting the same from the S content in the feed diesel (737 ppm), the S content adsorbed (removed) by the carbon sorbent is obtained. Lower the S content in the product obtained through the sorbent column, higher is the sorption capacity of the activated carbon under test.   The carbon materials are thus screened.   Adsorbent carbon and Calgon carbon showed good performance for the adsorption of S compounds in the SR diesel (Table 21).

Table 21. S sorbing ability of different commercial activated carbon materials

S. No.	Activated Carbon as Sorbent	*ml-diesel treated/g of adsorbent	S removed (ppm)
1	IG 18 x 40	4	134
2	IG 12 x 10	4	81
3	IG 8 x30	4	76
4	AC 4 x 8	4	12
5	AC 6 x 12	4	73
6	AC 12 x 30	4	92
7	Calgon carbon as received	4	181
8	Adsorbent carbon	4	229

* 20 ml initial product collected from the column packed with 5.0 g activated carbon and analyzed for S analysis

Different commercially available activated carbons, namely, IG 18 x 40, IG 12 x 10, IG 8 x 30, AC 4 x 8, AC 6 x 12, Ac 12 x 30, calgon carbon as received and adsorbent carbon as received as used as adsorbents for S containing compounds present in SR diesel. The results obtained on preliminary studies with the these adsorbents are presented in Table 21. The amount of S removed (in ppm) from 20 ml deisel by 5.0 g of sorbent is shown in extreme right column of Table 2. Among the eight carbons studied Adsorbent carbon as received and Calgon carbon as received showed outstanding performance by adsorbing 229 and 181 ppm of S. So Adsorbent carbon (A) and Calgon carbon (B) were selected and further intensive studies of adsorptive desulphurisation were carried out on these adsorbents.

Activation of Adsorbent carbon (A) and Calgon carbon (B):
Activation with Conc. HNO$_3$

HNO$_3$ treatment changes the surface chemistry of carbon materials. Such oxidative treatment results in the formation of oxygen containing surface functional groups (carbonyl and carboxyl). The presence of such surface functional groups, in most cases, enhances the adsorption capacity of carbon materials [218, 215].

Two commercial activated carbon materials, namely, the adsorbent carbon (A) and the calgon carbon (B) were treated with conc. HNO$_3$. The wt./wt.% ratio of carbon to conc. HNO$_3$ was 1:5. The oxidative treatment of carbon with conc. HNO$_3$ was carried out at 60 °C for 2 hrs under refluxing conditions in a 2 litre RB flask. The contents are then cooled to room temperature, washed with water and dried at 110 °C for 2 h.

Activation under Ar atmosphere: Ar activation involves the thermal activation of nitric acid treated carbon materials A and B at a temperature of 800 C under Ar atmosphere for 2 h in a cyclindrical quartz tube.

The carbon samples after activation were termed as nitic acid treated Ar activated carbon materials.

**Selected Sorbents for Adsorptive Desulphurization:**

Desulphurisation studies carried out with 5.0 g batch using adsorbent carbon, nitric acid treated adsorbent carbon and nitric acid treated Ar activated adsorbent carbon, calgon carbon, nitric acid treated calgon carbon and nitric acid treated Ar activated adsorbent carbon have been extended to 10.0 and 15.0 g batches. The process of adsorptive desulphurization has also been scaled upto 100 g batch using the same experimental set of glass column packed. In a typical process, diesel is continuously fed from a burette in to the column packed with the adsorbent. The product diesel is collected in aliquots of 20 ml at the bottom of the column. The S content in the product is analyzed by using *Oxford XRF analyzer*. The feed and the product diesel were also characterized for the detailed sulphur component analysis using *GC-PFPD (Gas Chromatography – Pulsed Flame Photometric Detector).*

**Characterization of Adsorbents for Desulphurization Application:**

Details of phase composition of carbon materials are obtained from X-ray diffraction studies. X-ray diffraction patterns of adsorbent carbon as received, adsorbent carbon treated with conc. HNO_3 and adsorbent carbon treated with HNO_3 followed by subsequent activation in Ar atmosphere are shown in Figs. 3(a), (b) and (c) respectively. Two broad diffraction peaks centered at 2θ values of 25.4 and 43.4 were observed in adsorbent carbon as well as modified adsorbent carbons. The two peaks can be indexed to (002) and (101) planes of crystalline hexagonal graphite lattice respectively [(JCPDS-41-1487), 311]
The phase composition of adsorbent carbon remained unaltered upon nitric acid treatment (Figs. 37 (a) and (b)). But in the case of adsorbent carbon treated with nitric acid followed by activation in Ar atmosphere an additional intense and narrow diffraction peak is seen at 2θ = 26.7 (Fig. 37 (c)). This is attributed to (002) reflection from highly crystalline graphitic carbon [312]. Nitric acid treated Ar activated adsorbent carbon (Fig. 37 (c)) is more crystalline than either adsorbent carbon as received or adsorbent carbon

treated with nitric acid alone. Thus Ar activation improved the crystallinity of nitric acid treated adsorbent carbon.
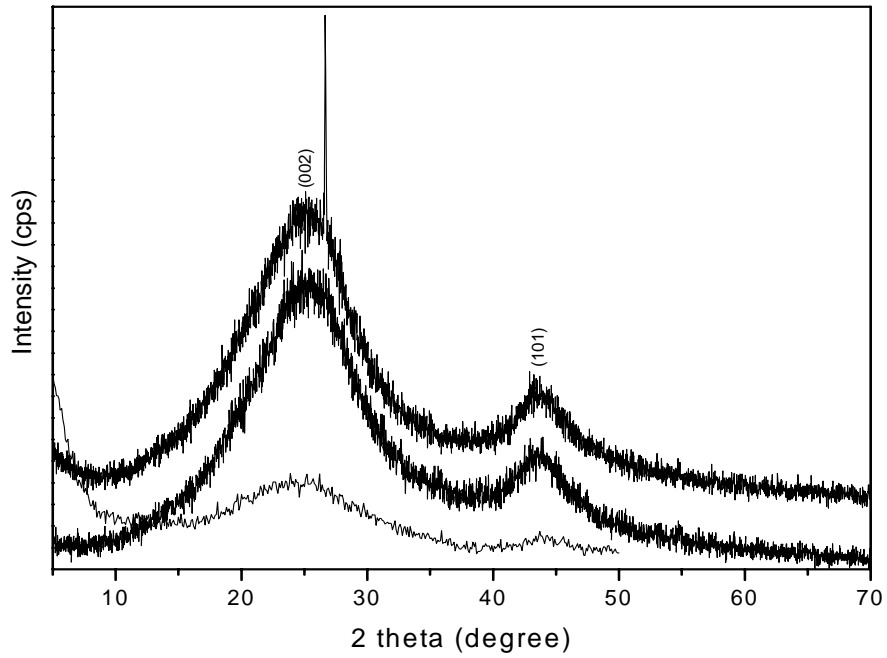
Fig. 37. XRD pattern of (a) Adsorbent carbon as received, (b) Adsorbent carbon treated with HNO_3 and (c) Adsorbent carbon treated with HNO_3 and activated with Ar
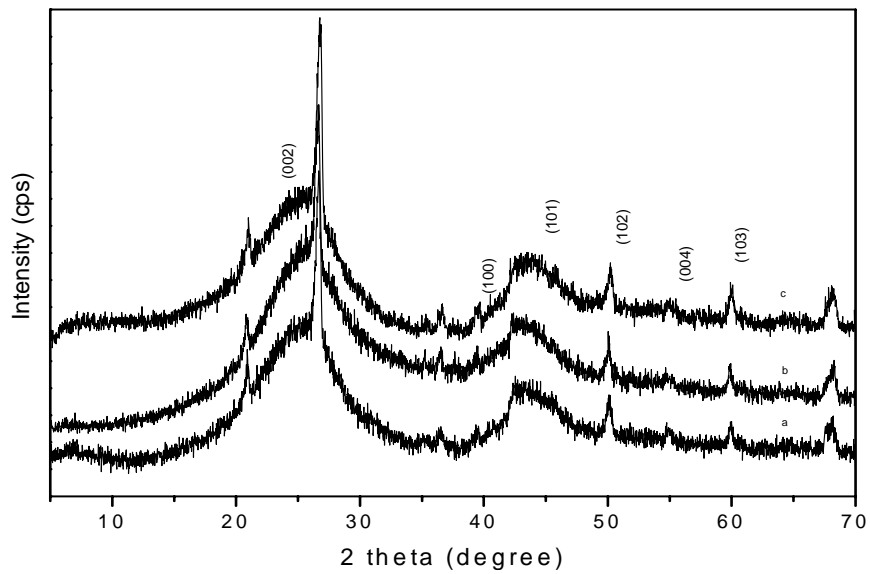
Fig. 38. XRD pattern of (a) Calgon carbon as received, (b) Calgon carbon treated with HNO_3 and (c) Calgon carbon treated with HNO_3 followed by Ar activation

X-ray diffraction patterns of calgon carbon as received, calgon carbon treated with HNO_3 and calgon carbon treated with HNO_3 followed by Ar activation are shown in Figs. 38. (a), (b) and (c) respectively.   The diffraction peaks arising from each of the mentioned carbon samples were indexed and are typical of graphitic carbon structure [312].

Neither HNO_3 treatment (Fig. 38 (b)) nor HNO_3 treatment with subsequent Ar activation (Fig. 38 (c)) altered the structure of original calgon carbon sample (Fig. 38 (a)). Thus either HNO_3 treatment or Ar activation has no effect on the phase structure of calgon carbon.

There is a marked difference in the structural order between adsorbent carbon and calgon carbon (Figs. 37 and 38). No diffraction peaks resulted from adsorbent carbon or modified adsorbent carbon beyond $2\theta = 50$ º   (Fig. 37) in sharp contrast to the characteristic diffraction peaks resulting from calgon and modified calgon carbon above $2\theta = 50$ º. Thus calgon based carbons are structurally more ordered than adsorbent based carbons.

Details of pore structure of carbon materials were obtained from N_2 sorption studies. N_2 adsorption-desorption isotherms of adsorbent carbon, modified adsorbent carbon, calgon carbon and modified calgon carbon are shown in Fig. 39.

The N_2 adsorption-desorption isotherms arising from adsorbent carbon as received (Fig. 39 (a)), HNO_3 treated adsorbent carbon (Fig. 39 (b)) and HNO_3 treated Ar activated adsorbent carbon (Fig. 39 (c)) are of typical type I isotherms in nature which are characteristic of microporous materials as per IUPAC classification [313].

The adsorption curves rose sharply at relative pressure upto 0.10. Beyond this value of p/p_0 the isotherms presented a plateau with increasing relative pressure. Also the adsorption and desorption branches were parallel over a wide range at higher relative pressure.   This is an indication of the narrow pore size distribution in microporous materials with slit-like or plate-like pores [314].

The shape of isotherms presented by calgon carbon as received (Fig. 39 (d)), calgon carbon treated with HNO_3 (Fig. 39 (e)) and calgon carbon treated with HNO_3 followed by Ar activation (Fig. 39 (f)) are distinctly different from the Type I isotherms

resulted from adsorbent and modified adsorbent carbons (Figs. 39 (a), (b) and (c)). The isotherms resulting from calgon and modified calgon carbon samples are a combination of type I and type II isotherms. Such isotherms indicate pore structure which is a combination of micropores and mesopores. Presence of such mesopores in addition to micropores enhances the adsorption capacity for relatively large adsorbate molecules [198, 315].
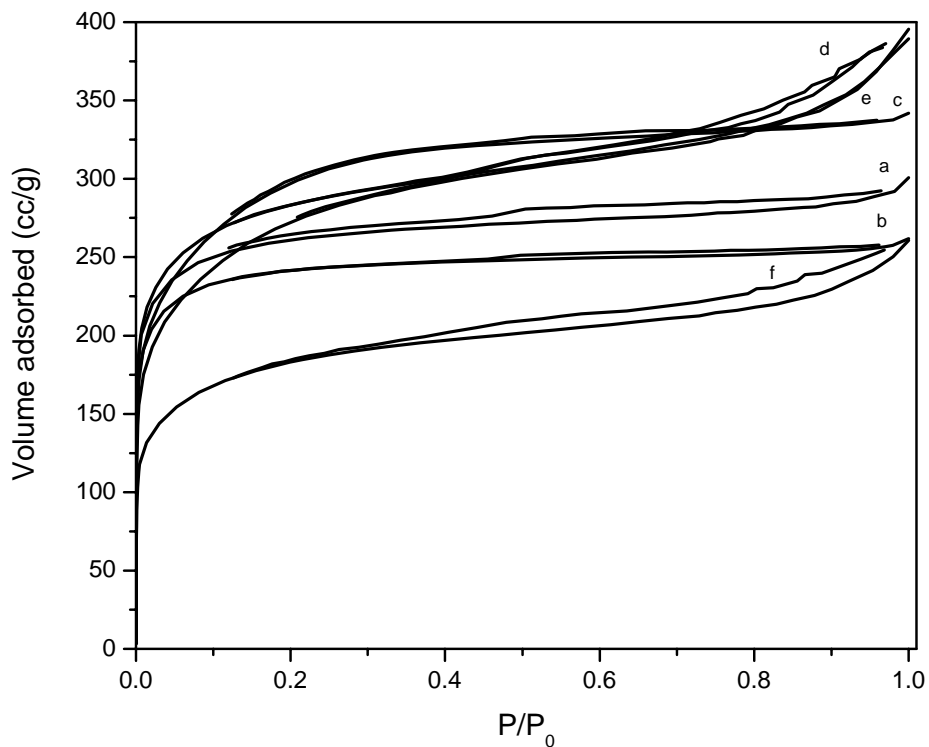
Fig. 39. Nitrogen adsorption-desorption isotherms of (a) Adsorbent carbon as received, (b) Adsorbent carbon treated with HNO_3, (c) Adsorbent carbon treated with HNO_3 followed by Ar activation, (d) Calgon carbon as received, (e) Calgon carbon treated with HNO_3 and (f) Calgon carbon treated with HNO_3 followed by Ar activation.

Details of oxygen containing surface functional groups on the surface of carbon materials are obtained from FT-IR studies. The FT-IR spectra of adsorbent carbon as received, adsorbent carbon treated with HNO_3 and adsorbent carbon treated with HNO_3 followed by Ar activation are shown in Figs. 40. (a), (b) and (c) respectively.

130

Table 22. Porosity characteristics of adsorbent, modified adsorbent, calgon and modified calgon carbon materials

Carbon Sorbent	Specific Surface Area Values (m^2/g)	Total Pore Volume (cm^3/g)
Adsorbent carbon as received	950	0.451
Adsorbent carbon treated with Conc. HNO$_3$	882	0.398
Adsorbent carbon treated with Conc. HNO$_3$ followed by Ar activation	1048	0.523
Calgon carbon as received	1014	0.587
Calgon carbon treated with Conc. HNO$_3$	649	0.387
Calgon carbon treated with Conc. HNO$_3$ followed by Ar activation	996	0.598

Details of oxygen containing surface functional groups on the surface of carbon materials are obtained from FT-IR studies. The FT-IR spectra of adsorbent carbon as received, adsorbent carbon treated with HNO$_3$ and adsorbent carbon treated with HNO$_3$ followed by Ar activation are shown in Figs. 40. (a), (b) and (c) respectively.
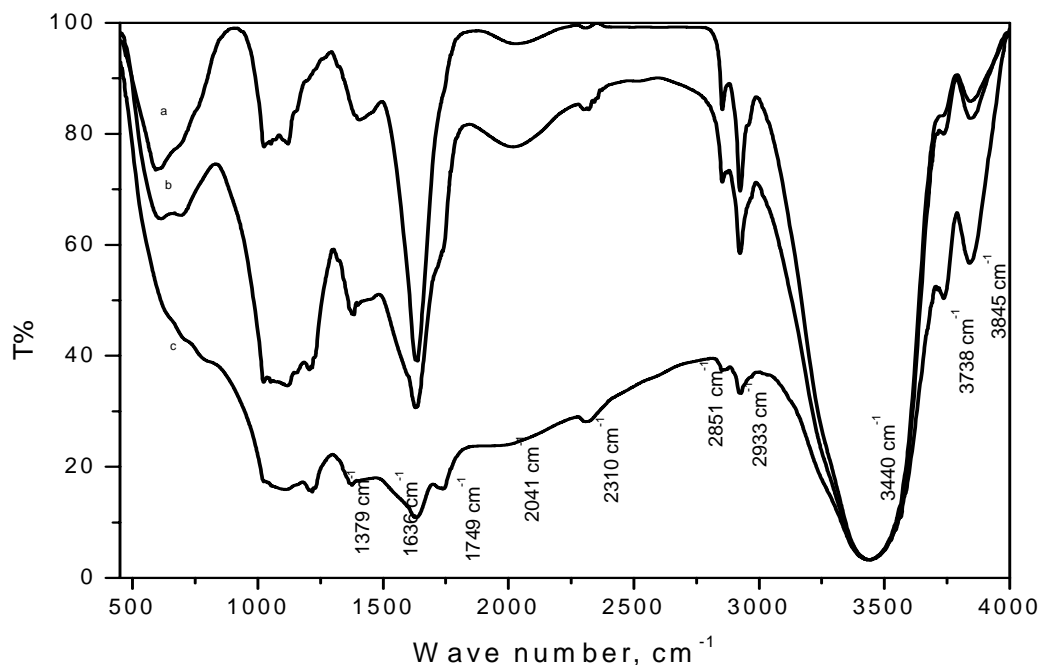
Fig. 40. FT-IR spectra of (a) Adsorbent carbon as received, (b) Adsorbent carbon treated with HNO$_3$ and (c) Adsorbent carbon treated with HNO$_3$ and activated with Ar .

The main distinguishing feature observed in the carbon samples after nitric acid treatment is the presence of shoulder at 1749 cm^{-1} (Fig. 40 (b)). This is a result of stretching vibration of C=O bond in aldehydes, ketones, lactones or carboxyl groups. Thus upon nitric acid treatment C=O group is generated on the adsorbent carbon surface which is absent otherwise. Also the shoulder at 1749 cm^{-1} became intense and developed in to sharp peak upon activation in Ar atmosphere (Fig. 40 (c)) [277, 205].

But for this difference all the three samples showed similar but rich surface chemistry with a variety of oxygen containing functional groups. The following functional groups are common to adsorbent carbon as well as modified adsorbent carbon (Figs. 40 (a), (b) and (c)): A sharp band at 3738 cm^{-1} is ascribed to isolated OH groups. A wide, intense band in the range of 3200-3600 cm-1 with a maximum at about 3440 cm-1 is assigned to the O-H stretching mode of hydroxyl groups and adsorbed water [316].

Two sharp, narrow and intense bands at 2922 and 2855 cm^{-1} are a result of asymmetric and symmetric C-H stretching vibrations of methylene group respectively [198, 202, 225]. It is to noted that the peak resulting from the asymmetric C-H stretching of methylene group is more intense than that arising from the symmetric stretching of methylene group. A sharp intense peak at 1640 cm^{-1} is attributed to the carbonyl groups in quinone. Broad bands observed in the range of 1300 – 1000 cm^{-1} are attributed to C-O stretching in acids, alcohols, phenols, ethers and esters. Broad bands in the range of 600 – 800 cm^{-1} are a result of the out of plane deformation mode of C-H in various substituted benzene rings [316, 198].

FT-IR spectra of calgon carbon as received, calgon carbon treated with conc. HNO$_3$ and calgon carbon treated with Conc. HNO$_3$ followed by Ar activation are shown in Figs. 41 (a), (b) and (c) respectively. There are striking differences in the surface chemistry (functionality) among the mentioned samples. This indicates that each of the methods of activation, whether it is HNO$_3$ treatment or Ar activation, has got a specific role to play and surface transformation to induce. Upon activation with Conc. HNO$_3$ several new bands originated at wave numbers corresponding to 3790, 2305 and 1387 cm^{-1} which can be attributed to isolated O-H groups, ketone surface groups [278] and the in-plane bending vibration of C-H in methyl group [164] respectively (Fig. 41 (b)). In addition to the generation of -OH, C=O and –CH$_3$ groups, a broad featureless shoulder is

observed in the range 2910-2990 cm^{-1} which is a result of aliphatic C-H stretching in methylene and methyl groups.

Ar activation of conc. HNO$_3$ treated calgon carbon induced certain specific changes in to the spectral features. The first and foremost change in the appearance of a broad shoulder at 1753 cm^{-1} attributable to the origin of C=O group of carboxylic acid (Fig. 41 (c)). Also the broad featureless shoulder presented by HNO$_3$ treated calgon carbon in the range 2910-2990 cm^{-1} developed into two clear sharp peaks centered at 2956 and 2918 cm^{-1} which are attributed to the asymmetric and symmetric stretching vibrations of C-H in methylene groups indicate the fact that Ar activation results in the generation of hydrophobic methylene C-H groups on the surface of calgon carbon which are other wise absent.
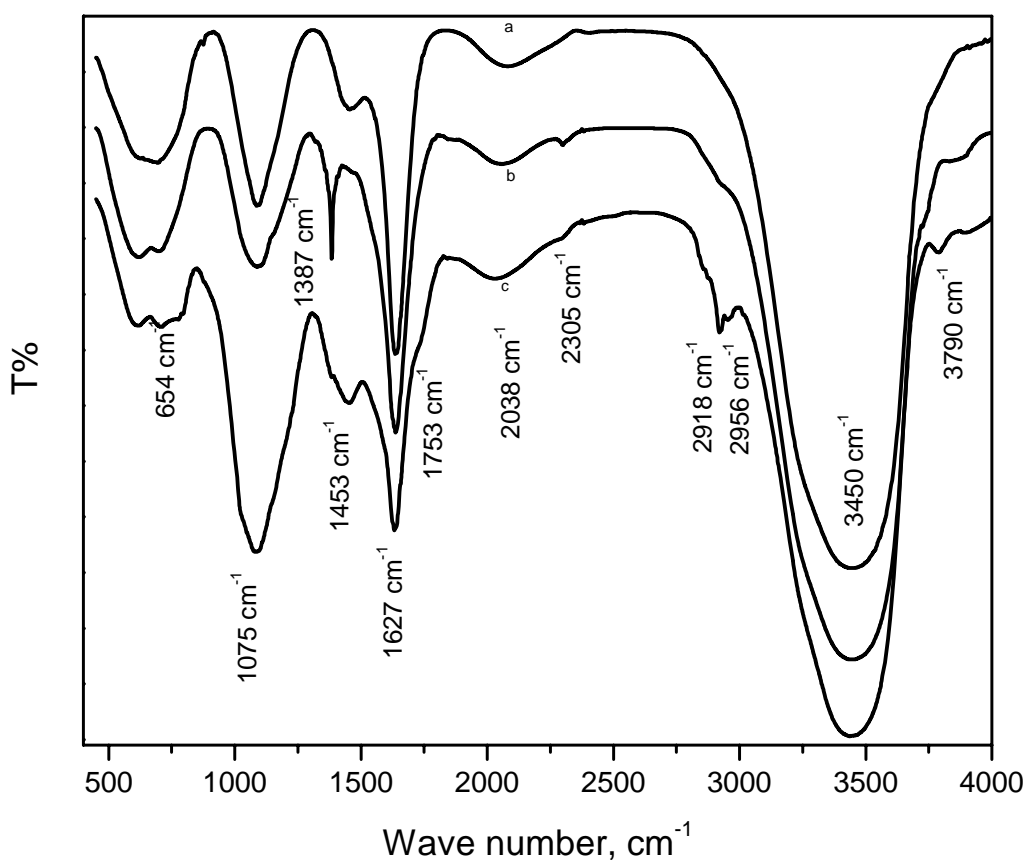
Fig. 41. FT-IR spectra of (a) Calgon carbon as received, (b) Calgon carbon treated with HNO$_3$ and (c) Calgon carbon treated with HNO$_3$ followed by Ar activation

In spite of the several striking changes brought about, as discussed above, into the surface functionality of calgon carbon upon treatment with conc. HNO_3 and subsequent Ar activation, some inherent functional groups of parent calgon carbon remained unaltered even after modification. The spectral features common to all the three samples shown in Figs. 41 (a), (b) and (c) are as follows: the broad intense transmission peak centered at 3450 cm^{-1} corresponding to OH stretching mode of hydroxyl groups and adsorbed water and the broad intense peak centered at 1075 cm^{-1} which can be attributed to C-O stretching in acids, alcohols, phenols, ethers and esters [202].

Thus a variety of surface functional groups, namely, the hydrophilic groups such as C=O (carboxylic and ketonic), isolated -OH groups and hydrophobic C-H groups of methylene were generated on the calgon carbon surface upon treatment with conc. HNO_3 and subsequent activation in Ar atmosphere. Interestingly such a transformation in surface chemistry is achieved by keeping intact the inherent surface functionality of parent calgon carbon (Fig. 41 (a)).
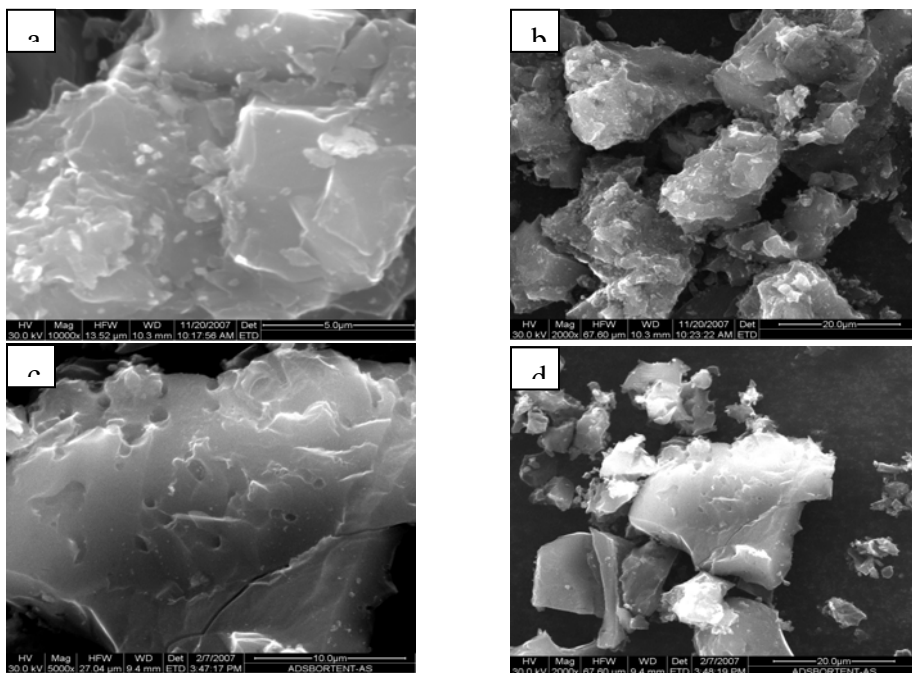

Fig. 42. SEM images (a) calgon carbon as received (magnification - 10, 000 x), (b) calgon carbon as received (magnification - 2, 000 x), (c) adsorbent carbon as received (magnification – 10, 000 x) and (d) adsorbent carbon as received (magnification - 2,000 x)

Details of surface microstructure of calgon carbon (as received) and adsorbent carbon (as received) are obtained from the scanning electronic microscopic studies. SEM images facilitate direct observation of the surface morphological features of adsobents. SEM images of calgon carbon as received at two different magnifications namely 10, 000 x and 2, 000 x are shown in Figs. 42 (a) and (b). The calgon carbon particles possess slate like morphology. The surface of calgon carbon is highly heterogeneous and rough with steps, kinks, edges and terraces.

SEM images of adsorbent carbon as received are recorded at two different magnifications namely 10, 000 x and 2000 x . The two images are depicted in Fig. 42 (c) and (d) respectively. There is close resemblances between the surface morphology of adsorbent carbon as received (Fig. 42 (c, d)) and calgon carbon as received. Both the carbon materials possess slate like particle morphology. But the surface of adsorbent carbon (Fig. 42 (c)) is relatively smoother than that offered by calgon carbon (Fig. 42 (a)). Unlike calgon carbon surface (Fig. 42 (a)), some porous network which is in its incipient stage is seen on the surface of adsorbent carbon (Fig. 42 (c)).

Evaluation of Adsorptive Desulphurization Potential of Adsorbent and Calgon based Carbon Materials

Adsorbent carbon as received, adsorbent carbon treated with HNO_3, adsorbent carbon treated with HNO_3 followed by Ar activation, calgon carbon as received, calgon carbon treated with nitric acid, calgon carbon treated with nitric acid followed by Ar activation were all employed as sorbents for S removal from SR diesel. The adsorptive desulphurization process was carried out using these sorbents at three different batch scales, namely, 5.0 g, 10.0 and 15.0 g. S sorption increased linearly as the amount of sorbent employed increased from 5 to 15 g irrespective of the sorbent used. Also nitric acid treatment and subsequent Ar activation greatly enhanced the S adsorption ability of both adsorbent carbon and calgon carbon. It is observed from the data presented in Table 23 that to derive the best from the oxidative treatment of carbon material, either adsorbent carbon or calgon carbon, subsequent activation in Ar atmosphere is a must.

Table 23.   Comparison of the S sorption capacity of Adsorbent carbon as received, Adsorbent carbon treated with HNO$_3$, Adsorbent carbon treated with HNO$_3$ followed by Ar activation, Calgon carbon as received, Calgon carbon treated with HNO$_3$, Calgon carbon treated with HNO$_3$ followed by Ar activation

Sorbent Amount	5.0 g	10.0 g	15.0 g
Sorbent Type	S removed*, (in ppm)		
Adsorbent carbon as received	229	380	410
Adsorbent carbon treated with HNO$_3$	105	186	577
Adsorbent carbon treated with HNO$_3$ followed by Ar activation	346	518	586
Calgon carbon as received	181	371	451
Calgon carbon treated with HNO$_3$	280	378	488
Calgon carbon treated with HNO$_3$ followed by Ar activation	340	399	619

* The product under consideration is the first 20 ml diesel obtained through the sorbent bed
* S content in the diesel feed – 737 ppm

Table 24. Type and amount of the S compounds in the feed and the product diesel (after passing through the carbon bed) as analyzed by GC – PFPD

Sulphur Species	S content (in ppm)		
	CBR diesel (Feed)	Adsorbent carbon HNO$_3$ followed by Ar treatment, 15.0 g	Calgon carbon, HNO$_3$ followed by Ar treatment, 15.0 g
C$_1$BT	4.6	Nil	Nil
C$_2$BT	119.6	Nil	Nil
C$_3$BT	137.5	75.2	67.2
C$_3^+$BT	79.6	68.9	47.4
DBT	91.5	2.6	1.3
C$_1$DBT	157.7	Nil	Nil
C$_2$DBT	116.7	Nil	Nil
C$_3$DBT	29.5	4.3	2.1
Total S	737	151	118

A combination of nitric acid treatment and Ar activation induces suitable surface functionality (discussed under FT-IR section), polarity (surface hydrophilic and hydrophobic functional groups), phase structure (discussed under XRD) and pore structure (discussed under BET sorptometry) into the carbon adsorbents facilitating enhanced adsorption for organo sulphur compounds present in the diesel feed stocks. The adsorptive desulphurization process utilizing carbon materials (activated by the

method which is a combination of nitric acid treatment and Ar activation) as adsorbents is an efficient and potent not only in terms of eliminating significant amounts of S from the feed as shown in Table x. but also the carbon materials are potential adsorbents for the removal of refractory S compounds. The nature of S components present in the product diesel was analyzed using GC – PFPD and the results obtained over 15.0 g sorbent bed using modified Adsorbent carbon (A) and Calgon carbon (B) are shown in Table 24.

Scaling up studies on s sorption - 100 g batch

Table 25. S adsorption studies on 100 g Adsorbent carbon HNO_3 treated, Ar activated and Calgon carbon as received

S. No.	ml-diesel/g adsorbent	S content in the product (S content removed) (in ppm)	
		Adsorbent carbon activated with HNO_3 followed by Ar activation	Calgon carbon as received
1	0.2	13 (724)	137 (600)
2	0.4	68 (669)	192 (545)
3	0.6	110 (627)	233 (504)
4	0.8	169 (568)	302 (435)
5	1.0	194 (543)	302 (435)
6	1.2	233 (504)	313 (424)
7	1.4	263 (474)	317 (420)
8	1.6	290 (447)	379 (358)
9	1.8	325 (412)	444 (293)
10	2.0	375 (362)	457 (280)
11	2.2	415 (322)	479 (258)
12	2.4	443 (294)	520 (217)
13	2.6	463 (274)	557 (180)
14	2.8	486 (251)	567 (170)
15	3.0	496 (241)	519 (218)
16	3.2	505 (232)	532 (205)
17	3.4	510 (227)	548 (189)

Apart from 5.0, 10.0, 15.0 g batches the process has been scaled up to 100 g batch too. But only two representative sorbents were tested, namely, calgon carbon as received and adsorbent carbon treated with HNO_3 and activated in Ar atmosphere. The result obtained from desulphurization studies are given in Table 25. Deisel with S content less

than 50 ppm and 200 ppm were obtained using adsorbent carbon treated with nitric acid followed by Ar activation and Calgon carbon as received which is a remarkable break through. Even after passing 3.4 ml diesel per gram of adsorbent, nearly 200 ppm of S is being removed from diesel feed indicating the effective function of the tailored carbon based adsorbents produced.

Regeneration of Adsorbent:

The carbon materials (adsorbent carbon, modified adsorbent carbon materials, calgon carbon and modified calgon carbon materials) employed for adsorptive desulphurization were found to be completely regenerable. The activity of the spent sorbent is regenerated by a simple process of elution with toluene. The performance of the regenerated sorbent bed is similar to that of the fresh adsorbent bed indicating the usefulness of the developed regeneration process.

Table 26. Comparison of the performance of fresh and regenerated sorbent (100 g Calgon carbon as received) for S sorption

S. No.	100 g Calgon as received	S content in the product (S removed) in ppm	
	ml-diesel/g adsorbent	Fresh sorbent	Regenerated sorbent
1	0.2	137 (600)	97 (640)
2	0.4	192 (545)	110 (627)
3	0.6	233 (504)	162 (575)
4	0.8	302 (435)	256 (481)
5	1.0	302 (435)	297 (440)
6	1.2	313 (424)	370 (367)
7	1.4	317 (420)	387 (350)
8	1.6	379 (358)	443 (294)
9	1.8	444 (293)	505 (232)
10	2.0	457 (280)	512 (225)
11	2.2	479 (258)	548 (189)
12	2.4	520 (217)	549 (188)
13	2.6	557 (180)	551 (186)
14	2.8	567 (170)	554 (183)

Solvent (Toluene) based regeneration method is employed. The spent sorbent used is the 100 g calgon carbon as received upon which desulphurization studies were

previously carried out (3rd column of Table 26). The Toluene solvent (500 ml) used to flush the spent sorbent is collected at the out let in the batches of 100 ml and labeled as T1, T2, T3, T4 and T5. The S content in T1, T2, T3, T4 and T5 are respective 757, 275, 81, 173 and 474. Thus essentially the spent sorbent is made S free as Toluene played an effective role in desorbing the adsorbed S compounds. The sorbent bed is then dried and used subsequently for next run of desulphurization.

Adsorptive desulphurization studies were then carried out on the regenerated sorbent bed. Diesel is fed through the column and the product diesel is collected from time to time in the amounts of 20 ml per batch at the outlet and analysed for S content. The process is stopped when S content of the outlet becomes equal to the S content of the feed. The S sorption results obtained on regenerated 100 g calgon carbon as received are presented in Table 26. For easy comprehension of the relative performance of fresh and regenerated sorbents the data in Table 26 are represented pictorially in Fig. 43. It is evident from the curves shown in Fig. 43. that regenerated sorbent's performance is on a par with that of the original fresh calgon carbon as received. Thus an effiecient, economic and environmentally benign regeneration method is developed.
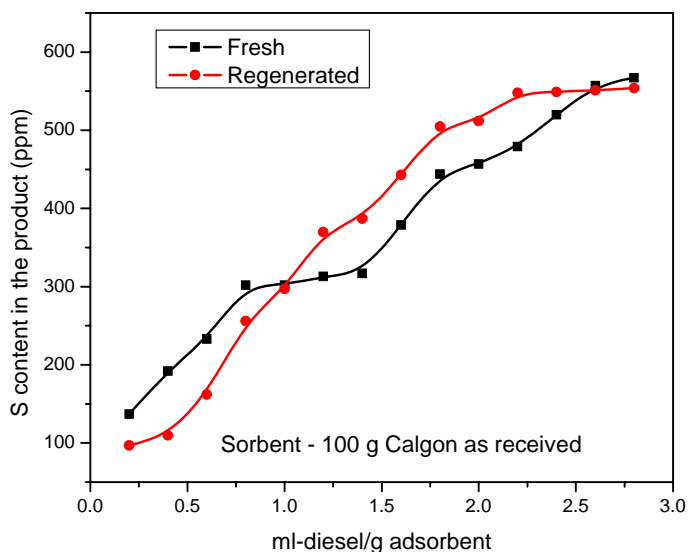

Fig. 43. Plot of S removal capacity of fresh Vs toluene regenerated sorbent (100 g calgon carbon as received)

An efficient desulphurization process based on adsorption, operated under modest conditions of temperature and pressure is developed. The potential of the process of adsorptive desulphurization lies in the elimination of refractive S containing compounds under mild process parameters. New method of activation, which is a unique combination of nitric acid treatment and Ar activation, of carbon based adsorbents to induced desired surface functionality, polarity, phase composition and pore texture, is developed. It was found that subsequent Ar activation of nitric acid treated carbon adsorbents are inevitable to derive the best out of oxidative modification of carbon surface chemistry. The utility of Adsorbent carbon as well as Calgon carbon and their tailored forms as adsorbents for organo sulphur compounds is elucidated. The process of adsorptive desulphurization is scaled upto 100 g (adsorbent) batch. In addition to the successful removal of appreciable amounts of S from diesel feed stocks using tailored carbon based adsorbents, simple, inexpensive, efficient, environmentally benign and reliable solvent (toluene) based regeneration has also been developed. The study strengthened our hope that newer desulphurization technologies are not too far to the refinery industry.

SECTION V

Conclusion

Methods of activation of carbon materials have opened up a new avenue to tune the structural, textural, morphological and surface properties of carbon materials to suit to the problem in hand. Activation methods based on environmentally benign activating agents (for instance organic acids and the alkali metal salts there of) with mild reaction conditions need to be developed. The sphere of usefulness of carbon materials increases manifold with the progress in the activation recipes.

SECTION VI
Acknowledgments

<div style="border:1px solid black;">

SECTION VII

References

</div>

[1]. Mansooreh Soleimani, Tahereh Kaghazchi, Bioresource Technology 99 (2008) 5374

[2] Xiaoge Chen, S. Jeyaseelan, N. Graham, Waste Management 22 (2002) 755

[3] M. Endo, C. Kim, K. Nishimura, T. Fujino, K. Miyashita, Carbon 38 (2000) 183

[4] A. G. Pandolfo, A. F. Hollenkamp, Journal of Power Sources, 157 (2006) 11

[5] Andrew L. Dicks, Journal of Power Sources, 156 (2006) 128

[6]. H. Fritzst Oeckli, Carbon 28 (1990) 6

[7] Michal Kruk, Bruno Dufour, Ewa B. Celer, Tomasz Kowalewski, Mietek Jaroniec and Krzysztof Matyjaszewski, J. Phys. Chem. B 2005, 109, 9216-9225

[8] An-Hui Ru and Jing-Tang Zheng, Journal of Colloid and Interface Science, 236 (2001) 369-374

[9] Junichi Hayashi, Atsuo Kazehaya, Katsuhiko Muroyama, A. Paul Watkinson, Carbon 28 (2000) 1873-1878

[10] Asa Don Dickinson, Great Leaders of the world, Stories of Achievement, , Garden City Publishing Co, Inc. Garden city, New York, 1937.

[11]. Timothy G. Rials and Wolfgang G Glasser, Journal of Applied Polymer Science 37 (1989) 2399

[12]. S. Kubo, Y. Uraki and Y. Sano, Carbon 36 (1998) 1119

[13]. Sanjay Sarkar, Basudam Adhikari, European Polymer Journal 37 (2001) 1391

[14]. M. Olivares – Marin, C. Fernandez – Gonzalez, A. Macias – Garcia, V. Gomez – Serrano, Applied Surface Science 252 (2006) 5967

[15]. J. Ganan, J. F. Gonzalez, C. M. Gonzalez-Garcia, A. Ramiro, E. Sabio, S. Roman, Applied Surface Science, 252 (2006) 5988

[16]. Maryam Kazemipour, Mehdi Ansari, Shabnam Tajrobehkar, Majdeh Majdzadeh, Hamed Reihani Kermani, Journal of Hazardous Materials, 150 (2008) 322

[17]. Y. Onal, C. Akmil-Basar, C. Sarici-Ozdemir, Journal of Hazardous Materials, 148 (2007) 727

[18] E. Demirbas, M. Kobya and M. T. Sulak, Bioresource Technology, 99 (2008) 5368

[19] Mansooreh Soleimani, Tahereh Kaghazchi, Chinese Journal of Chemical Engineering 16 (1) (2008) 112

 [20] Cigdem Sentorun – Shalaby, Mine G. Ucak-Astarhoglu, Levent Artok, Cigdem Sarici, Microporous and Mesoporous Materials, 88 (2006) 126

[21] M. Kobya, E. Demirbas, E. Senturk and M. Ince, Bioresource Technology 96 (2005) 1518

[22] B. H. Hameed, A. T. M. Din, A. L. Ahmed, Journal of Hazardous Materials 141 (2007) 819

[23] Yong-Jung Kim, Byoung-Ju Lee, Hiroaki Suezaki, Teruaki Chino, Yusuke Abe, Takashi Yanagiura, Kichul Park, Morinobu Endo, Carbon 44 (2006) 1592

[24] Dinesh Mohan, Kunwar P. Singh, Vinod K Singh, Journal of Hazardous Materials, 135 (2006) 280

 [25] Jeremias S Macedo, Larissa Otubo, Odair Pastor Ferreira, Iara de Fatima Gimenez, Italo Odone Mazali, Ledjane Silva Barreto, Microporous and Mesoporous Materials, 107 (2007) 276

[26] Badie S. Girgis, Amina A. Attia, Nady A. Fathy, Colloids and Surfaces A: Physico Chem. Eng. Aspects 299 (2007) 79

[27] Ru-Ling Tseng, Szu-kung Tseng, Journal of Hazardous Materials B 136 (2006) 671

[28] F. Suarez-Garcia, A. Martinez-Alonso, J. M. D. Tascon, Carbon 39 (2001) 1103

[29] F. Suarez-Garcia, A. Martinez-Alonso, J. M. D. Tascon, Journal of Analytical and Applied Pyrolysis, 62 (2002) 93

[30] F. Suarez-Garcia, A. Martinez-Alonso, J. M. D. Tascon, Journal of Analytical and Applied Pyrolysis, 63 (2002) 283

[31] Fabian Suarez Garcia, Amelia Martinez Alonso, Juan Manuel Diez Gascon, Manufacture of activated carbon from Apple pulp, Pat. No. ES 2173032

[32] Teresa Alvarez Centeno, Hermann Friedrich Stoeckli, Method of producing activated carbons from apple pulp for use as electrodes in electric double – layer capacitors (EDLC), PCT Int Appl. 2006, Pat. No. W02006103310

[33] E. C. Bernaro, R. Egashira, and J. Kawasaki, Carbon 35 (1997) 1217

[34] N. Syna, M. Valix, Minerals Engineering 16 (2003) 511

[35] Ashok Nagesh Gokam, Narendra Vasant Sankpal, An improved process for the manufacture of activated carbon, Patent No. IN 2000DE01216

[36] W. T. Tsai, C. Y. Chang, S. L. Lee, Carbon 35 (1997) 1198

[37] Chiung – Fen Chang, Ching – Yuan Chang, Wen – Tien Tsai, Jouranl of Colloid and Interface Science 232 (2000) 45

[38] Trivette Vaughan, Chung W. Seo, Wayne E Marshall, Bioresource Technology 78 (2001) 133

[39] Qing Cao, Ke-Chang, Yong-Kang Lv, Wei-Ren Bao, Bioresource Technology 97 (2006) 110

[40] Jorge Laine, Alvaro Calafat, Carbon 29 (7) (1991) 949

[41] Jorge Laine, Simon Yunes Carbon 30 (4) (1992) 601

[42] A. G. Pandolfo, M. Amini-Amoli and J. S. Killingley, Carbon 32 (5) (1994) 1015

[43] Beer Singh, S. Madhusudhanan, Vinita Dubey, Rabinder Nath, and N. B. S. N. Rao, Carbon 34 (1996) 327

[44] Zhonghua Hu and M. P. Srinivasan, Microporous and Mesoporous Materials, 27 (1) (1999) 11

[45] N. Yoshizawa, K. Maruyama, Y. Yamada and M. Zielinoka-Blajet, Fuel 79 (12) (2000) 1461

[46] Wenming Qiao, Yozo Korai, Isao Mochida, Yuuichi Hori, Takeshi Maeda, Carbon 40 (2002) 351-358

[47] Wei Su, Li Zhou, Yaping Zhou, Carbon 41 (4) (2003) 861

[48] Sandhya Babel, Tonni Agustiono Kurniawan, Chemosphere 54 (7) (2004) 951

[49] Wan Mohd Ashri Wan Daud, Wan Shabuddin Wan Ali, Bioresource Technology 93 (1) (2004) 63

[50] M. Sekar, V. Sakthi, S. Rengaraj, Bioresource Technology, 93 (1) (2004) 63

[51] Mukta S Dandekar, Girish Arabale, K. Vijaya Mohanan, Journal of Power Sources 141 (1) (2005) 198

[52] Diana C. S. Azevedo, J. Cassia S. Araujo, Moises, Bastos-Neto, A. Eurico B. Torres, Emerson F Jaguaribe, Celio L. Cavalcante, Microporous and Mesoporous Materials 100 (1-3) (2007) 361

[53] Osei-Wasu Achaw, George Afrane, Microporous and Mesoporous Materials 112 (1-3) (2008) 284

[54] Wei Li, Kunbin Yang, Jinhui Peng, Libo Zhang, Shenghui Guo, Hongying Xia, Industrial Crops and Products 28 (2008) 190

[55] Jinhui Peng, Libo Zhang, Kunbin Yang, Hongying Xia, Shimin Zhang, Sheng-hui Guo, Waste Management, 29 (2008) 756

[56] Feng Zhang, Hua Ma, Jun Chen, Guo – Dong Li, Yu Zhang, Jie – Sheng chen, Bioresource Technology, 99 (2008) 4803

[57] Badie S. Girgis, Abdel-Nasser A. El-Hendawy, Microporous and Mesoporous
   Materials 52 (2002) 105

[58] Zoulikha Merzougui, Fatima Addoun, Desalination 222 (2008) 394

[59] Shaheen A Al-Muhtaseb, Muftah H El-Naas, Sami Abdallah, Journal of Hazardous Materials 158 (2008) 300

[60] J. D. Rocha, A. R. Coutinho and C. A. Luengo, Brazilian Journal of Chemical Engineering, 19 (2002) 127-132

[61] I. A. Rahman and B. Saad, Malaysian Journal of Chemistry, 5 (2003) 8

[62] M. Fan, W. Marshall, D. Daugaard, R. C. Brown, Bioresource Technology 93 (2004) 103

[63] C. L. Chuang, M. Fan, M. Xu, R. C. Brown, S. Sung, B. Saha, C. P. Huang, Chemosphere 61 (2005) 478

[64] Margaret Iley, H Marsh and F. Rodriguez Reinoso, Carbon 11 (1973) 633

[65] J. de D. Lopez-Gonzalez, F. Martinez-Vilchez and F. Rodriguez-Reinoso, Carbon 18 (1980) 413

[66] M. T. Gonzalez, M. Malina-Sabio and F. Rodrignez-Reinoso, Carbon 32 (1994) 1407

[67] Carlos Moreno-Castilla, Francisco Carrosco-Marin, M. Victoria Lopez-Ramon, Miguel A. Alvarez-Merino, Carbon 39 (2001) 1415-1420

[68] Augustin F. Perez-Cadenas, Francisco J. Maldonado-Hodar, Carlos Moreno-Castilla, Carbon 41 (2003) 473-478

[69] Amjad H El-Sheikh, Alan P Newman, Hafid K al-Daffaee, Suki Phull, Neil Cresswell, Journal of Analytical and Applied Pyrolysis 71 (2004) 151

[70] M. L. Martinez, M. M. Torres, C. A. Guzman and D. M. Maestri, Industrial Crops and Products, 23 (2006) 23

[71] Ruth Ubago – Perez, Francisco Carrasco – Marin, David Fairen – Jimenez, Carlos Moreno – Castilla, Microporous and Mesoporous Materials, 92 (2006) 64

[72] Ibrahim Kula, Mehmet Ugurlu, Hamdi Karaoglu, Ali Celik, Bioresource Technology, 99 (2007) 492

[73] N. Spahis, A. Addoun, H. Mahmoudi, N. Ghaffour, Desalination, 222 (2008) 519

[74] Guillermo Rodriguez, Antonio Lama, Rocio Rodriguez, Ana Jimenez, Rafael Guillen, Juan Fernandez – Bolanos, Bioresource technology 99 (2008) 5261

[75] Mehmet Ugurlu, Ahmet Gurses Metin Acikyildiz, Microporous and Mesoporous Materials 111 (2008) 228

[76] Carlos Macias Gallego, Rafael Perez Castells, Franciso Agnado Arroyo, Activated carbon from plant sources and process for its preparation, Patent No. ES 2301381

[77] Badie S. Girgis, Samya S. Yunis, Ashraf M. Soliman, Materials Letters 57 (2002) 164

[78] Sayed A. Dastgheib, David A. Rockstraw, Carbon 39 (2001) 1849

[79] Ru-Ling Tseng, Feng-Chin Wu, Ruey-Shin Juang, Carbon 41 (2003) 487

[80] Nevin Yalcin, Vahdettin Sevinc, Carbon 38 (2000) 1943

[81] Yupeng Guo, Jurui Qi, Shaofeng Yang, Kaifeng Yu, Zichen Wang, Hongding Xu, Materials Chemistry and Physics, 78 (2002) 132

[82] Yupeng Guo, Hui Zhang, Nannan Tao, Yanhua Liu, Juirui Qi, Zichen Wang, Hongding Xu, Materials Chemistry and Physics 82 (2003) 107

[83] Yupeng Guo, Shaofeng Yang, Wuyon Fu, Jurui Qi, Renzhi Li, Zichen Wang, Hongding Xu, Dyes and Pigments, 56 (2003) 219

[84] Narsi Ram Bishnoi, Mini Bajaj, Nivedita Sharma, Asha Gupta, Bioresource Technology, 91 (2003) 305

[85] Jurui Qi, Zhi Li, Yupeng Guo, Hongding Xu, Materials Chemistry and Physics, 87 (2004) 96

[86] L. John Kennedy, K. Mohan das, G. Sekaran, Carbon 42 (2004) 2399

[87] Yupeng Guo, Jingzhe Zhao, Hui Zhang, Shaofeng Yang, Jurui Qi, Zichen Wang, Hongding Xu, Dyes and Pigments 66 (2005) 123

[88] Dimitrios Kalderis, Dimitrios Koutoulaskis, Panagiota Paraskeva, Evan Diamadopoulos, Emilia Otal, Joaquin Olivares del Valle, Constantino Fernandez-Pereira, Chemical Engineering Journal, 144 (2008) 42

[89] Gyu Hwan Oh, Chong Rae Park, Fuel 81 (2001) 327

[90] Chang Hun Yun, Yun Heum Park, Chong Rae Park, Carbon 39 (2001) 559

[91] Shan-Li Wang, Yu-Mind Tzon, Yi-Hsien Lu, Guangyao Sheng, Journal of hazardous materials, 147 (2007) 313

[92] A. A. M. Daifullah, S. M., Yakout, S. A. Elreefy, Journal of Hazardous Materials, 147 (2007) 633

[93] V. Gomez-Serrano, J. Pastor-Villegas, C. J. Duran-Valle, and C. Valenzuela-Calahorro, Carbon 34 (1996) 533

[94] J. Pastor-Villegas, C. J. Duran-Valle, Carbon 40 (2002) 397

[95] P. K. Malik, Journal of Hazardous Materials B113 (2004) 81

[96] S. Ismadji, Y. Sudaryanto, S. B. Hartono, L. E. K. Setiawan, A. Ayucitra, Bioresource Technology 96 (2005) 1364

[97] Vicente Gmez-Sarrano, Eduardo M. Cuerda-Correa, M Carmen Fernandez-Gonzalez, Maria F Alexandre-Franco and Antonio Macias-Garcia, Smart Mater. Struct.14 (2005) 363

[98]. D M Makay and P V Roberts 20 (1982) 87

[99] F. A. Cotton, and G. Wilkinson, Basic Inorganic Chemistry, John Wiley & Sons, 1976.

 [100]. M. M. Tang and Roger Bacon, Carbon 2 (1964) 211

[101] Wolfgang Heschel and Erhard Klose, Fuel 74 (1995) 1786

[102] Harry Marsh and Denis S. Yan, Carbon 22 (1984) 603

[103] Seong-Ho Yoon, Seongyop Lim, Yan Song, Yasunori Ota, Wenming Qiao, Atsushi Tanaka, and Isao Mochida, Carbon 42 (2004) 1723

[104] Byung – Joo Kim, Young – Seak Lee, Soo – Jin Park, Journal of Colloid and Interface Science, 306 (2007) 454

[105] Yupeng Guo, Shaofeng Yang, Kaifeng Yu, Jingzhe Zhao, Zichen Wang, and Hongding Xu, Materials Chemistry and Physics 74 (2002) 320

[106] Yong bin Ji, Tiehu Li, Li Xiaoxian Wang, and Qilang Lin, Applied Surface Science, 254 (2007) 506.

[107] Zengmin Shen, and Ruisheng Xue, Fuel Processing Technology 84 (2003) 95

[108] Hye - Ryun Hwang, Won-Joon Choi, Taek – Joon Kim, Jin-Seop Kim, Kwang - Joong Oh, Journal of Analytical and Applied Pyrolysis, 83 (2008) 220

[109] Joanna Gorka, Aleksandra Zawislak, Jerzy Choma, and Mietek Jaroniec, Carbon 46 (2008) 1159.

[110] Qi Jiang, Mei-Zhen Qu, Bo-Lan Zhang, Zuo-Long Yu, Carbon 40 (2002) 2743

[111] Yunfang Liu, Zengmin Shen, Kiyoshi Yokogawa, Materials Research Bulletin 41 (2006) 1503

[112] Q. Jiang , M.Z. Qu, G.M. Zhou, B.L. Zhang, Z.L. Yu, Materials Letters 57 (2002) 988–991

 [113] K. Kierzek, E. Frackowiak, G. Lota, G. Grygle Wicz and J. Machnikowski, Electrochimica Acta 49 (2004) 515

[114] Kim Konoshita, Carbon Electrochemical and Physicochemical Properties, John Wiley & Sons, 1988, p. 87

 [115] M. A. Lillo-Rodenas, D. Cazorla-Amoros, A. Linares – Solano, Carbon 41 (2003) 267

[116] Ru-Ling Tseng, Journal of Hazordous Materials 147 (2007) 10

[117] Yasumasa Yamashita and Koji Ouchi, Carbon 20 (1982) 47

[118] Jair C. C. Freitas, Miguel A. Schettino, Francisco G Emmerich, Alan Wong, Mark E Smith, Solid State Nuclear Magnetic Resonance 32 (2007) 109

[119] Jair C C Freitas, Miguel A. Schettino Jr., Alfredo G. Cunha, Franciso G. Emmerich, Antonio C. Bloise, Eduardo R De Azevedo, Tito J Bonagamba, Carbon 45 (2007) 1097

[120] Alejandro Robau – Sanchez, Federico Cordero – de la Rosa, Julia Aguilar – Pliego, Alfredo Aguilar – Elguezabal, Journal of Porous Materials 13 (2006) 123

[121] Kiyoshi Okada, Nohuo Yamamoto, Yoshikazu Kameshima and Atsuo Yasumori, Journal of Colloid and Interface Science 262 (2003) 179

[122] A. Addoun, J. Dentzer, P. Ehrburger, Carbon 40 (2002) 1131

[123] David A Fox and Alfred H White, Ind. Eng. Chem., 23 (3) (1931) 259

[124] Douglas W. Mckee, Fuel 62 (1983) 170

[125] L. S. Singer, 1961, p. 37-64, in Proceedings of the fifth conference on carbon, Volume 2, Symposium Publications Division, Pergamon Press, 1963.

[126] F Beguin, R Settan, Carbon 10 (1972) 539

[127] Isao Mochida, Ei-ichi Nakamura, Keiko Maeda and Kenjiro Takeshita, Carbon 13 (1975) 489

[128] Isao Mochida, Ei-ichi Nakamura, Keiko Maeda and Kenjiro Takeshita, Carbon 14 (1976) 123

[129] J. Hayashi, N. Yamamoto, T. Horikawa, K. Muroyama and V. G. Gomes, Journal of Colloid and Interface Science 281 (2005) 437

[130]. Wei Li, Li-bo Zhang, Jin − hui Peng, Ning Li, Xue − yun Zhu, Industrial Crops and Products 27 (2008) 341

[131] Ru-Ling Tseng, Journal of Hazardous Materials 147 (2007) 1020

[132] B. Viswanathan, T. K. Varadarajan, P. Indra Neel, A process for the preparation of activated carbon from botanical sources, , Indian Pat. Appl. (2008), IN 2007CH00376 A 20081128

[133]. Jair C. C. Freitas, Tito J. Bonagamba, Francisco G Emmerich, Carbon 39 (2001) 535

[134] Satoshi Kubo, Yasumitsu Uraki and Yoshihiro Sano, Journal of Wood Science, 49 (2003) 188

[135] Viboon Sricharoenchaikul, Chiravoot Pechyen, Duangdao Aht-ong, and Duangduen Atong, Energy and Fuels, 22 (2008) 31

[136] Stephen Brunauer, Lola S Deming, W. Edwards, Deming, Edward Teller, 62 (1940) 1723

[137] S. J. Greg and K. S. W. Sing, "Adsorption, Surface Area and Porosity", Second Edition, New York, Academic Press, 1982.

[138] M. D. Adams, Hydrometallurgy, 26 (1991) 201

[139] Y. Chen, J. Chen, H. Hu, M. A. Hamon, M. E. Itkis and R. C. Haddon, Chemical Physics Letters 299 (1999) 532

[140] S. Mrozowski, Carbon 17 (3) (1979) 227

[141] P.Indra Neel, B. Viwanathan and T K Varadarajan, (unpublished result)

[142]. R Sarathi, P Rajesh Kumar, R. H. Sahu, Polymer Degradation and Stability 92 (2007) 560

[143] L. S. Singer and G. Wagoner, Carbon 6 (1968) 199

[144] Vilas Ganpat Pol, Menachem Motiei, Aharon Gedanken, Jose Calderon-Moreno, Masahiro Yoshimura, Carbon 42 (2004) 111

[145] Willard, Merrit, Dean, Instrumental Methods of Analysis, 5th Edition, 1974, p. 236

[146] A. Manivannan, M. Chirila, N. C. Giles, M. S. Seehra, Carbon 37 (1999) 1741

[147] O. Chauvert, L. Forro, Physical Review B (Condensed Matter and Materials Physics), 52 (1995) R6963

[148] O. Zhuo, R. M. Fleming, D. W., Murphy, C. H. Chen, R. C. Haddon, A. P. Ramirez, S. H. Gharum, Science 263 (1994) 1744

[149] Jean Baptiste Donnet, Roopchand Bansal, Meng-Jiao Wang, Carbon Black – Science and Technology, Second Edition, Revised and Expanded, CRC publications,

[150] Zhonghua Hu and E. F. Vansant, Journal of Colloid and Interface Science, 176 (1995) 422

[151] F. Caturla, M. Molina-Sabio and F. Rodriguez-Reinoso, Carbon 29 (1991) 999

[152] F. Caturla, M. Molina-Sabio and F. Rodriguez-Reinoso, Carbon 29 (1991) 999

[153] A. Ahmadpour and D. D. Do, Carbon 34 (1996) 471

[154] K. Anoop Krishnan, Colloids and Surfaces A: Physicochem. Eng. Aspects 317 (2008) 344

[155] Reynaldo Nacco and Eugenio Aquarone, Carbon 16 (1978) 31

[156]. Rafael Kandiyoti, John I Lazaridis, Bo Dyrvold and C. Ravindra Weerasinghe, Fuel 63 (1984) 1583

[157] M. Z. Hussein, R. S. H. Tarmizi, Z. Zainal, R. Ibrahim and M. Badri, Carbon 34 (1996) 1447

[158]. Jale Yanik, Mehmet Saglam, Guldem Ustun and Mithat Yuksel, Fuel 71 (1992) 712

[159] C. Namasivayam and K. Kadirvelu, Bioresource Technology 62 (1997) 123

[160] A process for the preparation of activated carbon from botanical sources, B. Viswanathan, T. K. Varadarajan, P. Indra Neel, Indian Pat. Appl. (2008),
IN 2007CH00376 A 20081128

[161] Devarly Prahas, Y. Kartika, N. Indraswati, S. Ismadji, Chemical Engineering Journal, 140 (2008) 32

[162] W. Ruland, Advanced Materials, 2 (1990) 528

[163] W. Ruland, B. Smarsly, Journal of Applied Crystallography, 35 (2002) 624

[164] Ting Yang, Aik Chong Lua, Materials Chemistry and Physics, 100 (2006) 438

[165] F. Tuinstra and J. L. Koenig, Journal of Chemical Physics, 53 (1970) 1126

[166] M. Nakamizo, R. Kammereck and P. L. Walker, JR, Carbon 12 (1974) 259

[167] Diane S. Knight and William B White, Journal of Materials Research, 4 (1989) 385

[168] A. W. P. Fung, A. M. Rao, K. Kuriyama, M. S. Dresselhaus, G. Dresselhaus, M. Endo, N. Shindo, Journal of Materials Research, 8 (1993) 498

[169] A. M. Rao, A. W. P. Feng, M. S. Dresselhaus, M. Endo, Journal of Materials Research, 7 (1992) 1788

[170] X. K. Li, L. Liu, Zh. H. Li, D. Wu, Sh. D. Shen, Carbon 38 (2000) 623

[171] M. Nakamizo and H. Honda and M. Inagaki and Y. Hishiyama, Carbon 15 (1977) 295

[172] M. Nakamizo, H. Honda and M. Inagaki, Carbon 16 (1978) 281

[173] Y. Sato, M. Kamo and N. Setaka, Carbon 16 (1978) 279

[174] Terrence P. Mernagh, Ralph P. Cooney and Robert A. Johnson, Carbon 22 (1984) 39

[175] X. K. Li, L. Liu, Zh. H. Li, D. Wu, Sh. D. Shen, Carbon 38 (2000) 623

[176] Hee Jin Jeong, Seung Yol Jeong, Young Min Shin, Jeong Ho Han, Seong Chu Lim, Sung Jin Eum, Cheol woong Yang, Nam-gyun Kim, Chong – Yum Park, Young Hee Lee, Chemical Physics Letters 361 (2002) 189

[177] Jieshan Qiu, Yongfeng Li, Yunpeng Wang, Changhai Liang, Tonghua Wang, Dehe Wang, Carbon 41 (2003) 767

[178] P.Indra Neel, B. Viswanathan and T K Varadarajan, (unpublished results)

[179] P. Lespade, R. Al-Jishi and M. S. Dresselhaus, Carbon 20 (1982) 427

[180] Tanzil Haider Usmani, Tamoor Wahab Ahmed and A. H. K. Yousufzai, Bioresource Technology 48 (1994) 31

[181] W. T. Tsai, C. Y. Chang and S. L. Lee, Bioresource Technology 64 (1998) 211

[182] Virote Boonamnuayvitaya, Srisuda Sae-ung, Wiwut Tanthapanichokoon, Separation and Purification Technology, 42 (2005) 159

[183] Kaustubha Mohanty, D. Das, M. N. Biswas, Chemical Engineering Journal, 115 (2005) 121

[184] Canan Akmil Basar, Journal of Hazardous Materials B135 (2006) 232

[185] Y. Onal, C. Akmil-Basar, C. Sarici-Ozdemir, S. Erdogan, Journal of Hazardous Materials, 142 (2007) 138

[186] C. Namasivayam, D. Sangeetha, Desalination 219 (2008) 1

[187] Jyothikusum Acharya, J. N. Sahu, C. R. Mohanty, B. C. Meikap, Chemical Engineering Journal (Article in Press)

[188] D. W. Mckee, Carbon 17 (1979) 419

[189] Yasumasa Yamashita and Koji Ouchi, Carbon 20 (1982) 55

[190] J. Laine, A. Calafat and M. Labady, Carbon 27 (1989) 191

[191] Marit Jogtoyen and Frank Derbyshire, Carbon 31 (1993) 1185

[192] M. Molina – Sabio, F. Rodriguez – Reinoso, F. Caturla and M. J. Selles, Carbon 33 (1995) 1105

[193] M. Molina – Sabio, F. Rodriguez – Reinoso, F. Caturla and M. J. Selles, Carbon 34 (1996) 457

[194] Marit Jagtoyen and Frank Derbyshire, Carbon 36 (1998) 1085

[195] Christopher A Toles, Wayne E. Marshall, Mitchell M. Johns, Carbon 37 (1999) 1207

[196] H. Benaddi, T. J. Bandosz, J. Jagiello, J. A. Schwarz, J. N. Rouzaud, D. Legras, F. Beguin, Carbon 38 (2000) 669

[197] A. M. Puziy, O. I. Poddubnaya, A. Martinez-Alonso, F. Suarez – Garcia, J. M. D. Tascon, Applied Surface Science 200 (2002) 196

[198] A. M. Puziy, O. I. Poddubnaya, A. Martinez – Alonso, F. Suarez – Garcia, J. M. D. Tascon, Carbon 41 (2003) 1181

[199] A. Marcias – Garcia, M. A. Diaz – Diez, V Gomez – Serrano and M. C. Fernandez Gonzalez, Smart Materials and Structures 12 (2003) N24-N28

[200] M. Molina-Sabio, F. Rodriguz-Reinoso, Colloids and Surfaces A: Physicochem. Eng. Aspects, 241 (2004) 15

[201] I. Martin – Gullon, J. P. Marco – Lozar, D. Cazorla – Amoros, A. Linores – Salano, Carbon 42 (2004) 1339

[202] Alexander M. Puziy, Olga I Poddubnaya, Amelia Martinez – Alonso, Fabian Suarez – Garcia, Jaun M. D. Tascon, Carbon 43 (2005) 2857

[203] I. A. Rahman, B. Saad, S. Shaidan, E. S. Sya Rizal, Bioresource Technology, 96 (2005) 1578

[204] V. Gomez – Serrano, E. M. Cuerda – Correa, M. C. Fernandez – Gonzalez, M. F. Alexandre – Franco, A. Macias – Garcia, Materials Letters 59 (2005) 846

[205] T. Budinova, E. Ekinci, F. Yardim, A. Grimm, E. Bjornbom, V. Minkova, M. Goranova, Fuel Processing Techonology 87 (2006) 899

[206] B. Corcho-Corral, M. Olivares – Marin, C. Fernandez – Gonzalez, V. Gomez – Serrano, A. Macias – Garcia, Applied Surface Science, 252 92006) 5961

[207] J. I. Paredas, F. Suarez-Garcia, A. Martinez – Alonso and J. M. D. Tascon, Langmuir 22 (2006) 9730

[208] A. M. Puziy, O. I. Poddubnaya, B. Gawdzik, M. Sobiesiak and M. M. Tsyba, Applied Surface Science 253 (2007) 5736

[209] S. Girgis, Amina A. Attia, Nady A. Fathy, Colloids and surfaces A: Physico chem. Eng. Aspects, 299 (2007) 79

[210] Yanping Guo, David A. Rockstraw, Bioresource Technology, 98 (2007) 1513

[211] Yanping Guo, David A. Rockstraw, Microporous and Mesoporous Materials 100 (2007) 12

[212] Amina A. Attia, Badie S. Girgis, Nady Fathy, Dyes and Pigments 76 (2008) 282

[213] Jorge Bedia, Juana Maria Rosas, Josefa Marquez, Jose Rodriguez – Mirasol, Tomas Cardero, Carbon 47 (2009) 286

[214] P. Battistoni, S. Bompadre and G. Fava, Materials Chemistry and Physics, 11 (1984) 339

[215] Joong S. Noh and James A. Schwarz, Carbon 28 (1990) 675

[216] P. Vinke, M. Van Der Eijk, M. Verbree, A. F. Voskamp and H. Van Bekkum, Carbon 32 (1994) 675

[217] A. Gil, G. Dela Puente, P. Grange, Microporous Materials 12 (1997) 51

[218] V. Gomez-Serrano, M. Acedo-Ramos, A. J. Lopez-Peinado, C. Valenzuela-Calahorro, Thermo Chimica Acta 291 (1997) 109

[219] Jae – Woon Shim, Soo – Jin Park, Seung – Kon Ryu, Carbon 39 (2001) 1635

[220] Abdel-Nasser A. El-Hendaway, Carbon 41 (2003) 713f

[221] . Naiqin Zhao, Nawei, Jiajun Li, Zhijun Qiao, Jing Cui, Fei He, Chemical Engineering Journal 115 (2005) 133

[222] E. M. Cuerda – Correa, M. Olivares – Marin, J. Ganan – Gomez, Applied Surface Science, 252 (2006) 5972

[223] J. A. Caballero, A. Marcilla and J. A. Conesa, Journal of Analytical and Applied Pyrolysis 44 (1997) 75

[224] Patricia Alvarez, Clara Blanco, Marcos Granda, Journal of Hazardous Materials 144 (2007) 400

[225] Ozgul Gercel, Adnan Ozcan, A. Safa Ozcan, H. Ferdi Gercel, Applied Surface Science, 253 (2007) 4843

 [226] Nzongola Kayembe and Allen H. Pulsifer, Fuel 55 (1976) 211

[227] K. Otto and M. Shelef, Carbon 15 (1977) 317

[228] D.W. McKee and D. Chatterji, Carbon 16 (1978) 53

[229] J. C. Gonzalez, M. T. Gonzalez, M. Molina – Sabio, F. Rodriguez-Reinoso and A. Sepulveda-Escribano, Carbon 33(1995) 1175

[230] M. J. Lazaro, M. E. Galvez, S. Artal, J. M. Palacios and R. Moliner, Journal of Applied Pyrolysis, 78 (2007) 301

[231] A. Aranda, R. Murillo, T. Garcia, M. S. Callen, A. M. Mastral, Chemical Engineering Journal, 126 (2007) 79

[232] Francisco Salvador, M. Jesus Sanchez – Montero, Jessica Montero and Carmen Izquierdo, Journal of Physical Chemistry C 112 (2008) 20057

[233] P. Gonzalez – Vilchez, A. Linares – Solano, J. de D. Lopez – Gonzalez and F. Rodriguez – Reinoso, Carbon 17 (1979) 441

[234] C. Salinas-Martinez de Lecea, A. Linares – Solano, Carbon 19 (1981) 65

[235] John H. Marsh and S. Walter Orchard, Carbon 30 (1992) 895

[236] O. C. Kopp, E. L. Fuller, C. R. Sparks, M. R. Rogers and M. L. McKinney, Carbon 35 (1997) 1765

[237] Vicento Gomez – Serrano, Fernando Piriz – Almeida, Carlos Javier Duran – Valle, Jose Pastor – Villegas, Carbon 37 (1999) 1517

[238] Man S. Tam and Michael Jerry Antal Jr., Ind. Eng. Chem. Res. 38 (1999) 4268

[239] F. Rodriguez – Reinoso, J. de D. Lopez – Gonzalez and C. Berenguer, Carbon 20 (1982) 513

[240] Rosa Torrgrosa and Jose Miguel Martin – Martinez, Fuel 70 (1991) 1173

[241] J. Pastor – Villegas, C. Valenzuela 0 Calahorro, A. Bernalte – Garcia, and V. Gomez – Serrano, Carbon 31 (1993) 106

[242] Nestor Tan Credi, Tomas Cordero, Jose Rodriguez – Mirosol and Jaun J. Rodriguez, Fuel 75 (1996) 1701

[243] Francisco carrasco – Marin, Miguel A. Alvarez – Merino and Carlos Moreno – Castilla, Fuel 75 (1996) 966

[244] J. Alcaniz – Monge, M. A. Dela Casa – Lillo, d. Cazorla – Amoros and A. Linares – Solano, Carbon 35 (1997) 291

[245] H. Teng, J. A. Ho and Y. F. Hsu, carbon 35 (1997) 275

[246] Aik Chong Lua, Jia Guo, Carbon 38 (2000) 1089

[247] Alejandro Robau Sanchez, Alfredo Aguilar Elguezabal, Luis de La Torre Saenz, Carbon 39 (2001) 1367

[248] W. T. Tsai, C. Y. Chang, S. Y.Wang, C. F. Chang, S. F. Chien, H. F. Sun, Bioresource Technology 78 (2001) 203

[249] S. B. Lyubchik, Ro. Benoit and F. Beguin, Carbon 40 (2002) 1287

[250] D. Lozano – Castello, D. Cazorla – Amoros, a. Linares – Solano, Fuel Processing Technology, 77 (2002) 325

[251] Jia Guo, Aik Chong Lua, Journal of Collid and Interface Science 251 (2002) 242

[252] Jia Guo and Aik Chong Lua, Materials Letters 55 (2002) 334

[253] Guillermo San Miguel, Geoffrey D. Fowler, Christopher J. Sollars, Carbon 41 (2003) 1009

[254] Ting Yang and Aik Chong Lua, Journal of Collid and Interface Science, 267 (2003) 408

[255] E. Arenas and F. Chejue, Carbon 42 (2004) 245

[256] M. Turmuzi, W. R. W. Daud, S. M. Tasirin, M. S. Takriff, S. E. Iyuke, Carbon 42 (2004) 423

[257] Tengyan Zhang, Walter P. Walawander, L. T. Fan, Maohong Fan, Daren Daugaard, R. C. Brown, Chemical Engineering Journal 105 (2004) 53

[258] A. Zabaniotou, P. Madau, P. D. Oudenne, C. G. Jung, M. P. Delplancke, A. Fontana, Journal of Analytical and Applied Pyrolysis, 72 (2004) 289

[259] Maria Jasienko – Halat, Katarzyna Kedzior, Carbon 43 (2005) 944

[260] Feng – Chin Wu, Ru Ling Tseng, Journal of Colloid and Interface Science, 294 (2006) 21

[261] J. I. Paredes, F. Suarez – Garcia, A. Martinez – Alonso, and J. M. D. Tascon, Langmuir 22 (2006) 9730

[262] Juan F. Gonzalez, Jose M. Encinar, Carmen, M. Gonzalez – Garcia, E. Sabio, A. Ramiro, Jose L. Canito, Jose Ganan, Applied Surface Science, 252 (2006) 5999

[263] Chi-Chang Hu, Chen-Ching Wang, Feng – Chin Wu, Ru-Ling Tseng, Electrochimica Acta 52 (2007) 2498

[264] Manuel Maria Mahamad, Applied Surface Science 253 (2007) 6019

[265] B. Viswanathan and M. Aulice Scibioh, Fuel Cells : Principles and Applications, Universities Press, 2006

[266] Sonia A. C. Carabineiro and David T. Thompson, Catalytic Applications of Gold Nanotechnology in Nanoscience and Technology, Nanocatalysis, U. Heiz, U. Landman (Eds.), Springer-Verlag, Berlin Heidelberg, 2007, p. 463.

[267] Gang Wu, Bo-Qing Xu, Journal of Power Sources, 174 (2007) 148

[268] Yicheng Liu, Xinping Qiu, Zhenguo Chen, Wentao Zhu, Electrochemistry Communications 4 (2002) 550

[269] P. V. Samant, C. M. Rangel, M. H. Romero, J. B. Fernandes, J. L. Figueiredo, Journal of Power Sources 151 (2005) 79

[270] J. L. Gomez de la Fuente, M. V. Martinez-Huerta, S. Rojas, P. Terreros, J. L. G. Fierro, M. A. Pena, Catalysis Today 116 (2006) 422

[271] B. Ren, X. Q. Li, C. X. She, D. Y. Wu, Z. Q. Tian, Electrochimica Acta 46 (2000) 193

[272] Mohindar S. Seehra and Arthur S. Pavlovic, Carbon 31 (1993) 557

[273] V. Suresh Babu and M. S. Seehra, Carbon 34 (1996) 1259

[274] Yongbin Ji, Tiehu Li, Li Zhu, xiaoxian Wang, Qilang Liu, Applied Surface Science, 254 (2007) 506

[275] S. Biniak, G. Szymanski, J. Siedlewski and A. Swiatkowski, Carbon 35 (1997) 1799

[276] Chang Yu, Jie Shan Qiu, Yu Feng Sun, Xian Hui Li, Gang Chen, Zong Bin Zhao, Journal of Porous Materials, 15 (2008) 151

[277] C. Ishizaki and I Marti, Carbon, 19 (1981) 409

[278] A. Macias – Garcia, M. A. Diaz – Diez, E. M. Cuerda – Correa, M. Olivares – Marin, J. Ganan – Gomez, Applied Surface Science 252 (2006) 5972

[279] C. Moreno-Castilla, M. V. Lopez-Ramon, F. Carrasco-Marin, Carbon 38 (2000) 1995

[280]. B. Viswanathan, Catalysis Today, 141 (2009) 52

[281] B. Rajesh, Ph. D., Thesis, Indian Institute of Technology, Madras, 2002.

[282]. A. R. West, Solid State Chemistry and its Applications, Wiley, Chichester, 1984, Pp. 734

[283] M. Carmo, V. A. Paganin, J. M. Rosolen, E. R. Gonzalez, Journal of Power Sources 142 (2005) 169

[284] Zhaolin Liu, Xing Yi Ling, Xiaodi Su and Jim Yang Lee, J. Phys. Chem. B., 108 (2004) 8234

[285] R. Manohara, J. B. Goodenough, Journal of Materials Chemistry, 2 (1992) 875

[286] Zhaolin Liu, Jim Yang Lee, Weixiang Chen, Ming Han and Leong Ming Gan, Langmuir 20 (2004) 181

[287] M. Sevilla, C. Sanches, T. Valdos-Sols, E. Moralln, A. B. Fuertes, Journal of Physical Chemistry C, 111 (2007) 9749

[288] Jun Jie Niu, Jian Nong Wang, Li Zhang and Yiqing Shi, Journal of Physical Chemistry C, 111 (2007) 10329

[289] Zhibin Lei, Shiying Bai, Yi Xiao, Liqin Dang, Lizhen Au, Guangning Zhang, and Qian Xu, Journal of Physical Chemistry C, 111 (2008) 722

[290] Shu-Fa Zheng, Jin-song Hu, Liang – Shu, Zhong, Li – Jun Wan, Wei-Guo Song, Journal of Physical Chemistry C 111 (2007) 11174

[291]. J. Sobkowski, K. Franaszczuk and K. Dobrowolska, Journal of Electroanalytical Chemistry, 330 (1992) 529

[292]. Meng-Liang Lin, Chun-Chieh Huang, Man-Yin Lo, and Chung-Yuan Mou, Journal of Physical Chemistry C, 112 (2008) 867

[293]. Zhibin Lei, Lizhen An, Liquin Dang, Mingyi Zhao, Jingying Shi, Shiying Bai, yindicao, Microporous and Mesoporous Materials 119 (2009) 301.

[294]. H. J. Wang, H. Yu, F. Peng, P. Lv, Electrochemistry communications 8 (2006) 499

[295] G. L. Che, B. B. Lakshmi, C. R. Martin, E. R. Fisher, Langmuir 15 (1999) 750

[296] S. J. Sardhar Basha, P. Vijayan, K. Santhi, D. K. Setua, Catalysis Communications 8 (2007) 619

[297] J. M. Manoli, P. Da Costa, M. Brun, M. Vrinat, F. Mauge and C. Potvin, Journal of Catalysis, 221 (2004) 365

[298] John R Anderson and Michel Boudart, Catalysis Science and Technology, Volume 11, Springer Verlag, 1996

[299]. Michele Breysse, Gerald Djega – Mariadassou, Stephanie Pessayre, Christophe Geantet, Michel Vrinat, Guy Perot, Marc Lemaire, Catalysis Today 84 (2003) 129

[300] Frances M. Collins, Andrew R. Lucy, Christopher Sharp, Journal of Molecular Catalysis A: Chemical, 117 (1997) 397

[301] Beatriz Castro, Michael J. Whitecombe, Evgeny N. Vulfson, Rafael Vazquez – Duhalt, Eduardo Barzana, Analytica Chimica Acta, 435 (2001) 83

[302] Chunshan Song, Xiaoliang Ma, Applied Catalysis B: Environmental, 41 (2003) 207

[303] Hai Mei, B. W. Mei, Teh Fu Yen, Fuel 82 (2003) 405

[304] Chunshan Song, Catalysis Today 86 (2003) 211

[305] Jorgge Aburto, Antonio Mendez – Orozco, Sylvie Le Borgne, Chemical Engineering and Processing, 43 (2004) 1587

[306] Yosuke Sano, Ki-Hyonk Choi, Yozo Korai, Isao Mochida, Applied Catalysis B : Environmental 49 (2004) 219

[307] Xiaoliang Ma, Subramani Velu, Jae Hyung Kim, Chunshan song, Applied Catalysis B: Environmental 56 (2005) 137

[308] Chang Yu, Jie Shan Qiu, Yu Feng Sun, Xian Hui Li, Gang Chen, Zong Bin Zhao, Journal of Porous Materials 15 (2008) 151

[309] Yahia A. Alhamed, Hisham S. Bamufleh, Fuel 88 (2009) 87

[310] V. Selvavathi, A. Meenakshisundaram, B. Sairam, P. Indra Neel, M. Rajasekaran, B. Viswanathan, Adsorptive desulphurization of diesel by modified carbons, 6th International Symposium on Fuels and Lubricants (ISFL-2008)",March 9-12,2008 at New Delhi.

[311] Mingwang Shao, Debao Wang, Guihua-Yu, Bing Hu, Weichao Yu, Yitai Qian, Carbon 42 (2004) 183-185.

[312] J. A. Macia – Agullo, B. C. Moore, D. Cazoria – Amoros, A. Linares – Solana, Microporous Materials 101 (2007) 397

[313] S. J. Gregg, K. S. W. Singh, Adsorption, Surface Area and Porosity, Second ed. Academic Press, London, 1982, pp. 195-288

[314] Qingrong Qian, Motoi Machida, Hideki Tatsumoto, Bioresource Technology, 98 (2007) 353-360

[315] Thio Christine Chandra, M. M. Mirna, Y. Sudaryanto, S. Ismadji, Chemical Engineering Journal, 127 (2007) 121

[316] M. Madhava Rao, A. Ramesh, G. Purna Chandra Rao, K. Seshaiah, Journal of Hazardous Materials B129 (2006) 123